THE UNIVERSITY OF MANITOBA

Studies of High-T_c Superconductors

BY

XUE ZHI ZHOU

A THESIS SUBMITTED TO THE FACULTY OF GRADUATE STUDIES OF THE UNIVERSITY OF MANITOBA IN PARTIAL FULFILLMENT OF THE REQUIREMENTS OF THE DEGREE OF DOCTOR OF PHILOSOPHY

DEPARTMENT OF PHYSICS

WINNIPEG, MANITOBA

February 1990

ISBN 0-315-63265-8

Studies of High-T_c Superconductors

by

Xue Zhi Zhou

A thesis submitted to the Faculty of Graduate Studies of the University of Manitoba in partial fulfillment of the requirements of the degree of

DOCTOR OF PHILOSOPHY

Abstract

In early 1987 the high-T_c superconductor, $YBa_2Cu_3O_{7-\delta}$, with $T_c \simeq 90K$ was successfully made in our laboratory by a standard ceramic technique. Later $Tl_2Ca_2Ba_2Cu_3O_{10}$ with $T_c \simeq 120K$ was produced by a special procedure. Structural analysis by x-ray diffraction showed that $YBa_2Cu_3O_{7-\delta}$ was responsible for the high-T_c, the so called 123 phase. It is an oxygen deficient perovskite with the orthorhombic structure, space group $Pmmm$, lattice constant a=3.8243, b=3.8862 and c=11.667Å. Oxygen vacancies are very important to the superconducting properties. An impurity, Y_2BaCuO_5, with a green colour, was identified as a semiconducting phase. A technique to grow single crystals of $YBa_2Cu_3O_{7-\delta}$ is described. The crystals are rectangular up to $2 \times 2 \times 0.2$ mm^3 in size. Two phases, $Tl_2CaBa_2Cu_2O_8$ (the 2122 phase) and $Tl_2Ca_2Ba_2Cu_3O_{10}$ (the 2223 phase), are responsible for the high-T_c in the Tl-system; they have a tetragonal or pseudotetragonal structure with space group $I4/mmm$.

Resistivity and magnetic ac susceptibility results show that high-T_c materials have a sharp superconducting transition and many properties in common with conventional superconductors. The shielding effect is closely related to the properties of grain boundaries. Magnetic ordering at low temperature (below 10K) of high-T_c materials was discovered by Mössbauer experiments with ^{57}Fe doped samples. Substitution of Fe for Cu reduced the superconducting transition temperature and the shielding effect. Theories of superconductivity for conventional and the new superconductors are reviewed and related to the experimental results.

Acknowledgements

I am very grateful to my advisor, Professor A. H. Morrish for his encouragement and guidance throughout this research project and carefully reading my thesis. I have benefited greatly in many ways by working with him.

I wish to thank Dr. R. J. Pollard and Dr. Q. Pankhurst for their computer programs to fit Mössbauer spectra, Dr. M. Raudsepp for his x-ray diffraction data analysis and Dr. I. Maartense for the use of his ac susceptometer. Thanks are also due for their very useful discussions and sharing their knowledge.

I am grateful to professors J. H. Page, R. M. Roshko, J. P. Svenne and L. K. Chan for their spending time for my project.

Thanks are also due to Mr. G. Roy for his great deal of invaluable technical help, to Dr. H. Kunkel, Ms. Y. L. Luo, Mr. Z. W. Li, Mr. N. Ball and Ms. G. Pelletier for their assistance. I am also grateful to the staff in the Electronics and Mechanical workshops for their patience and skill.

The financial support received from the Department of Physics, University of Manitoba in the form of research grants is gratefully acknowledged.

Finally I wish to express my gratitude to my family for their support in completing this research project, especially my wife, Yulin Luo, for her assistance with all the diagrams and my son, Yuchuan Zhou, for his partially typing of thie thesis.

Contents

List of Figures

List of Tables

Introduction

It is well known that in 1911, H. Kamerlingh Onnes discovered that the resistance of mercury sharply disappeared at 4.2 K and it is said that the mercury enters a superconducting state. Since then the development of this field followed mainly three directions: theoretical works to find the origin of superconductivity, material researches to search for new materials which have higher transition temperatures, and applications to make devices that benefit mankind.

In order to understand the mechanism of superconductivity several macroscopic theories, such as London's theory, Ginzberg's theory, and so on, were presented. It took a long time to find the origin of the superconductivity because of the extremely small energy difference between the normal and the superconductive state. In 1950 H. Fröhlich suggested that the electron-phonon interaction, which implies an attractive electron-electron interaction, was responsible for the superconductivity. It was confirmed by the discovery of the isotope effect. In 1956 Cooper showed that the Fermi sea is unstable against pair formation when there exists any attractive interaction between electrons no matter how weak. About a half century later after the initial discovery of superconductivity, a microscopic theory was completed by Bardeen, Cooper and Schriefer in 1957, it is usually referred to as the BCS theory. It showed that the electron-phonon interaction was responsible for the superconductivity in conventional superconductors. It also agrees well with most experimental results.

Ever since superconductivity was first observed, it has been man's dream to utilize the zero-resistance property for the benefits of mankind. With development

of type-II superconductors, it became possible to make superconducting solenoids that produced large magnetic fields. Because liquid helium was still required as a refrigerant, these device were primarily restricted to laboratory uses. To make superconductivity useful for more practical applications, it is better that the materials have T_c above 77K. Then liquid nitrogen can be used as the refrigerant.

On the other hand experimental physicists have been trying to search for new materials which possess much higher T_c since 1911. Attempts mostly were concentrated on metals and alloys. The T_c was enhanced slowly from 4.2 K for mercury to 23.3 K for Nb_3Ge during the past 75 years.

In 1986, J. G. Bednorz and K. A. Müller (IBM, Zürich, Switzerland) found an oxide $LaBaCuO_4$[1], which had $T_c \simeq 30$ K; this is higher than 23.3K, the highest T_c in alloys. This discovery stimulated scientists over the world to attempt further to find a new compound with a higher T_c. In early 1987, indeed, materials with $T_c > 77$K were reported, including our own discovery [2,3]. Later this material was identified as $YBa_2Cu_3O_{7-\delta}$ with onset temperature 93K and zero resistivity at about 90K. That is the so called 123 phase. In early 1988, other new materials, the BiCaSrCuO system with T_c=80-110K and the TlCaBaCuO system with T_c=90-125K were reported [4,5]. To date, attempts to enhance T_c are still in the progress.

The discovery of high-T_c superconductivity opened up many new vistas to scientists. In view of the applications, it appears that high-T_c materials promise a bright future for superconductivity since liquid nitrogen can be used as a refrigerant. But the ceramic property and low critical current make applications of

the new materials very difficult in some fields, such as power transmission, supermagnets and so on. It also makes some difficulties for the BCS theory. No doubt scientists will be encouraged to modify the BCS theory or to find an entirely new one.

In this thesis some early results on high-T_c superconductors during this period are presented. The preparation of high-T_c superconductors is described. The structure analysis is performed by x-ray diffraction. Resistivity and ac susceptibility results show that the new materials have a sharp superconducting transition and many properties in common with conventional superconductors. Magnetic ordering at low temperature was observed by Mössbauer experiments in ^{57}Fe doped samples. Theories of superconductivity for conventional and new high-T_c superconductors are also reviewed. Our accomplishments are summarised in chapter 8. In addition, some suggestions for future investigations are made.

Chapter 1

Basic Properties of Superconductors

1.1 Perfect Conductivity

For most metals and alloys, the electrical resistivity decreases when they are cooled. At and above room temperature the electrical resistance of most metals is approximately a linear function of temperature. At sufficiently low temperature ($T << \Theta$, The Debye temperature) the resistivity varies as T^5 [6]. The resistance arises from the scattering of conduction electrons by the thermal vibrations of the lattice and randomly-distributed impurities and imperfections in the crystalline lattice.

For certain metals, when they are cooled their electrical resistance decreases in the usual way, but on reaching a certain temperature they suddenly lose all of their resistance. An example is mercury, which loses its resistance at 4.2 K, as was first discovered by H. Kamerlingh Onnes. Then these materials are said to have passed into the superconducting state. The temperature at which a

superconductor loses its resistance is called the transition temperature or critical temperature, denoted by T_c.

The electrical property of the superconductor discovered earliest is that its resistance vanishes below T_c. Naturally the superconductor is a *perfect conductor*, namely its conductivity is infinite ($\sigma \to \infty$).

What is the magnetic property of a perfect conductor (not a superconductor)? In a perfect conductor, the equation of motion of the charge carrier with mass m, charge q, and the density n_s in a constant electrical field $\mathbf{E}$ is

$$m\frac{d\mathbf{v}}{dt} = q\mathbf{E} \tag{1.1}$$

where $\mathbf{v}$ is the velocity of the charge carrier. The current density by general definition is

$$\mathbf{j}_s = n_s q\mathbf{v} \tag{1.2}$$

From (1.1) and (1.2), it follows that

$$\frac{d\mathbf{j}_s}{dt} = \frac{n_s q^2}{m}\mathbf{E}$$

On using Maxwell's equation

$$\nabla \times \mathbf{E} = -\frac{\partial \mathbf{B}}{\partial t}$$

We obtain

$$\nabla \times \frac{d\mathbf{j}_s}{dt} = \frac{n_s q^2}{m} \nabla \times \mathbf{E} = -\frac{n_s q^2}{m} \frac{\partial \mathbf{B}}{\partial t} \tag{1.3}$$

or

$$\frac{d}{dt}\left[\nabla \times \mathbf{j}_s + \frac{n_s q^2}{m}\mathbf{B}\right] = 0 \tag{1.4}$$

Since

$$\nabla \times \mathbf{B} = \mu_0 \mathbf{j} \qquad \text{and} \qquad \nabla \cdot \mathbf{B} = 0$$

So that

$$\begin{aligned} \nabla \times \frac{d\mathbf{j}_s}{dt} &= \nabla \times \left(\frac{1}{\mu_0} \nabla \times \frac{\partial \mathbf{B}}{\partial t}\right) \\ &= \frac{1}{\mu_0}\left[\nabla(\nabla \cdot \frac{\partial \mathbf{B}}{\partial t}) - \nabla^2 \frac{\partial \mathbf{B}}{\partial t}\right] \\ &= -\frac{1}{\mu_0} \nabla^2 \frac{\partial \mathbf{B}}{\partial t}, \end{aligned}$$

$$\nabla^2 \frac{\partial \mathbf{B}}{\partial t} = \frac{\mu_0 n_s q^2}{m} \frac{\partial \mathbf{B}}{\partial t} = \frac{1}{\lambda^2} \frac{\partial \mathbf{B}}{\partial t} \tag{1.5}$$

where

$$\lambda^2 = \frac{m}{\mu_0 n_s q^2}$$

The solution of equation(1.5) is

$$\frac{\partial \mathbf{B}}{\partial t} = \frac{\partial \mathbf{B}_0}{\partial t} e^{-x/\lambda} \tag{1.6}$$

where $\mathbf{B}_0$ is the magnetic field outside the conductor, and x is the distance measured from the surface of the perfect conductor. When $x \gg \lambda$, in the interior of a perfect conductor $\frac{\partial \mathbf{B}}{\partial t} = 0$, namely the magnetic induction in the interior of a perfect conductor is a constant over time, which depends on the initial magnetic state of the perfect conductor.

1.2 Perfect Diamagnetism

Until 1933 it was assumed that infinite conductivity was the essential property of a superconductor. In 1933, Meissner and Ochesenfeld showed that the superconducting state possessed the additional and entirely independent property; viz *the magnetic flux is expelled from the interior of the superconductor and the magnetic induction* $\mathbf{B}$ *vanishes.* This is called the Meissner effect, which indicates $\mathbf{B} = 0$ inside a superconductor independent of its initial state. This is quite different from the situation for a perfect conductor.

In order to explain the Meissner effect, F. London and H. London in 1935 postulated a more restrictive condition in which the equation (1.4) was replaced by

$$\nabla \times \mathbf{j}_s + \frac{n_s q^2}{m} \mathbf{B} = 0 \tag{1.7}$$

This is called the London equation. Equation (1.7) can be reduced to

$$\nabla^2 \mathbf{B} = \frac{1}{\lambda^2}\mathbf{B} \tag{1.8}$$

which is similar to equation (1.5) with $\lambda^2 = \frac{m}{\mu_0 n_s q^2}$. For a one-dimensional material which occupies the halfspace $x > 0$, while other halfspace, $x < 0$, is vacuum, equation (1.8) can be simplified to

$$\frac{d^2 B_y(x)}{dx^2} = \frac{1}{\lambda^2} B_y(x).$$

The solution of this equation is

$$\mathrm{B}_y(x) = \mathrm{B}_0 e^{-x/\lambda} \tag{1.9}$$

where B_0 is the magnetic induction at $x = 0$ in the vacuum.

Figure 1 shows the distribution of magnetic induction $\mathrm{B}_y(x)$ inside the superconductor. In the region of $x >> \lambda$, $\mathrm{B}_y(x) \rightarrow 0$; while $0 < x < \lambda$, the flux can penetrate the superconductor. From Maxwell's equation

$$\mu_0 j_{sz} = (\nabla \times \mathbf{B})_z = \frac{d}{dx}\mathrm{B}_y(x) = -\frac{\mathrm{B}_0}{\lambda} e^{-x/\lambda}$$

There is a current on the surface of superconductor along the direction of the z axis. The current attenuates exponentially along the x direction; the length characterizing the attenuation is called the penetration depth, λ. It is this surface current J_{sz} that produces a magnetic field in the region of $x > \lambda$ along

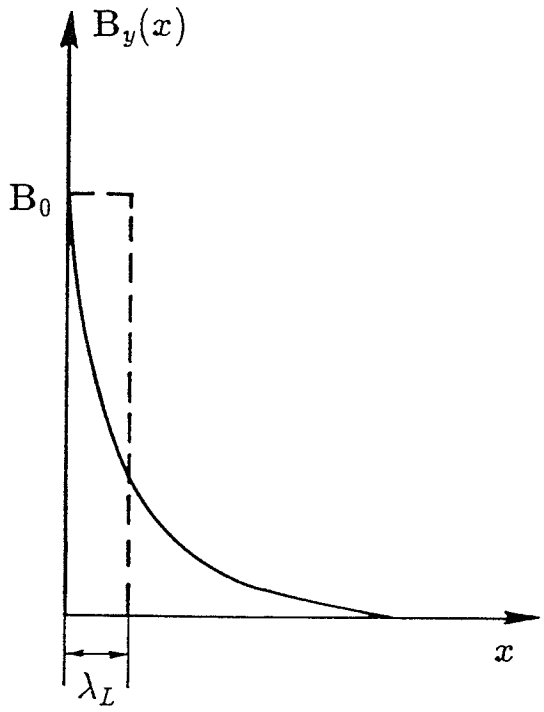

Figure 1.1: The distribution of magnetic induction **B** on the surface of a superconductor as given by London equation.

the negative y direction which cancels the applied field to make the total field inside the superconductor zero. This surface current is called the diamagnetic or shielding current.

In the Meissner effect, the total magnetic induction $\mathbf{B}$ inside the superconductor vanishes as long as the applied field is less than a critical field H_c. We can deduce that

$$\mathbf{B} = \mathbf{B_0} + \mu_0 \mathrm{M} = 0$$

where $\mathbf{B_0}$ is the applied magnetic field, μ_0 the permeability and M the magnetic moment of the superconductor. The magnetic susceptibility is then

$$\chi = \frac{\mu_0 \mathrm{M}}{\mathbf{B_0}} = -1 \tag{1.10}$$

The negative unity value of χ means the superconductor is a *perfect diamagnet.* The Meissner effect reveals clearly the difference between a superconductor and a perfect conductor. Thus perfect conductivity, (ρ=0), alone is not sufficient to describe superconductors. We also need perfect diamagnetism ($\mathbf{B}$=0). The Meissner effect also shows that the superconducting transition is reversible and that the superconducting state is a thermodynamic phase independent of the way it is entered.

1.3 Specific Heat

It has been found experimentally that the specific heat has a jump at the superconducting transition. The specific heat of the superconducting state is greater than that of normal state.

To understand this phenomenna we consider a thermodynamic system in which a specimen with a long needle-like shape (to avoid a complicated calculation of the demagnetization field effect) aligned parallel to an applied magnetic field H_a. The first thermodynamic law has the form

$$dU = TdS - P\Delta V + \mu_0 V H_a dM$$

where U is the internal energy, S the entropy, P the pressure, V the volume, H_a the applied field and M the magnetic moment per unit volume. This equation means that the increase of the internal energy dU equals the sum of the heat absorbed by the specimen, TdS, the work done by the specimen, $-P\Delta V$, and the work done by the applied field on the specimen, $\mu_0 H_a dM$. At the transition experiment shows that the change in volume can be neglected. Therefore

$$dU = TdS + \mu_0 V H_a dM.$$

The Gibbs function density (or free energy density) has the form

$$g = u - Ts - \mu_0 H_a M$$

so that

$$dg = -sdT - \mu_0 M dH_a$$

Under constant temperature (dT=0)

$$dg = -\mu_0 M dH_a.$$

The superconductors are not ferromagnets. In the normal state M$\simeq$0, then dg_n = 0, i.e. g_n is a constant.

$$g_n(T, H_a) = g_n(T, 0)$$

In the superconducting state $dg_s = -\mu_0 M dH_a$. After integration we obtain

$$g_s(T, H_a) - g_s(T, 0) = \frac{1}{2}\mu_0 H_a^2 \tag{1.11}$$

From thermodynamic theory a necessary condition for the two phases to coexist is that the density of Gibbs function has the same value in both phases. Thus the critical field is determined by the condition

$$g_s(T, H_c) = g_n(T, H_c) \tag{1.12}$$

Since the normal state has been assumed to nonmagnetic, g_n is independent of

the field, i.e.

$$g_n(T, H_c) = g_n(T, 0) \tag{1.13}$$

Therefore

$$g_n(T, 0) - g_s(T, 0) = \frac{1}{2}\mu_0 H_c^2 \tag{1.14}$$

Because the density of entropy is $s = -\left(\frac{\partial g}{\partial T}\right)_{p,H_a}$,

$$s_n(T, 0) - s_s(T, 0) = -\mu_0 H_c \frac{dH_c}{dT} \tag{1.15}$$

The density of the specific heat is $c = dQ/dT = Tds/dT$, so the difference in the density of specific heat between the normal and superconducting states is

$$\begin{aligned}
\Delta c &= c_s - c_n \\
&= T\left[\frac{ds_s}{dT} - \frac{ds_n}{aT}\right] \\
&= T\frac{d}{dT}\left[\mu_0 H_c \frac{dH_c}{dT}\right] \\
&= \mu_0 T\left[\left(\frac{dH_c}{dT}\right)^2 + H_c \frac{d^2 H_c}{dT^2}\right]
\end{aligned}$$

In particular, at T=T_c, H_c=0 and for the transition in the absence of an applied

magnetic field we have

$$(c_s - c_n)_{T_c} = \mu_0 T_c \left(\frac{dH_c}{dT}\right)^2_{T_c} \tag{1.16}$$

That means in the absence of an applied field and at T_c the specific heat of the superconducting state is greater than that of the normal state by an amount of $\mu_0 T_c (\frac{dH_c}{dT})^2_{T_c}$, which agrees well with experimental results.

From equation (1.15) we can obtain the latent heat L, i.e. the heat absorbed by the sample per unit volume during the transition from the superconducting to the normal state, viz

$$\begin{aligned} L = T\Delta s &= T[s_n(T, H_c) - s_s(T, 0)] \\ &= -\mu_0 T H_c \frac{dH_c}{dT} \end{aligned}$$

When $0 < T < T_c$, $\frac{dH_c}{dT} < 0$ and then $L > 0$. The transition from the superconducting to the normal state absorbs heat. On the other hand, the transition from the normal to the superconducting state releases the heat and $L < 0$. This is a first-order transition. At $T=T_c$, $H_c = 0$ and then L=0. In this case there is no change of L at the transition. Then the superconducting transition at $H_c = 0$ is a second-order transition.

In both the superconducting and the normal states there are two contributions to the specific heat of a metal; these are from the crystal lattice and from

the conduction electrons. We therefore may write the specific heat as

$$c_n = c_{Ln} + c_{en}$$

$$c_s = c_{Ls} + c_{sn}$$

The experimental results show that the properties of the lattice do not change during the transition; hence $c_{Ln} = c_{Ls}$. The difference in the specific heat between the superconducting and the normal states arises only from the contribution of the conduction electrons, that is

$$c_s - c_n = c_{es} - c_{en}$$

It was found that the specific heat of the superconducting state at very low temperatures (T< $\frac{1}{3}\Theta_D$, Θ_D is the Debye temperature) is given by

$$c_{es} = ae^{-b/k_BT} \tag{1.17}$$

where a and b are constants and k_B is Boltzmann's constant. Such a exponential variation suggests that as the temperature is raised electrons are excited across an energy gap above their ground state. The number of electrons excited across such a gap would vary exponentially with temperature. Each excited electron absorbs an energy of about k_BT_c. This may account for the rapid increase in the specific heat of a superconducting metal as the temperature approaches T_c.

1.4 Energy Gap

It was found that between the superconducting state (ground state) and the normal state (excited state) there is an enery gap. The magnitude of the energy gap is about $10^{-4}\ eV$.

As mentioned previously, at low temperature the contribution of the conduction electrons to the specific heat in the superconducting state is proportional to e^{-b/k_BT}. It is very hard to understand such a temperature dependence, except as a consequence of an energy gap. If there is an energy gap then as the temperature is raised, the electrons are thermally excited aross the gap and for each of these electrons an amount of energy equal to the energy gap E_g is absorbed in the process. The number of the electrons in the energy level above the gap at temperature T according to a Boltzmann statistic is proportional to $e^{-E_g/2k_BT}$, where k_B is Boltzmann's constant. The thermal energy absorbed in exciting these electrons is therefore proportional to $E_g e^{-E_g/2k_BT}$. The specific heat is proportional to the derivative of the energy with respect to temperature, i.e. to $\left(\frac{1}{T^2}\right) e^{-E_g/2k_BT}$. The T^2 term varies much more slowly with T than the exponential term. So the variation of specific heat should be very nearly exponential.

Besides the specific heat, many other experiments, such as low temperature thermal conductivity [7], the microwave absorption spectrum [8], ultrasonic attenuation [9] and tunneling experiments [10] and so on, all confirm the existence of an energy gap in superconductors. The existence of energy gap is also important for the development of the microscopic theory of superconductivity.

1.5 Isotope Effect

In 1950 E. Maxwell [11], and C. A. Reynold, B. Serin [12] independently discovered the isotope effect, wherein the transition temperatures of the sample made from different isotopes of a given element are different. Often the transition temperature, T_c, varies inversely with the square root of the isotope mass M, that is

$$M^{1/2}T_c = \text{constant}$$

This relation links the superconducting properties of the metal to the masses of the ions in the lattice even though the lattice itself does not change during the transition. This effect strongly indicates that the electron-phonon interaction is the origin of the superconductivity.

Other experiments show a relationship $M^{\alpha}T_c = c$, where $\alpha = 0.5 \pm 0.03$ for most isotopes, few of them have a very small α value, such as Ru, Os and Zr. This may be attributed to the special band structure of these metals. The isotope effect is absent or very small in the new high T_c ceramic superconductors. This absence or very small isotope effect may imply that a new mechanism is resposible for high-T_c superconductivity.

1.6 Two Types of Superconductors

When $T < T_c$ a magnetic field could destroy the superconducting state and restore the normal state. The minimum magnetic field required to destroy the

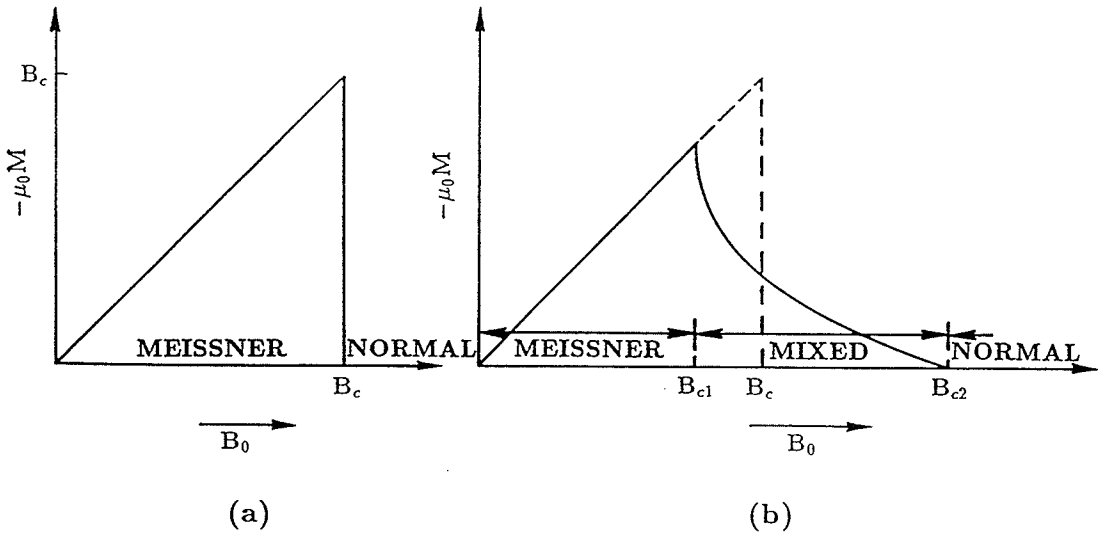

Figure 1.2: The magnetization curve of two types of superconductors.

superconducting state is called the critical field H_c or ($B_c = \mu_0 H_c$). For most metal-element superconductors H_c is a function of temperature given by

$$H_c = H_{c0}\left(1 - \frac{T^2}{T_c^2}\right) \tag{1.18}$$

where H_{c0} is the critical field at T=0 K and T_c is the transition temperature.

Superconductors can be classified into two types. Type I superconductors have only one critical field H_c. The magnetization curve is shown in Fig. 1.2(a). It has the Meissner effect and the supercurrent on the surface maintains the complete diamagnetism inside the sample. Most elemental superconductors, except V, Nb

and Tc, belong to type I.

Type II superconductors have two critical fields, a lower critical field H_{c1} and an upper critical field H_{c2}, as shown in Fig. 1.2(b). When the applied field $H_a < H_{c1}$, the properties of type II and type I superconductors are similar. Both have the Meissner effect and no flux penetrates the sample. When $H_{c1} < H_a < H_{c2}$, the type II superconductor is in a mixed state, a characteristic of type II superconductor. In the mixed state the magnetic flux partially penetrates the sample body and forms a lot of small cylinders which are in the normal state and can be penetrated by a fluxon. The region between the normal cylinders is in the superconducting state (Fig. 1.3).

When a type II superconductor is in the mixed state it not only has diamagnetism but also has zero resistance. As the applied field increases each cylindrical normal region does not expand, but instead the number of the cylindrical regions increases. When $H_a=H_{c2}$, all the cylindrical regions connect with each other. Then sample loses the superconducting state and recovers to the normal state. Figure 1.4 shows the various states for type II superconductors. The mixed state has been confirmed in the conventional and as well as in the new high-T_c ceramic superconductors by some elegant experimemts [13,14,15]. Most alloys and the new high-T_c materials are type II superconductors.

Since there are some boundaries between the normal and superconducting states in type II superconductors and these are absent in type I superconductors, it can be expected that the surface energy of a normal-superconducting interface is very important to classify these two types of superconductors. When a magnetic

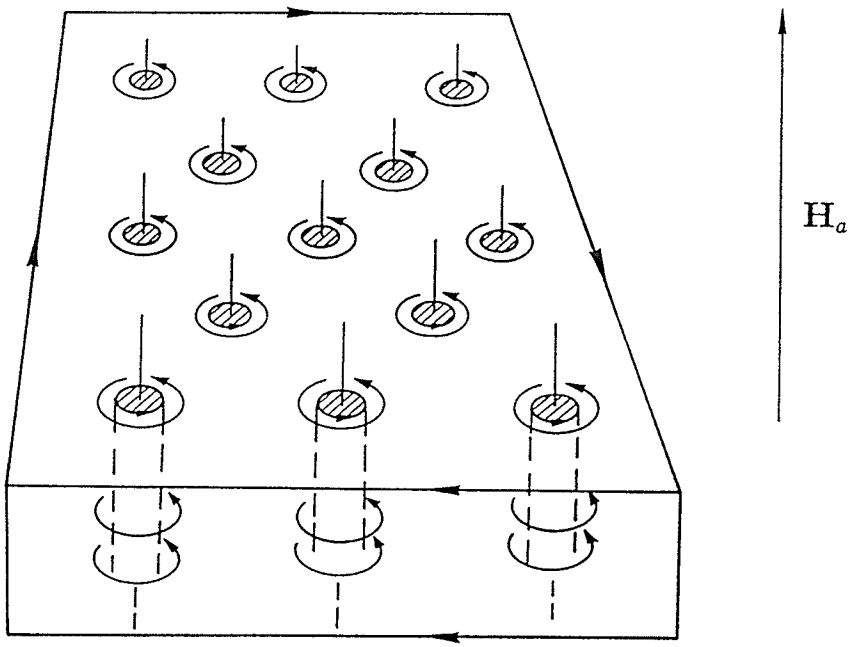

Figure 1.3: The mixed state, showing normal cylindrical regions and encircling supercurrent vortices. The vertical lines represent the flux threading the normal cylinder region. The surface current maintains perfect bulk diamagnetism.

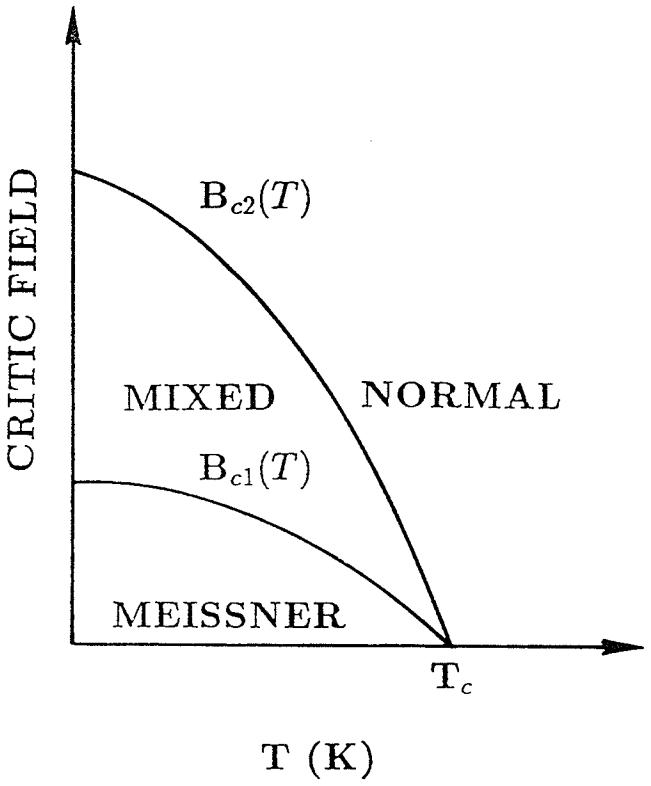

Figure 1.4: Various states of type II superconductor.

field, $H_{c1} < H_a < H_{c2}$, is applied to a type II superconductor a cylindrical structure is formed. In the coherence length range, ξ, the superelectron density decreases as compared to the superconducting region and energy must be provided to split up the electron pairs. As an approximation the appearance of the interface will result in a local increase in free energy of $\xi \cdot \frac{\mu_0 H_c^2}{2}$ per unit area of the interface. Meanwhile in the penetration depth range, λ, the material is not diamagnetic. So there is a local decrease in magnetic energy that is approximately equal to $\lambda \cdot \frac{\mu_0 H_a^2}{2}$ per unit area. Therefore the surface energy per unit area at the normal-superconducting interface is

$$\sigma_{ns} = \xi \cdot \frac{\mu_0 H_c^2}{2} - \lambda \cdot \frac{\mu_0 H_a^2}{2}$$

According to this relation, when $H_a < H_c$ (a necessary condition for the mixed state), if $\xi > \lambda$, $\sigma_{ns} > 0$, that is the surface energy is positive. Then the surface of the normal- superconducting interface is energetically unfavourable; this occurs for type I superconductors. When $\xi < \lambda$, $\sigma_{ns} < 0$, that is, the surface energy is negative. The surface of normal-superconducting interface is then energetically favourable; a type II superconductor will be in the mixed state.

Ginzburg and Landau define a parameter

$$\kappa = \frac{\lambda}{\xi}$$

where λ is the penetration depth and ξ the coherence length. The κ varies for different superconductors and is called Ginzburg-Landau costant. A more detailed

calculation shows that

for	$\kappa < \sqrt{2}$,	the surface energy is positive (type I)
for	$\kappa > \sqrt{2}$,	the surface energy is negative (type II)

Type II supercondutors have much larger upper critical fields than those for type I materials; they are therefore techanically important and used to make the solenoids with large magnetic fields.

Chapter 2

The Microscopic Theory of Superconductivity

After the discovery of the superconductivity by H. Kamerlingh Onnes a number of phenomenological theories, such as the two-fluid model, the Ginzberg–Landau theory [16] and so on, had been proposed to understand and explain superconducting properties. About half century later (in 1957) the complete microscopic theory of superconductivity was established by Bardeen, Cooper and Schrieffer, usually referred to as the BCS theory [17]. The isotope effect and the quantization of magnetic flux strongly supported and confirmed this theory. It also agrees well with most properties of conventional superconducting materials.

The discovery of the high-T_c superconducting materials ($T_c \geq 90K$) makes some difficulties for the BCS theory. Specially a very small or zero isotope effect in the new materials has been experimentally shown [18,19]. Whether the BCS theory merely needs to be modified or if a complete new theory is required for the high-T_c superconductors is currently a controversial subject in physics.

2.1 BCS theory

Before the BCS theory it took a long time to find the interaction responsible for the superconductivity. Experimental evidence pointed to the fact that in the transition to the superconductive state the lattice and its properties were essentially unchanged whereas some of the properties of conduction electrons were changed radically. In the first instance, it was reasonable to assume that the transition was caused by a change in the state of the electrons alone. The early attempts suggested that a theory based on an independent particle model of the conduction electrons did not have the possibility of explaining the fundamental property of superconductors which is their infinite conductivity. Thus the simplest model was that of a gas of electrons interacting with each other through some two-particle interaction; this was the model to which Bardeen, Cooper and Schrieffer addressed themselves.

The Coulomb interaction was first considered. But it is repulsive. Measurements of the magnetic field required to destroy superconductivity near the absolute zero show that the condensation energy of each electron within a energy band of width $k_B T_c$ around the Fermi surface is about 10^{-8} eV; however the energy of the Coulomb interaction between the electrons is about 1 eV [20]. Even if it were attractive the magnitude would be too large to be resposible for the superconductivity. Thus the Coulomb interaction was rejected.

In 1950 Fröhlich[21] pointed out that electron–phonon interaction provides a mechanism for a weak attraction between two electrons which is responsible for superconductivity.

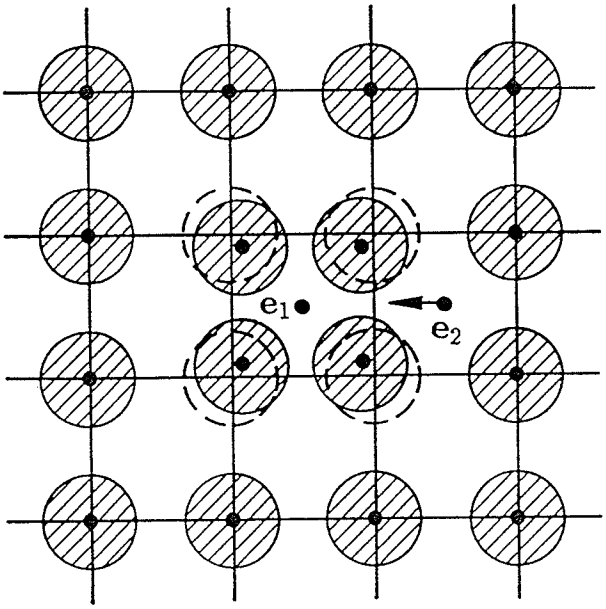

Figure 2.1: The electron polarized crystal.

2.1.1 The Attraction Between Electrons

Free electrons repel each other through their Coulomb interaction. Therefore the attraction between the electrons must be transmitted by another mechanism. In a crystal an electron, e_1, will attract the positive ions around it at lattice points. It is said that the electron polarized the crystal. This slightly increases the density of positive ion cores in the immediate region of the electron(Fig. 2.1).

The other electrons, such as e_2, in this general vicinity will be drawn towards this region because of the higher density of positive charge; hence the electrons are attracted to each other via the movement of the ions. If this attractive force overcomes the repulsive Coulomb interaction there is a net attractive force between the two electrons.

To describe this indirect attractive force let us analyse the process in which the two electrons exchange a *virtual phonon.*

An electron with wave vector $\mathbf{k}_1$ emits a phonon $\mathbf{q}$ and is scattered into a state with wave vector $\mathbf{k}_1'(=\mathbf{k}_1-\mathbf{q})$ (Fig. 2.2(a)). This phonon is absorbed by a second electron which changes its wave vector from $\mathbf{k}_2$ to $\mathbf{k}_2'(=\mathbf{k}_2+\mathbf{q})$. Both processes conserve crystal momentum

$$\mathbf{k'}_1 + \mathbf{k'}_2 = \mathbf{k}_1 + \mathbf{k}_2$$

According to second order perturbation theory the contribution of this process before the phonon was absorbed to the energy is

$$< \mathbf{k}_1 - \mathbf{q}, \mathbf{k}_2 + \mathbf{q}|V_1|\mathbf{k}_1, \mathbf{k}_2 >= \frac{M_{\mathbf{k}_1,\mathbf{k}_1-\mathbf{q}} \cdot M^{*}_{\mathbf{k}_2,\mathbf{k}_2+\mathbf{q}}}{E(\mathbf{k}_1) - E(\mathbf{k}_1 - \mathbf{q}) - \hbar\omega_q}$$

where $E(\mathbf{k}_1)$ and $E(\mathbf{k}_1-\mathbf{q})$ are the energies of electron in the state $\mathbf{k}_1$ and $\mathbf{k}_1-\mathbf{q}$ respectively. $M_{\mathbf{k}_1,\mathbf{k}_1-\mathbf{q}}$ is the matrix element of the interaction potential $V(\mathbf{r}_1)$ between the first electron and the phonon and $M_{\mathbf{k}_2,\mathbf{k}_2+\mathbf{q}}$ is the matrix element of the interaction potential $V(\mathbf{r}_2)$ between the second electron and the phonon.

It is possible that the other scattering process occurs, as shown in Fig.

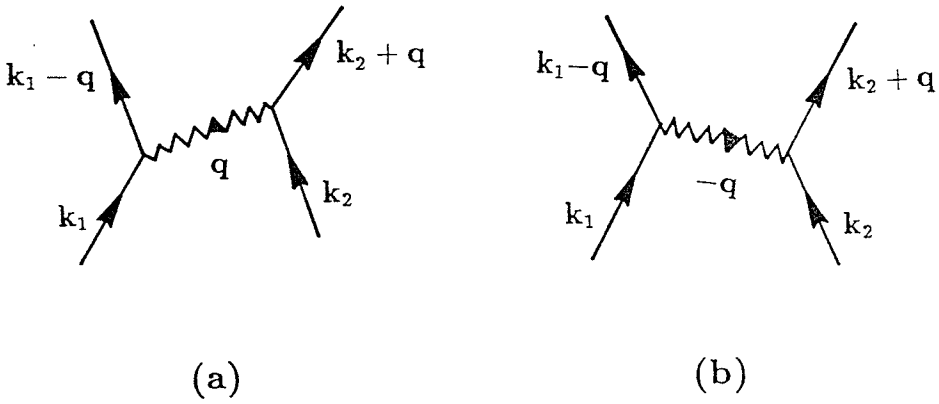

Figure 2.2: The interaction between the electrons and the phonon.

2.2(b). The first electron absorbs a phonon with wave vector $-\mathbf{q}$ and is scattered from state $\mathbf{k}_1$ to $\mathbf{k}_1-\mathbf{q}$. This phonon is emitted from the second electron which is scattered from state $\mathbf{k}_2$ to $\mathbf{k}_2+\mathbf{q}$. The contribution of this process to the energy is

$$< \mathbf{k}_1 - \mathbf{q}, \mathbf{k}_2 + \mathbf{q}|V_2|\mathbf{k}_1, \mathbf{k}_2 >= \frac{M^{*}_{\mathbf{k}_1,\mathbf{k}_1-\mathbf{q}} \cdot M_{\mathbf{k}_2,\mathbf{k}_2+\mathbf{q}}}{E(\mathbf{k}_2) - E(\mathbf{k}_2 + \mathbf{q}) - \hbar\omega_{-q}}$$

Since energy conservation requires that

$$E(\mathbf{k}_1) - E(\mathbf{k}_1 - \mathbf{q}) = E(\mathbf{k}_2 + \mathbf{q}) - E(\mathbf{k}_2)$$

and on assuming that

$$M_{\mathbf{k}_1,\mathbf{k}_1-\mathbf{q}} = M_{\mathbf{k}_2,\mathbf{k}_2+\mathbf{q}}.$$

the total contribution of these two processes to the energy is

$$< \mathbf{k}_1 - \mathbf{q}, \mathbf{k}_2 + \mathbf{q}|V_1 + V_2|\mathbf{k}_1, \mathbf{k}_2 >= \frac{|M_{\mathbf{k}_1,\mathbf{k}_1-\mathbf{q}}|^2 2\hbar\omega_q}{[E(\mathbf{k}_1) - E(\mathbf{k}_1 - \mathbf{q})]^2 - (\hbar\omega_q)^2} \qquad (2.1)$$

When $|E(\mathbf{k}_1) - E(\mathbf{k}_1 - \mathbf{q})| < \hbar\omega_q$, this energy is *negative* and corresponds to an attractive force. This means that only the electrons within the $\pm\hbar\omega_q$ band measured at the Fermi surface have this indirect attraction, since the states in the Fermi sea far from the Fermi surface are all fully occupied by the electrons which can not interact with the other electrons in the neighboring energy levels by absorbing or emitting a phonon.

2.1.2 Cooper Pairs

The ground state of a free electron gas is represented by a sea of the electrons which fill the Fermi sphere. The above section showed that the attraction between two electrons can be transmitted by a (virtual) phonon. Cooper[22] indicated that in the presence of an attractive interaction, no matter how weak, the Fermi sea becomes energetically unstable (a lower energy state, with Cooper pairs, exists).

Consider that two electrons are added to a metal at absolute zero so that they are forced by the Pauli principle to occupy states $\mathbf{k}_1$ and $\mathbf{k}_2$, respectively, where $|\mathbf{k}_1|, |\mathbf{k}_2| > k_F$. The positions of the two electrons in the space are at $\mathbf{r}_1$ and $\mathbf{r}_2$, respectively. The wave function of these two electrons taken to be a plane wave is

$$\begin{aligned} \varphi(\mathbf{r}_1, \mathbf{r}_2) &= \frac{1}{V_c} e^{i(\mathbf{k}_1 \cdot \mathbf{r}_1 + \mathbf{k}_2 \cdot \mathbf{r}_2)} \\ &= \frac{1}{V_c} e^{i\mathbf{K} \cdot (\frac{\mathbf{r}_1 + \mathbf{r}_2}{2})} e^{i\mathbf{k} \cdot (\mathbf{r}_1 - \mathbf{r}_2)} \end{aligned}$$

where V_c is the volume of the crystal within which the wave function was normalized, $\mathbf{K}=\mathbf{k}_1+\mathbf{k}_2$ is the wave vector of the mass center, $(\mathbf{r}_1 + \mathbf{r}_2)/2$, of the two electrons, and $\mathbf{k}=(\mathbf{k}_1+\mathbf{k}_2)/2$ is the wave vector for the relative motion of the two electrons. In the mass center coordinate system, the wave function of these two electrons becomes:

$$\varphi(\mathbf{r}_1, \mathbf{r}_2) = \frac{1}{V_c} e^{i\mathbf{k} \cdot (\mathbf{r}_1 - \mathbf{r}_2)}$$

If the two electrons interact, then the wave function should have the form

$$\Psi(\mathbf{r}_1, \mathbf{r}_2) = \sum_{\mathbf{k}} g(\mathbf{k}) \varphi_{\mathbf{k}}(\mathbf{r}_1, \mathbf{r}_2)$$

or

$$\Psi(\mathbf{r}_1, \mathbf{r}_2) = \frac{1}{V_c} \sum_{\mathbf{k}} g(\mathbf{k}) e^{i\mathbf{k}\cdot(\mathbf{r}_1 - \mathbf{r}_2)} \tag{2.2}$$

where $g(\mathbf{k})$ is the probability amplitude for finding the electrons in the state $(\mathbf{k}_1,\mathbf{k}_2)$ and $g(\mathbf{k})$=0 for $|\mathbf{k}_1|, |\mathbf{k}_2| < k_F$.

Substitution of $\Psi(\mathbf{r}_1, \mathbf{r}_2)$ into the Schrödinger equation yields

$$-\frac{\hbar^2}{2m}(\nabla_1^2 + \nabla_2^2)\Psi(\mathbf{r}_1, \mathbf{r}_2) + V(\mathbf{r}_1, \mathbf{r}_2)\Psi(\mathbf{r}_1, \mathbf{r}_2) = E\Psi(\mathbf{r}_1, \mathbf{r}_2)$$

or

$$\frac{1}{V_c} \sum_{\mathbf{k}} \frac{\hbar^2 k^2}{m} g(\mathbf{k}) e^{i\mathbf{k}\cdot(\mathbf{r}_1 - \mathbf{r}_2)} + \frac{1}{V_c} V(\mathbf{r}_1, \mathbf{r}_2) \sum_{\mathbf{k}} g(\mathbf{k}) e^{i\mathbf{k}\cdot(\mathbf{r}_1 - \mathbf{r}_2)} = \frac{E}{V_c} \sum_{\mathbf{k}} g(\mathbf{k}) e^{i\mathbf{k}\cdot(\mathbf{r}_1 - \mathbf{r}_2)}$$

We can also change $\mathbf{k}$ to $\mathbf{k}'$ and $(\mathbf{r}_1 - \mathbf{r}_2)$ to $\mathbf{r}$ and rewrite the equation as

$$\frac{1}{V_c} \sum_{\mathbf{k}'} \frac{\hbar^2 k'^2}{m} g(\mathbf{k}') e^{i\mathbf{k}'\cdot\mathbf{r}} + \frac{1}{V_c} V(\mathbf{r}_1, \mathbf{r}_2) \sum_{\mathbf{k}'} g(\mathbf{k}') e^{i\mathbf{k}'\cdot\mathbf{r}} = \frac{E}{V_c} \sum_{\mathbf{k}'} g(\mathbf{k}') e^{i\mathbf{k}'\cdot\mathbf{r}}$$

Now multiply by $e^{-i\mathbf{k}\cdot\mathbf{r}}$ on the left of both sides equation and integrate over $\mathbf{dr}$; then

$$\frac{\hbar^2 k^2}{m} g(\mathbf{k}) + \sum_{\mathbf{k}'} g(\mathbf{k}') V_{\mathbf{k},\mathbf{k}'} = E g(\mathbf{k})$$

and

$$\left(E - \frac{\hbar^2 k^2}{m} \right) g(\mathbf{k}) = \sum_{\mathbf{k}'} g(\mathbf{k}') V_{\mathbf{k},\mathbf{k}'} \tag{2.3}$$

where

$$V_{\mathbf{k},\mathbf{k}'} = \frac{1}{V_c} \int V(\mathbf{r}) e^{i(\mathbf{k}'-\mathbf{k})\cdot\mathbf{r}} d\mathbf{r} \tag{2.4}$$

Here E is the eigenvalue of the energy of the interaction two-electron system and $\hbar^2 k^2/2m$ is the energy of the unperturbed plane wave, denoted by $\varepsilon(\mathbf{k})$. $V_{\mathbf{k},\mathbf{k}'}$ describes the scattering of a pair of electrons from the state $\mathbf{k}'(=(\mathbf{k}_1'-\mathbf{k}_2')/2)$ to the state $\mathbf{k}(=(\mathbf{k}_1-\mathbf{k}_2)/2)$ with the same total energy via the interaction potential $V(\mathbf{r})$ (this will be related to electon–phonon coupling).

Cooper assumed that the interaction between the two electrons is attractive and constant in an energy band $\hbar\omega_D$ above Fermi level

$$V_{\mathbf{k},\mathbf{k}'} = \begin{cases} -V_0 & E_F \le \varepsilon(\mathbf{k}) \text{ and } \varepsilon(\mathbf{k}') \le (E_F + \hbar\omega_D) \\ 0 & \varepsilon(\mathbf{k}) \text{ and } \varepsilon(\mathbf{k}') > E_F + \hbar\omega_D \end{cases} \tag{2.5}$$

where ω_D is the Debye frequency, V_0 is a positive and denotes the magnitude of the interaction between the two electrons. Let $\varepsilon(\mathbf{k}) = \hbar^2 k^2/2m$ be the energy of a single electron. Then

$$[E - 2\varepsilon(\mathbf{k})]g(\mathbf{k}) \;=\; -V_0 {\sum_{\mathbf{k}'}}' g(\mathbf{k}')$$

or

$$g(\mathbf{k}) \;=\; \frac{V_0 {\sum_{\mathbf{k}'}}' g(\mathbf{k}')}{2\varepsilon(\mathbf{k}) - E}$$

where $\sum'$ designates a sum restricted by equation (2.5).

On summing both sides over $\mathbf{k}$ and cancelling $\sum_{\mathbf{k}} g(\mathbf{k})$, we obtain

$$1 \;=\; \sum_{\mathbf{k}}{}' \frac{V_0}{2\varepsilon(\mathbf{k}) - E}$$

or

$$\frac{1}{V_0} \;=\; \sum_{\mathbf{k}}{}' \frac{1}{2\varepsilon(\mathbf{k}) - E} \tag{2.6}$$

Let us introduce the density of states per spin orientation,

$$N(\varepsilon)d\varepsilon = \frac{V_c}{8\pi^3} 4\pi k^2 dk$$

and replace the summation in equation (2.6) by an integration. Since $\hbar\omega_D << E_F$

we have $N(\varepsilon) \simeq N(E_F)$; then

$$\begin{aligned} \frac{1}{V_0} &= \int_{E_F}^{E_F+\hbar\omega_D} \frac{N(\varepsilon)d\varepsilon}{2\varepsilon(\mathbf{k}) - E} \\ &\simeq \frac{N(E_F)}{2} \ln\left(1 + \frac{2\hbar\omega_D}{2E_F - E}\right) \end{aligned}$$

or

$$\frac{2}{N(E_F)V_0} = \ln\left(1 + \frac{2\hbar\omega_D}{2E_F - E}\right)$$

and

$$e^{\frac{2}{N(E_F)V_0}} = 1 + \frac{2\hbar\omega_D}{2E_F - E}$$

In the limit of weak interaction $N(E_F)V_0 << 1$, and we can neglect 1 on the right side of the equation. Then

$$E = 2E_F - 2\hbar\omega_D e^{-\frac{2}{N(E_F)V_0}} \tag{2.7}$$

Thus there is a bound state with a *negative* energy relative to the Fermi surface made up entirely of electrons with $|\mathbf{k}| > k_F$, that is, with kinetic energies in excess of E_F. The contribution to the energy by the attractive potential outweighs this excess kinetic energy leading to binding regardless of how small V_0 is. Therefore the normal state in the Fermi sea of single electrons is unstable for the formation of at least one Cooper pair, since any perturbation that moves two

electrons above E_F, where scattering is possible, will lower the system energy.

2.1.3 The Superconducting Ground State

The above section showed that when two extra electrons are added to a metal at absolute zero they will form a bound state, a Cooper pair, that has a lower energy than the Fermi level. Of course, the original full sea could have contained (N−2) electrons and the pair could be formed out of the last two electrons to complete the N-particle sea. What will be happened when a system has many Cooper pairs?

Assume that the probability of finding a Cooper pair in the state $\Psi_{1\mathbf{k}}(\mathbf{k}\uparrow, -\mathbf{k}\downarrow)$ (occupied state) is $v_{\mathbf{k}}^2$ and that the probability of this pair state being empty (empty state) is $u_{\mathbf{k}}^2$, denoted as $\Psi_{2\mathbf{k}}(\mathbf{k}\uparrow, -\mathbf{k}\downarrow)$. The superconducting ground state Ψ can be described by a linear combination of $\Psi_{1\mathbf{k}}$ and $\Psi_{2\mathbf{k}}$, viz;

$$\Psi = u_{\mathbf{k}}\Psi_{2\mathbf{k}} + v_{\mathbf{k}}\Psi_{1\mathbf{k}} \tag{2.8}$$

The $u_{\mathbf{k}}$ and $v_{\mathbf{k}}$ must satisfy the normalization condition

$$u_{\mathbf{k}}^2 + v_{\mathbf{k}}^2 = 1. \tag{2.9}$$

We now calculate the energy of the ground state. Since the probability of

the Cooper pair appeared is $v_{\mathbf{k}}^2$ and its kinetic energy is

$$2\varepsilon(\mathbf{k}) = 2\left(\frac{\hbar^2 k^2}{2m}\right),$$

the total kinetic energy of all Cooper pairs is

$$W_{kin} = \sum_{\mathbf{k}} 2\varepsilon(\mathbf{k}) v_{\mathbf{k}}^2$$

The interaction between the Cooper pairs is important. When the occupied state of a Cooper pair $(\mathbf{k}\uparrow, -\mathbf{k}\downarrow)$ is scattered into an empty state $(\mathbf{k}' \uparrow, -\mathbf{k}' \downarrow)$ by exchanging a phonon, the initial Cooper pair $(\mathbf{k}\uparrow,-\mathbf{k}\downarrow)$ became an empty state while the $(\mathbf{k}' \uparrow, -\mathbf{k}' \downarrow)$ state became the occupied state. The contribution of this process to the interaction energy using Cooper's simplication (2.5) is

$$\varepsilon_{int} = -V_0 u_{\mathbf{k}} u_{\mathbf{k}'} v_{\mathbf{k}} v_{\mathbf{k}'}$$

Since the initial state is $v_{\mathbf{k}} u_{\mathbf{k}'}$ and the final state $v_{\mathbf{k}'} u_{\mathbf{k}}$, the energy is lowered by V_0 after this scattering. The total interaction energy of the system is

$$W_{int} = -\sum_{\mathbf{k}} \sum_{\mathbf{k}'} V_0 u_{\mathbf{k}} v_{\mathbf{k}} u_{\mathbf{k}'} v_{\mathbf{k}'}$$

The total energy of the ground state at T=0 is then

$$W_0 \;=\; W_{kin} + W_{int}$$

$$= 2\sum_{\mathbf{k}} \varepsilon(\mathbf{k}) v_k^2 - V_0 \sum_{\mathbf{k}} \sum_{\mathbf{k}'} u_{\mathbf{k}} v_{\mathbf{k}} u_{\mathbf{k}'} v_{\mathbf{k}'} \tag{2.10}$$

Now consider $v_{\mathbf{k}}$ as a variation parameter. From the minimizing condition $\partial W_0/\partial v_{\mathbf{k}}=0$, the $v_{\mathbf{k}}$ and W_0 are obtained as follows

$$u_{\mathbf{k}} = \sqrt{1 - v_{\mathbf{k}}^2},$$

so that

$$\frac{\partial u_{\mathbf{k}}}{\partial v_{\mathbf{k}}} = \frac{-v_{\mathbf{k}}}{\sqrt{1 - v_{\mathbf{k}}^2}}.$$

Hence

$$\frac{\partial W_0}{\partial v_{\mathbf{k}''}} = 4\varepsilon(\mathbf{k}'') v_{\mathbf{k}''} - V_0 \sum_{\mathbf{k}'} u_{\mathbf{k}'} v_{\mathbf{k}'} \frac{\partial (u_{\mathbf{k}''} v_{\mathbf{k}''})}{\partial v_{\mathbf{k}''}} - V_0 \sum_{\mathbf{k}} u_{\mathbf{k}} v_{\mathbf{k}} \frac{\partial (u_{\mathbf{k}''} v_{\mathbf{k}''})}{\partial v_{\mathbf{k}''}}$$

and

$$\frac{\partial W_0}{\partial v_{\mathbf{k}''}} = 4\varepsilon(\mathbf{k}'') v_{\mathbf{k}''} - 2V_0 \left(\sum_{\mathbf{k}} u_{\mathbf{k}} v_{\mathbf{k}} \right) \frac{1 - 2v_{\mathbf{k}''}^2}{\sqrt{1 - v_{\mathbf{k}''}^2}}. \tag{2.11}$$

Let

$$\Delta_0 = V_0 \sum_{\mathbf{k}} u_{\mathbf{k}} v_{\mathbf{k}} \tag{2.12}$$

where Δ_0 refers to the energy-gap parameter at T=0. From $\partial W_0/\partial v_{\mathbf{k}} = 0$, equation (2.11) becomes

$$2\varepsilon(\mathbf{k})v_{\mathbf{k}}\sqrt{1-v_{\mathbf{k}}^2} = \Delta_0(1-2v_{\mathbf{k}}^2) \tag{2.13}$$

From(2.13) we can obtain

$$v_{\mathbf{k}}^2 = \frac{1}{2}\left(1-\frac{\varepsilon(\mathbf{k})}{\sqrt{\varepsilon^2(\mathbf{k})+\Delta_0^2}}\right) \tag{2.14}$$

$$u_{\mathbf{k}}^2 = \frac{1}{2}\left(1+\frac{\varepsilon(\mathbf{k})}{\sqrt{\varepsilon^2(\mathbf{k})+\Delta_0^2}}\right) \tag{2.15}$$

so that

$$u_{\mathbf{k}}^2 v_{\mathbf{k}}^2 = \frac{1}{4}\left(\frac{\Delta_0^2}{\varepsilon^2(\mathbf{k})+\Delta_0^2}\right)$$

In order to ensure that the energy gap parameter $\Delta_0 = V_0 \sum_{\mathbf{k}} u_{\mathbf{k}} v_{\mathbf{k}}$ is positive, take

$$u_{\mathbf{k}} v_{\mathbf{k}} = \frac{1}{2}\frac{\Delta_0}{\sqrt{\varepsilon^2(\mathbf{k})+\Delta_0^2}}$$

On substituting $u_{\mathbf{k}}v_{\mathbf{k}}$ into Δ_0,

$$1 = \frac{V_0}{2}\sum_{\mathbf{k}}\frac{1}{\sqrt{\varepsilon^2(\mathbf{k})+\Delta_0^2}} \tag{2.16}$$

When the number of states within dε intervel is N(E_F)dε, the summation in (2.16) can be replaced by the integral

$$1 = \frac{V_0}{2}\int_{-\hbar\omega_D}^{\hbar\omega_D}\frac{N(E_F)d\varepsilon(\mathbf{k})}{\sqrt{\varepsilon^2(\mathbf{k})+\Delta_0^2}} \tag{2.17}$$

$$1 = N(E_F)V_0\text{arcsh}\left(\frac{\hbar\omega_D}{\Delta_0}\right) \tag{2.18}$$

In the weak interaction limit, $N(E_F)V_0 << 1$, (2.18) can be reduced and the energy gap parameter can be obtained as

$$\Delta_0 \;=\; 2\hbar\omega_D e^{-\frac{1}{N(E_F)V_0}} \tag{2.19}$$

Then, by substituting (2.12) and (2.14) into (2.10) yields the total energy of the superconducting ground state at T=0 as

$$W_0 \;=\; \sum_{\mathbf{k}}\varepsilon(\mathbf{k})\left(1-\frac{\varepsilon(\mathbf{k})}{\sqrt{\varepsilon^2(\mathbf{k})+\Delta_0^2}}\right)-\frac{\Delta_0^2}{V_0} \tag{2.20}$$

Obviously the energy of the superconducting ground state, W_0, is lower than that of the normal state system in which the electrons are independent. Therefore the transition from the normal state to superconducting state will certainly occur.

2.1.4 Some Properties Predicted by the BCS Theory

I. The critical temperature

When $T > 0$, BCS theory indicates that the energy gap Δ is a function of T; the equation for Δ(T) is [23]

$$1 = \frac{V_0}{2}\int_{-\hbar\omega_D}^{\hbar\omega_D} \tanh\left(\frac{\sqrt{\varepsilon^2+\Delta^2(T)}}{2k_BT_c}\right)\frac{N(E_F)}{\sqrt{\varepsilon^2+\Delta^2(T)}}d\varepsilon \tag{2.21}$$

The critical temperature is the temperature at which $\Delta(T) \rightarrow 0$. In this case equation (2.21) becomes

$$\begin{aligned} 1 &= \frac{V_0}{2}\int_{-\hbar\omega_D}^{\hbar\omega_D} \tanh\left(\frac{\varepsilon}{2k_BT_c}\right)\frac{N(E_F)}{\varepsilon}d\varepsilon \\ &= N(E_F)V_0\int_0^{\hbar\omega_D} \tanh\left(\frac{\varepsilon}{2k_BT_c}\right)\frac{d\varepsilon}{\varepsilon} \\ &\simeq N(E_F)V_0\left[\ln\left(\frac{\hbar\omega_D}{k_BT_c}\right) - \int_0^{\infty} dx\ln(x)\frac{d}{dx}(\tanh x/2)\right] \end{aligned}$$

Since $k_BT_c << \hbar\omega_D$, which corresponds to a weak electon-phonon-electron coupling defined by N$(E_F)V_0 << 1$, and the intergal coverges rapidly, we can replace the upper limit by infinity. The integral is a number which can be evaluated in terms of Euler's constant γ, as $-\ln(\frac{2\gamma}{\pi})$. The ratio $2\gamma/\pi$ is 1.13. Thus we have

$$1 = N(E_F)V_0\ln\left(\frac{2\gamma}{\pi}\frac{\hbar\omega_D}{k_BT_c}\right)$$

or

$$k_B T_c = 1.13\hbar\omega_D e^{-\frac{1}{N(E_F)V_0}} \tag{2.22}$$

This result suggests that the critical temperature of a superconductor depends on three factors: the Debye frequecy of the lattice vibration, ω_D, the density of states of the electrons at the Fermi surface $N(E_F)$, and the interaction constant between the electron and phonon, V_0. The material will show superconducting behavior only if the net interaction between the electrons resulting from the combination of the phonon-induced and Coulomb interaction is attractive. This is why normal good conductors like silver and copper, which have a weak electron-phonon interaction, do not exhibit superconductivity at the lowest temperature achieved to date. However some materials that are poor conductors at normal temperature, but which have a strong electron-phonon interaction, are superconductors. Indeed, the poorer the conductivity at normal temperatures the higher the critical temperature at low temperatures. This supports the viewpoint that the electron-phonon interaction that causes resistivity at normal temperatures gives rise to superconductivity at the low temperatures.

II. Isotope effect

The Debye frequency ω_D is inversely proportional to the square root of the isotope mass M. Therefore from (2.22) one obtains

$$T_c \propto M^{-\frac{1}{2}} \tag{2.23}$$

This explains the origin of the isotope effect.

III. Energy gap

By comparing equation (2.19) and (2.22) we find that the energy gap at T=0

$$E_g = 2\Delta_0 = 3.5 k_B T_c \tag{2.24}$$

where k_B is Boltzmann's constant. Equation (2.24) predicts that the critical temperature is simply related to the energy gap at T=0. The experimental values of most conventional superconducting materials are close to this value, but the deviations for some materials are outside the experimental error, this can be attribute to simplifications made in the theory.

IV. Flux Quantization

The motion of the mass center of the Cooper pairs can be described by a plane wave

$$\Psi(\mathbf{r}, t) = u e^{i(\mathbf{k}.\mathbf{r} - \omega t)} \tag{2.25}$$

If the supercurrent is assumed to be along the x axis, then

$$\Psi(x, t) = u e^{i(\frac{2\pi x}{\lambda} - \omega t)} \tag{2.26}$$

where $\lambda = 2\pi/k$. Along the x axis the phase difference between the wave function at points a and b is

$$\varphi_b - \varphi_a = 2\pi \int_a^b \frac{dx}{\lambda} \tag{2.27}$$

where $\lambda = \frac{h}{2mv_s} = \frac{hn_se}{2mj_s}$, and j_s is the supercurrent density, $j_s = n_s e v_s$. Here n_s is the density of superelectrons so that the density of Cooper pairs is $\frac{1}{2}n_s$. Therefore

$$\varphi_b - \varphi_a = \frac{2m}{\hbar n_s e} \int_a^b j_s dx$$

Now when a magnetic field is applied the momentum of the Cooper pair is

$$\mathbf{P} = 2m\mathbf{v}_s + 2e\mathbf{A}$$

where $\mathbf{A}$ is the magnetic vector potential with $\nabla \times \mathbf{A} = \mathbf{B}$ and $\lambda = h/|\mathbf{P}|$. Hence

$$\varphi_b - \varphi_a = \frac{2m}{\hbar n_s e} \int_a^b \mathbf{j}_s \cdot d\mathbf{l} + \frac{2e}{\hbar} \int_a^b \mathbf{A} \cdot d\mathbf{l}$$

Suppose a superconductor encloses a non-superconducting region N in which there is a flux density $\mathbf{B}$ due to the supercurrent $\mathbf{j}_s$ along the boundary of N. Such a situation might arise when N is a hole through the material or, in the case of a solid piece of superconductor where the magnetic field generated by the encircling current maintains the region N in the normal state. Around a closed path, such as the dotted curve in Fig. 2.3, which encircles the normal region, the total phase

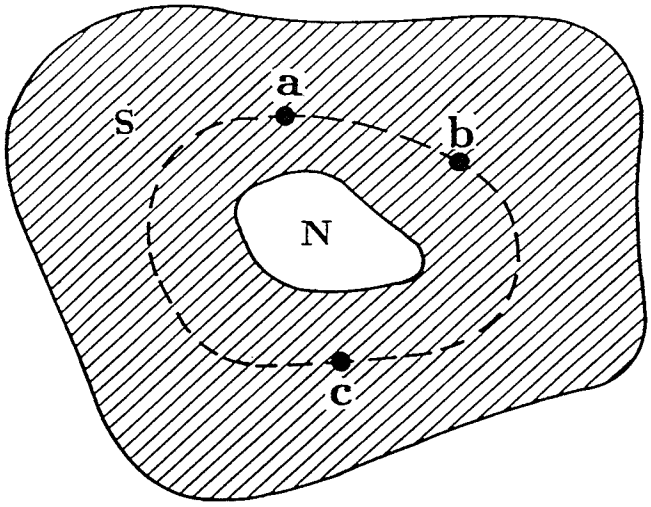

Figure 2.3: A normal region N in the superconductor.

difference will be

$$\Delta\varphi = \frac{2m}{\hbar n_s e}\oint \mathbf{j}_s \cdot d\mathbf{l} + \frac{2e}{\hbar}\oint \mathbf{A}\cdot d\mathbf{l}. \tag{2.28}$$

Now by Stoke's theorem

$$\oint \mathbf{A} d\mathbf{l} = \int\int \nabla \times \mathbf{A}\cdot d\mathbf{S}$$

where $d\mathbf{S}$ is an element of area. Then

$$\frac{m}{n_s e^2}\oint \mathbf{j}_s \cdot d\mathbf{l} + \int\int \mathbf{B}\cdot d\mathbf{S} = \frac{\hbar}{2e}\Delta\varphi \tag{2.29}$$

F. London and H. London named the quantity on the left hand side of the equation

the *fluxoid* and gave it the symbol Φ',

$$\Phi' = \frac{m}{n_s e^2} \oint \mathbf{j}_s d\mathbf{l} + \int\int \mathbf{B} \cdot d\mathbf{S} \tag{2.30}$$

where Φ' is called London fluxoid. Because of the single-valuedness of the wave, the phase difference, $\Delta\varphi$, can only take integer multiples of 2π, that is, $\Delta\varphi = n \cdot 2\pi$, where n is an integer. Therefore

$$\frac{m}{n_s e^2} \oint \mathbf{j}_s d\mathbf{l} + \int\int \mathbf{B} \cdot d\mathbf{S} = n\frac{h}{2e} = n\Phi_0 \tag{2.31}$$

The fluxoid within a closed curve is closely related to the magnetic flux within the curve. The first term on the left hand side of the equation contains the line integral of the current density around the closed curve, but because the penetration depth is very small, nearly all the circulating current will in fact be concentrated very close to the boundary of the normal region N. This term can be neglected. The second term on the left side is just the magnetic flux contained within N and the penetration depth around it where

$$\Phi_0 = \frac{h}{2e} = 2.07 \times 10^{-15} \text{Weber},$$

Φ_0 is called a *fluxon*. We see that any flux within a superconductor should only exist as multiples of a quantum, the fluxon Φ_0. The factor 2 in the denominator is a strong suggestion that the supercurrent is carried by pairs of the electrons.

In 1961 B. S. Deaver and W. M. Fairbank [24], Doll and Näbauer [25] had experimentally observed flux quantization and confirmed that fluxon $\Phi_0 =$

$h/2e$. For the new high-T_c superconductor, $YBa_2Cu_3O_{7-\delta}$, $Bi_{2.2}Sr_2CaCu_2O_x$, and $Tl_2Ba_2CaCu_2O_x$, the flux quantization has also been observed and the value, $\Phi_0 = h/2e$, is also confirmed by the experiments [26,27].

2.2 The Theory of the New High-T_c Superconductors

It is well known that the transition temperature of mercury, the superconductor discovered first, was 4.2 K. About 75 years later, prior to 1985, the highest transition temperature observed among the thousands of alloys prepared was only 23.3 K in Nb_3Ge. The discoveries of superconductivity in $La_{2-x}Ba_xCuO_4$ with a transition temperature, T_c, above 30 K [1], in $YBa_2Cu_3O_{7-\delta}$ above 90 K [2], and in $Tl_2Ca_2Ba_2Cu_3O_{10+\delta}$ above 120 K [5], have come as a shock to most physicists. These cuprate ceramics superconduct at temperatures many times higher than in any other materials, as confirmed by many groups and laboratories in the world. A huge amount of work has been done studying the electric, magnetic,thermal, structural and optical properties. In response, a flood of theories has come forth, which range from modifying the BCS theory to totally new ones. To develop a new theory, it is necessary to ask why the new materials have a such high T_c? Is the electron-phonon interaction still responsible for the superconductivity and do Cooper pairs still exist in the new materials?

In conventional superconductors the Cooper pairs were confirmed by the beautiful magnetic flux quantization experiments of Deaver and Fairbank and Doll and Näbauer in 1961[24,25]. In these experiments it was shown that the magnetic

flux trapped in a hollow superconducting cylinder was an integral multiple of a fundamental unit of flux, $(h/2e)$. Here h is Planck's constant, and e is the charge of the electron. The presence of the factor 2 in the denominator implies that the carriers are pairs of electrons.

For the new high-T_c materials similar experiments have been done by Gough et al[26]. The value of the flux trapped in a superconducting ring of $YBa_2Cu_3O_{7-\delta}$ was measured and the value of the flux quantum is 0.97 ± 0.04 $(h/2e)$.

Experiments based on the Josephson effect between $YBa_2Cu_3O_{7-\delta}$ and an alloy of Pb and Sn also give the flux quantum value of $(h/2e)$[28]. The factor 2, again suggests that the charge carriers in $YBa_2Cu_3O_{7-\delta}$ are indeed electron pairs. Hence Cooper pairs are still present in the new high-T_c superconductors.

If the isotope effect still exists in $YBa_2Cu_3O_{7-\delta}$, then substituting isotope O^{18} for O^{16} in the superconductor with T_c of 90 K should shift T_c by at about 5 K, assuming an ideal value of 1/2 for α (in $T_c \propto M^{-\alpha}$) and that the all phonon modes relevant for superconductivity involve vibrations of oxygen atoms only. But the experimental results [18] show that the changes of T_c after O^{18} replaces O^{16} range from 0.0 to 0.5 K corresponding to a value of α ranging from 0.0 to 0.02 which is much smaller than $\alpha = 0.5$. This means that there is a very small or null oxygen isotope effect in $YBa_2Cu_3O_{7-\delta}$. Similar experiments have been done by substituting Cu^{65} for Cu^{63} in $YBa_2Cu_3O_{7-\delta}$ [19]. It is found that the transition temperature is the same within experimental error of ± 0.2 K for the samples before and after substitution. This indicates the isotope effect of copper is also absent in $YBa_2Cu_3O_{7-\delta}$.

The absence of an isotope effect for oxygen and copper gives rise to different points of view about the interaction responsible for high-T_c superconductivity. One extreme point of view considers that the electron-phonon interaction is no longer responsible for the superconductivity in the new materials; the other extreme point of view suggests that the absence of an isotope effect for oxygen and copper by itself does not completely rule out the phonon mechanism, because in many transition metal superconductors – molybdenum, zirconium, and ruthenium, for example – isotopic substitution leads to no observable change in T_c, even though few doubt that pairing in these superconductors is mediated by phonons. The other argument is that the unit cell in high T_c materials is quite large and the lattice may have many phonon modes that do not involve significant motion of oxygen and copper atoms. If these modes were important for pairing, one would of course not see any isotope effect if only a heavier isotope of oxygen or copper is substituted in a sample.

On the other hand, an alternative view to the traditional electron-phonon theory considers the Cu-O bond vibration modes to be central. The absence of an isotope effect in high-T_c materials then indicates that the BCS theory has to be modified; a reduced isotope effect is characteristic of a small electron-phonon interaction. It follows that the electron-phonon interaction by itself is not sufficient to produce high-T_c and some other kinds of interaction are responsible for the electron pairs.

Based on the above experimental data there are mainly two extreme points of view concerning the theory of high-T_c materials. According to one of them,

the mechanism is totally different from the BCS model. The Resonating-Valence-Bond model (RVB) suggested by P. W. Anderson [29] and similar models suppose that the origin of high-T_c superconductivity lies in a spin liquid, which in conventional superconductors is the electric Fermi liquid. In the RVB model, Anderson proposed a singlet ground state in which every spin is paired in a singlet configuration with another one, so that the total spin of the whole lattice is zero. The pairs are not fixed; a spin has a finite probability of paring with any one of its nearest neighbors. The ground-state wavefunction, therefore, is a linear combination of the quantum mechanical states for different configurations of singlet spin pairs on the lattice. If the spin pairs are represented by bonds connecting the corresponding lattice sites, then the configurations may be transformed into one another by moving the bonds[30]. In Anderson's words, using a term from organic chemistry, the bonds defined by spin pairs *resonate* between different configurations. This model is very interesting but up to now has not been confirmed either theoretically or experimentally. For example, a linear temperature dependence of the specific heat is predicted at $T << T_c$ in the models, although several new measurements fail to show the existence of such a linear term in some high-T_c superconductors. Furthermore in the high-temperature superconductor $Ba_{0.6}K_{0.4}BiO_3$, there apparently are no magnetic moments and so no spin liquid can exist [31]. If, as seems reasonable, the origin of superconductivity in this and the cuprates is the same, then they also can not be spin liquids.

The other extreme point of view is that the superconductivity of high-T_c materials is very similar to that in the conventional superconductors. Both

are described by the BCS model. However the source of the high value of T_c appears to be in the exchange of electronic excitations that are not connected with spin effects. The attractive interaction responsible for the electron pairs may be the polarization of an electron subsystem rather than the lattice. Under appropriate circumstances this could lead to superconductivity near room temperature. In a simple picture the Debye energy, $\hbar\omega_D$, in the BCS expression $k_B T_c = 1.13\hbar\omega_D exp(-\frac{1}{N(E_F)V_0})$, is replaced by a much larger electronic energy, $\hbar\omega$, consequently if the coupling constant $\frac{1}{N(E_F)V_0}$ is the same the transition temperature will be raised [32].

This BCS-like model has most aspects of the BCS theory and does not contradict the experimental results. Some experimental data [33], such as $2\Delta_0 = 3.5k_B T_c$, connecting the energy gap at T=0 with T_c, have provided strong evidence for this model. The main difference as compared to conventional BCS superconductors is in the mode of coupling. Evidence suggests that some charge excitation with an energy several times that of the phonons, provides this coupling. However this model remains to be confirmed either theoretically or experimentally.

Chapter 3

The Equipment

Polycrystalline high-T_c superconductors are ceramic materials. To make samples a standard ceramic procedure including weighing chemicals, ball milling, pressing, preheating, regrounding and firing, are used. In this chapter we describe some equipment used to make and characterize the superconductors.

The chemicals used for making the superconductors were weighted by a gram-atic *balance* made by E. Mettler with a maximum weight 200 g and accuracy of 0.0005 g.

A *ball milling machine* consists of a rolling device and a container. The rolling device makes the container move with a three-dimensional rotation. The container is a wide-mouth glass bottle (240ml) made by Fisher Scientific Co. Alumina balls in various diameters from 8 to 15mm were used for milling and mixing.

Three kinds of *furnace*, namely a tube furnace, a box furnace and a single-crystal furnace were used for heat treatment. The dimensions of the tube furnace are 36 cm in length, 32 cm in width and 33 cm in hight. There is a tunnel of

4.8 cm in diameter and 36 cm in length in the centre of the furnace. A Fe-Cr-Al helically-coiled wire was wound on the tunnel as the heating element. A quartz tube of 90 cm in length and 3.0 cm in diameter was put into the tunnel. A small alumina boat containing the samples can easily go in and out of the quartz tube. A chromium-aluminum thermocouple measures the temperature. The maximum temperature available is 1200°C. The constant temperature region is 10 cm in length near the centre; at about 900°C the temperature is within ±1°C. Oxygen gas controlled by a flowmeter can pass through the quartz tube as necessary. The exhaust gas is introduced into water by a flexible tube and is then released to the air as shown in Fig. 3. 1. The tube furnace has a small chamber. It is convenient for heating small amounts of samples and for using various atmospheres.

The box furnace, made by Lindburg, chamber dimension 7.5 × 5.25 × 14 ($W \times H \times D$) inches is used to preheat and heat. The heating elements are a composite of helically-coiled iron, chrome and aluminum alloy wire and moldatherm, Lindburg's unique ceramic-fiber insulation. The heating elements are provided on the top, bottom and sides of the chamber for uniform heat distribution. A platinel II thermocouple with a long life and good stability is located at the top of the chamber center both to measure and to control the temperature. A digital temperature control instrument made by Lindburg can keep the temperature stable within ±1°C. The constant temperature region of this furnace is about 10×15 (W×D) cms near the center of the furnace. An oxygen atmosphere can be introduced into the chamber as required from the front window by a quartz tube which has a funnel outlet. The box furnace has a large chamber. It is suitable for

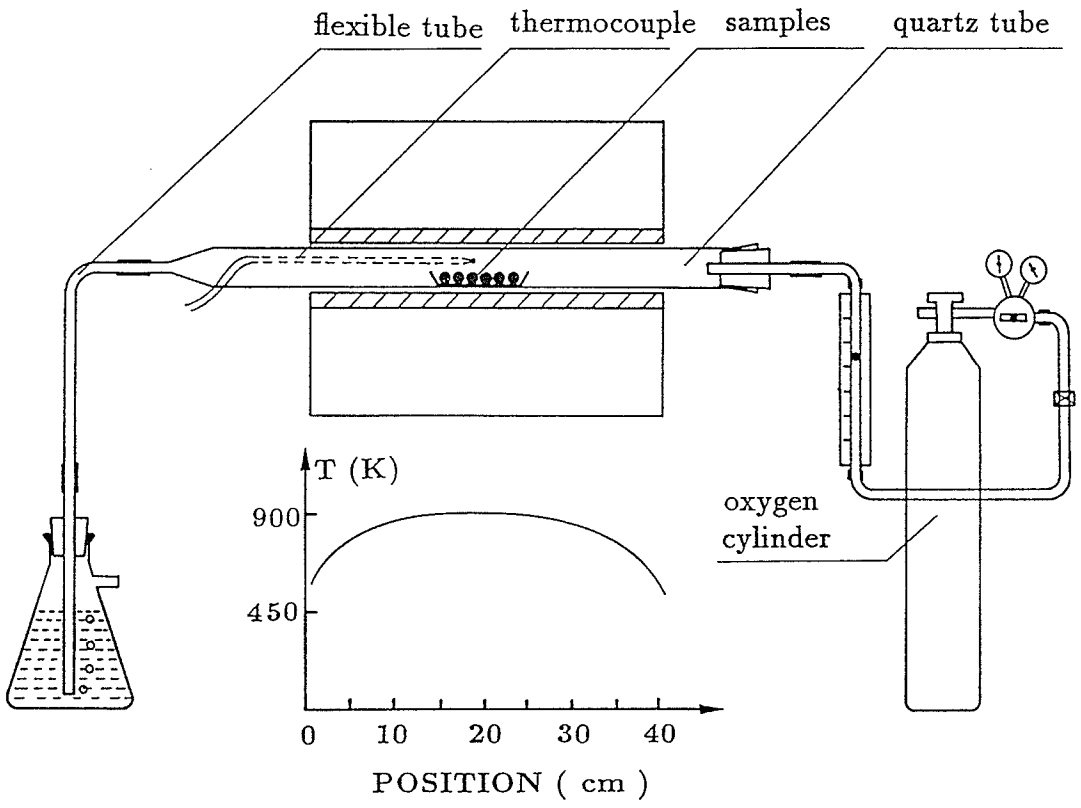

Figure 3.1: A schematic illustration of the tube furnace and its temperature distribution.

larger samples.

The single-crystal furnace and a program controller were made by Leeds and Northrup Canada Ltd. The heating elements consist of 8 globars (SiC). A Pt 10% Rh and Pt thermocouple was employed for measuring and controlling the temperature. The furnace can reach a maximum temperature of 1380°C at a rate of up to 200°C/hr. The rise speed of temperature is controlled by an input current. The drop speed of the temperature can be chosen from 0.1°C per hour to 9°C per hour in the 800°-1200°C range. Oxygen gas can be introduced into the furnace during the crystal growth from the bottom of the furnace via a quartz tube. The exhaust gas directly goes to outside the building passing into a fume hood which is located to the left top of the furnace.

The *ac susceptometer* was made by Dr. I. Maartense. Two symmetric coils with about 4100 turns, with a resistance of 600–700Ω, are 13 mm in inner diameter and 11 mm in thickness; they pass a small ac current and are used as sensor coils. The equipment is adjusted so that both χ' and χ'' equal zero with no sample. When the sample is put into one coil, the induced signal was decomposed into two components: a real component, χ' and an imaginary component, χ''. The details are described in reference [34]. The temperature of the sample can be varied from 55 K by pumping liquid nitrogen up to room temperature by heating the sample holder or by absorbing heat naturally(Fig. 3.2).

The sensor coils and dc magnetic field coils are inserted into a wide-mouth liquid-nitrogen dewar. A two layer glass cylinder with a tail of 10 mm in diameter and 60 mm in length was used as a variable temperature dewar. There is a vacuum

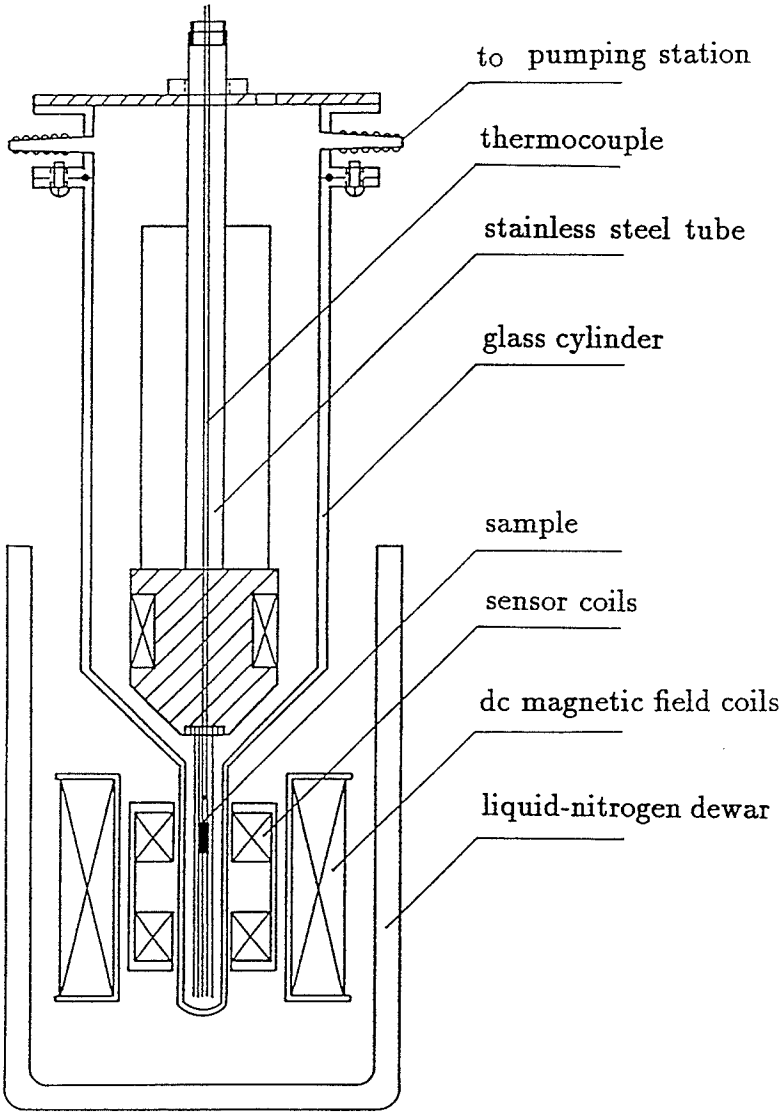

Figure 3.2: A schematic illustration for ac susceptibility measurement.

between the two layers. The sample is located in the middle of the tail by a sample holder. The tail is put into the sensor coil during the measurements. The copper-constantan thermocouple was put near the sample in order to measure the temperature. The leads of the thermocouple and heating wires pass through a central stainless steel tube and are connected to a millivoltmeter and power supply, respectively (Fig. 3.2).

To perform *resistivity* measurements, a simple stainless steel cylinder was designed in which the sample temperature could be varied from 77 K to room temperature. A stainless steel cylinder, 48 mm in diameter, was placed directly into liquid nitrogen contained in a glass dewar. A copper sample holder made contact with the wall of the cylinder by a copper leaves (Fig. 3.3) in order to make the heat exchange fast. Raising and lowering the temperature can be achieved by moving the cylinder down and up, respectively. The four leads used for the four probe technique make contact with the sample at one end; at the other end they pass through a stainless steel tube and connect to a constant current source, 60 mA maximum and a millivoltmeter, 10^{-6} V minimum, respectively. The temperature of the sample was measured with a copper-constantan thermocouple. The sensor point of the thermocouple was fixed in the sample holder and made contact with the sample surface. To reduce the contact resistance between the leads and sample, silver pads were evaporated onto the surface of the sample and indium was used as solder in order to join the leads to the silver pads.

The drive system of the *Mössbauer spectrometer* consists of a MFG-N-5 function generator, a MDF-N-5 driver and a MVT-4 velocity transducer made

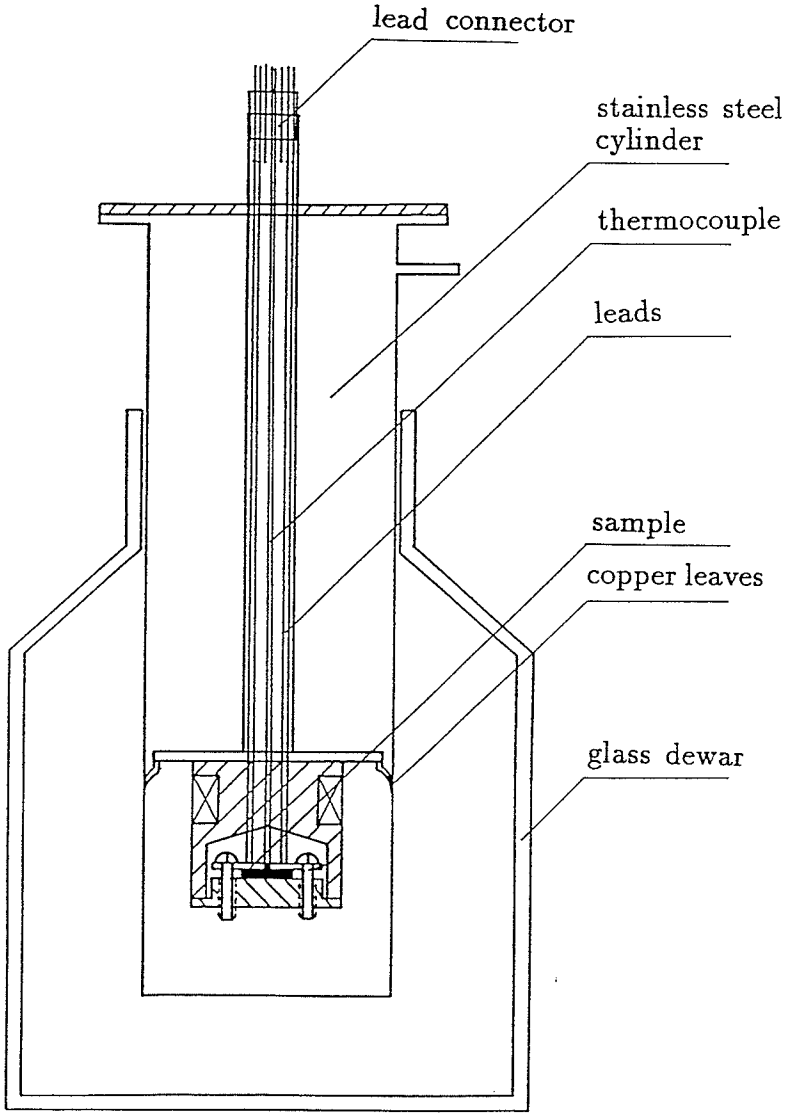

Figure 3.3: A schematic illustration of low temperature dewar for resistivity measurements.

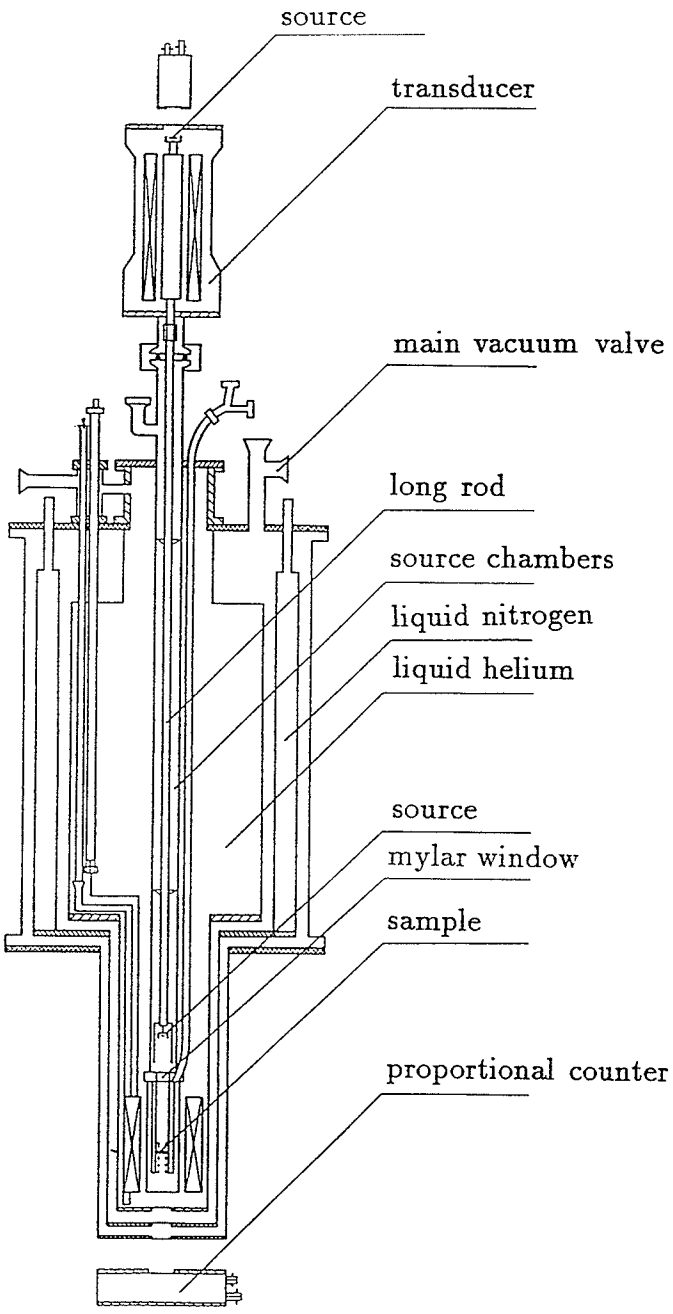

Figure 3.4: Schematic illustration of the cryogenic system made by Oxford.

by Elscint Ltd, which can be operated with a sawtooth, triangular or linearized-sine waveform. The frequency varies from 3 to 22 Hz and the velocity can be adjusted from 0 to $\pm$100 mm/sec for the sawtooth mode and to $\pm$500 mm/sec for the triangular and sine modes. The amplifier (570) and SCA (551) were made by Ortec. A multichannel analyser (CMCA-1000A) was made by Wissel and is controlled by IBM XT personal computer. Two Mössbauer spectrometers can be operated simultaneously. The data collected can be either storied in floppy disks or sent to the Amdahl main-frame computer system for further analysis.

The experiments at low temperatures and in magnetic fields were performed in the Oxford cryogenic system shown in Fig. 3.4. In this system, the sample is placed in the sample holder which can be heated to various temperatures. This holder is sealed into the sample chamber and separated from the source chamber by a mylar window. The temperature of the sample and the source can be controlled separately. The source of ^{57}Co in Rh was driven by the transducer at the top of the system via a long rod. The γ-ray absorption is measured by a proportional counter, which is not affected by the stray magnetic field at the bottom. A weak source, mounted on the other end of the transducer, together with a suitable absorber and a NaI scintillation counter were used for calibration purposes.

Low temperatures can be obtained with liquid nitrogen at 77 K, liquid helium at 4.2 K, and below 4.2 K by pumping on the liquid helium from a exhaust-gas outlet. Temperatures can be continuously varied by a capacitance controller (model CSC 400 made by Lake Shore Cryotronics Inc.). An Au 0.7%Fe

vs. chromel thermocouple measures the source's temperature with 77 K as its reference point. A Rh-Fe thermister measures for the sample's temperature. The temperature of the superconducting coil is monitored by two 270Ω carbon sensors fixed to the top and bottom of the magnet. To get the minimum boiling rate of He at a certain temperature the exchange gas pressure in the sample and source chambers have to be adjusted by the pumping station. Of course, the main vacuum has to be better than 1×10^{-5} torr. Usually the boiling rate is about 160-180 mL per hour (less than 4.5L each day).

The magnetic field is generated by a superconducting coil of NbTi with a maximum of 6 Tesla at 57 Amps. The ratio of magnetic field to the current is about 0.105 T/A. To avoid quenching of the magnetic field some precautions have to be taken, such as keeping the helium level above the superconducting coil (no less than 2 L), keeping the charging rate less than the critical value, and so on.

This system is suitable for measuring one sample at various temperatures or in various magnetic fields. It is not suitable for measuring various samples since a lot of helium is required when the sample is changed.

A PW-1360 Philips X-ray diffractometer is used for structure analysis. Usually Cu Kα radiation with a Ni filter was used. The structure refinement was performed by the computer controlled x-ray diffractometer in the Department of Geological Science. Microstructure and composition of the samples are determined with an ISI-100 B scanning electron microscope (SEM) equiped with EDAX.

Chapter 4

Sample Preparation

4.1 Polycrystalline Samples

The high-T_c superconductors in polycrystalline form are ceramics. These materials are made by a solid-state reaction in which the starting chemicals react with each other at high temperatures but below the melting points. The general ceramic procedure includes weighing the appropriate amount of chemicals, mixing, pelletizing, preheating, regrinding, heating and cooling. The procedure used for a desired ceramic compound is tailored to the properties of the chemicals used and to the specific solid state reaction.

4.1.1 The YBaCuO System

To make samples of the YBaCuO system, the chemicals Y_2O_3 (99.99%, Alfa), CuO (Technical, Fisher), and $BaCO_3$ (A.C.S. Fisher) or BaO (Technical, K and K) were used as starting materials. Appropiate amounts (total weight of about 5 grams) of the chemicals were weighed by a balance described in chapter 3 and thoroughly mixed and ground in a ballmill (with a 240 mL glass container and

about 30 alumina balls, 8 to 15 mm in diameter) using about 40 mL of acetone as the active agent. (Usually a liquid, such as water, alcohol, actone and so on, is used in ball milling to make mixing more efficient and to increase the activity of the chemicals.) Since BaO dissolves in water, we had to choose acetone as the liquid. Powders or pellets of the mixture were preheated at 860 to 900°C for 6 hours and reground. The final pellets were put in an alumina boat, heated in a tube furnace at 900 to 920°C for 6 hours and furnace cooled in flowing oxygen. Since the superconducting properties, especially the transition temperature, of this material is very sensitive to the oxygen content, slow cooling and an oxygen atmosphere is important in order to get superior samples.

In early 1987 the scientific news bulletin anounced that the superconducting transition temperature had been enhanced to above liquid nitrogen temperatures, but there was no details given concerning the materials. In March 1987, after various compositions of $(Y_{1-x}Ba_x)CuO_3$ were tried, we found that when x was in a range 0.4 to 0.8 the samples all had a superconducting transition ($R \rightarrow 0$, when $T<T_c$), but had a different transition width. Some pellets had a black colour with some green or some dark black spots. Only the composition of $Y_{0.4}Ba_{0.6}CuO_3$ (i.e. for x=0.6) was pure black in colour and had the highest transition temperature, 93 K, and a narrow transition width, as shown in Fig. 4.1 [3]. Later this composition was identified as $YBa_2Cu_3O_{7-\delta}$, called 123 phase, and is responsible for the superconductivity. The structure and properties of $YBa_2Cu_3O_{7-\delta}$ will be discussed later.

To determine the properties of the green parts in the samples we also made

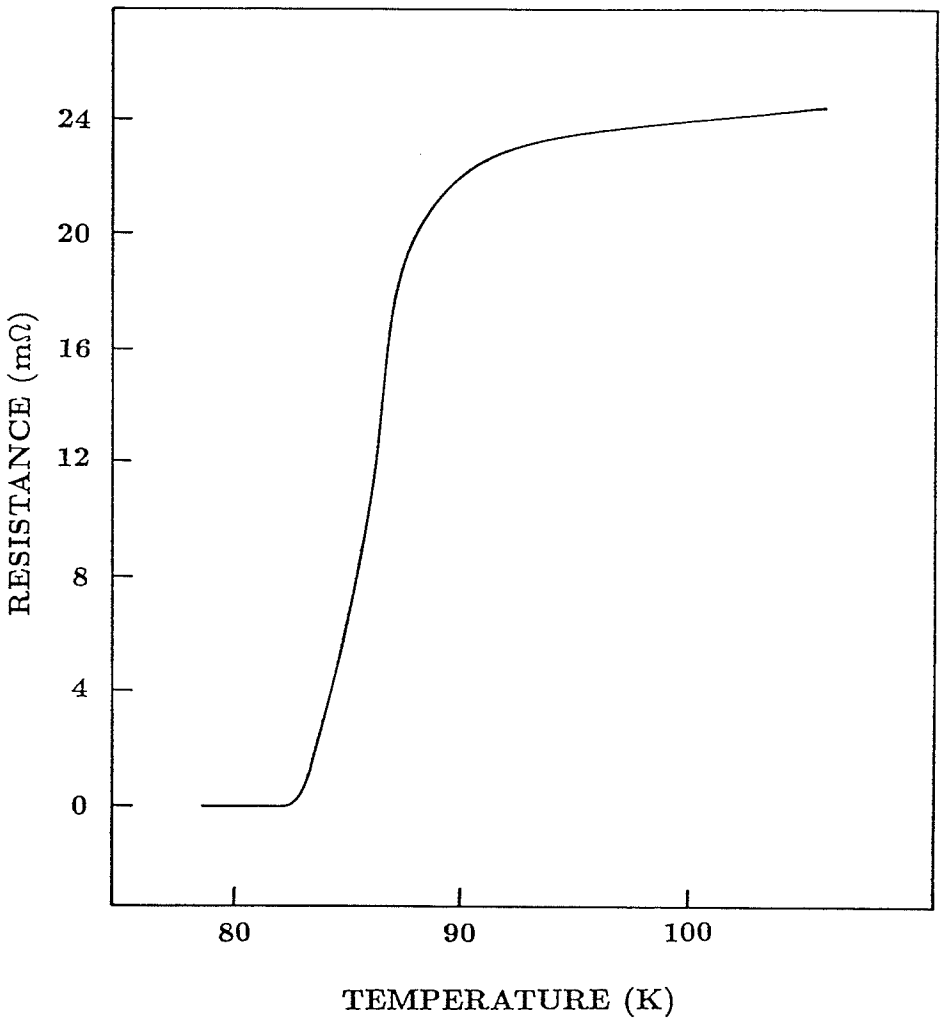

Figure 4.1: The resistance of a sample $Y_{0.4}Ba_{0.6}CuO_3$ versus temperature.

Figure 4.2: The x-ray diffraction pattern of Y_2BaCuO_5 with Cu Kα radiation.

a sample with a pure green phase; this was identified as Y_2BaCuO_5, a semiconducting phase[35]. Its x-ray diffraction pattern with Cu Kα radiation is shown in Fig. 4.2 and the d values are listed in Table 4.1. The lattice constants are a=7.1294(9), b=12.172(1) and c=5.6552(7) Å. Space group is $Pbn*$ (* can be a, b or c).

In detailed experiments, the compositions of the superconducting phase $YBa_2Cu_3O_{7-\delta}$ and the semiconducting phase Y_2BaCuO_5 in the samples for different x were estimated from the x-ray diffraction patterns and are given in Table 4.2. The ac susceptibility measurements indicate that the transition temperature differs only a little between the samples, while the transition width and the magnitude of the susceptibility, χ', below T_c are significantly different. The implication is that the superconducting properties of mixed phases mainly depend on the 123 phase.

4.1.2 TlCaBaCuO System

It is relatively easy to make close to single-phase 123 superconductors (though it is less easy to control the exact oxygen content). In the thallium system there are two phases responsible for the high-T_c, viz the $Tl_2CaBa_2Cu_2O_8$ (2122) and $Tl_2Ca_2Ba_2Cu_3O_{10}$ (2223) phases. It is very difficult to make single-phase thallium compounds since the phase formation of the thallium superconductors with $T_c > 100$ K is very sensitive to the heat treatment [36,37]. Sometimes starting with a 2223 mixture results in a 2122 phase; often both 2122 and 2223 phases coexist in the final pellet.

To make good quality samples some steps of the procedure used in making

Table 4.1: Powder x-ray diffraction pattern for Y_2BaCuO_5 with Cu Kα radiation.

h	k	l	$2\theta_{obs}$	d_{cal}	d_{obs}	I/I_0
2	1	0	26.02	3.421	3.422	8.0
2	2	0	29.00	3.076	3.076	6.2
0	4	0	29.26	3.043	3.049	8.8
1	3	1	29.83	2.992	2.993	100
2	1	1	30.50	2.927	2.928	64
0	0	2	31.60	2.828	2.829	49
1	4	0	31.94	2.799	2.799	20
2	2	1	33.12	2.702	2.703	18
1	1	2	34.90	2.569	2.569	7.3
1	4	1	35.78	2.508	2.508	12
2	3	1	37.11	2.420	2.421	9.9
3	1	0	38.59	2.332	2.331	5.9
1	5	0	39.07	2.304	2.304	11.2
3	2	0	40.72	2.214	2.214	22
2	1	2	41.39	2.179	2.180	14
3	1	1	41.87	2.156	2.156	6.3
0	4	2	43.68	2.071	2.071	8.4
0	6	0	44.63	2.029	2.029	9.4
1	4	2	45.56	1.989	1.989	29.0
2	3	2	46.64	1.944	1.946	8.3
3	4	0	48.56	1.873	1.873	11
1	6	1	49.38	1.845	1.845	4.1
1	5	2	51.16	1.786	1.784	10.2
2	6	0	51.81	1.763	1.763	7.3
3	2	2	52.47	1.743	1.743	14.3
2	6	1	54.44	1.683	1.684	7.0
1	3	3	55.20	1.662	1.663	16.0
2	1	3	55.63	1.651	1.651	13.5
1	7	1	56.84	1.619	1.619	4.9
2	2	3	57.30	1.607	1.607	5.5
3	4	2	59.12	1.561	1.561	12.9

Table 4.2: The superconducting phase $YBa_2Cu_3O_{7-\delta}$ and semiconducting phase Y_2BaCuO_5 in the nominal formula $Y_{1-x}Ba_xCuO_3$ for different x estimated by x-ray diffraction patterns.

x	$YBa_2Cu_3O_{7-\delta}$(%)	Y_2BaCuO_5 (%)
0.4	31	69
0.5	63	37
0.6	83	17
0.66	92	8
0.70	95	5
0.80	85	15

$YBa_2Cu_3O_{7-\delta}$ samples have to be adjusted, since the thallium oxide (Tl_2O_3) has a low melting point (717° C) and is easily evaporated. It is also highly toxic.

First, extreme precautions have to be taken to prevent the vapour of thallium compounds (Tl_2O_3, Tl_2O) directly entering the atmosphere. The chemicals were mixed in a dry box and the heating of the pellets was carried out in a closed system. During the heating the oxygen gas was introduced from one end of the quartz tube. After reacting the exhaust gas exited via an outlet through a flexible tube into water and then was released into the air. Most waste thallium compounds were deposited on the wall of the flexible tube. A small amount of leftover was deposited in the water.

Secondly we used two kinds of short heating procedure. In one all the chemicals in an appropriate amount were mixed together by a ballmill. The pellets were placed in an Al_2O_3 boat, heated in a quartz tube at 850-900°C for 3-30 min. and furnace cooled to room temperature in flowing oxygen [36]. The samples made by this procedure mostly are mixed phases of 2122 and 2223, but we can get nearly pure 2122 phase. This procedure produces less thallium contamination.

In the other, the $BaCO_3$ and CuO were reacted first at 925°C for 24 hours and then reground with Tl_2O_3 and CaO. The mixture was pelletized into disks 6 mm in diameter and 1.5-2.0 mm in thickness. The pellets were placed into a tube furnace, which has been heated at 860-920°C. The samples were heated for 3-10 min. and furnace cooled to room temperature under flowing oxygen[37]. To make the 2122 phase the starting materials were close to a 2223 atomic ratio, but with slighly less CaO and final heating was at 890°C for 5 to 10 min. For the 2223 phase, the Tl_2O_3 and CaO slightly exceeded a 2223 ratio and the final heating was at 915°C for 3 to 5 min. The structure and properties of 2122 and 2223 phase will be discussed later.

4.2 Single Crystals of $YBa_2Cu_3O_{7-\delta}$

Many research works have been made on the synthetic ceramic oxide superconducors of $YBa_2Cu_3O_{7-\delta}$ since the polycrystalline samples are easy to prepare. To have a better understanding of the basic mechanism and the dependence of their properties on crystallographic directions single crystals of sufficient size are required. Attempts to grow single crystals of $YBa_2Cu_3O_{7-\delta}$ have been described by several groups [38,39,40,41]. However the details of the growth techniques used are not given.

Single crystals of oxide materials usually are prepared by *flux* growth, also called *High Temperature Solution* growth (HTS). In this method the components of the desired crystal are dissolved in a solvent, the so-called flux. The process is analogous to crystal growth from an aqueous solution, but the solvent solidifies

before reaching room temperature.

The main advantage of this method is that the crystals are grown at temperatures below the melting point. This is very important if the materials melt incongruently. The flux method is also helpful if the melting point is very high or if the vapour pressure is high at the melting point. Thermal strain is minimized due to the relatively low growth temperature and the free growth into a liquid, allowing the formation of growth facets.

The main disadvantage is that during the growth some ions of the flux go into the crystal lattice as impurities. The low growth rate of this method is another shortcoming. The choice of a suitable flux, a larger crucible and automation of the growth procedure can minimize these disadvantages; the flux growth method still is widely used in many laboratories and industries [42].

At first we used the standard flux method and tried various fluxes, including PbO, B_2O_3, PbF_2, and Bi_2O_3, and various ratios of flux to the nutrient in attempts to grow single crystals of $YBa_2Cu_3O_{7-\delta}$. After completion there were some black shiny crystal points (they may correspond to the superconducting 123 phase) and some transparent shiny points (they may be the semiconducting phase of Y_2BaCuO_5) on the surface of the solidified flux. In order to separate them from the flux, the usual methods of boiling the crucible in acetic acid, nitric acid or a mixture (acetic acid : nitritic acid : water = 1:1:3) were used. Then an anomalous event occurred. After boiling in the acid solution we did not get the black crystals but we did get some small transparent crystals which had lost their corners and edges and became ball-shapes. We realized that the superconducting crystals of

$YBa_2Cu_3O_{7-\delta}$ reacted with acid; this led us to do systematic experiments of the deterioration of the 123 phase in various environments. Hence the usual fluxes used are not suitable for growing single crystals of this superconductor. We sought new fluxes.

We found that BaO_2 and CuO can be used as fluxes. Now BaO_2 has a low melting point (450°C) and decomposes at 800°C. These properties ensure that divalent barium ions are available for the single crystal and perhaps also some oxygen ions. The presence of CuO in the flux will avoid any lack of copper when the starting conditions use stoichiometric mixtures . For the nutrient, Y_2O_3 : BaO_2 : CuO molecular ratios of 0.5:2:3 were used; for the flux the BaO_2 : CuO molecular ratios lay beween 1:3 and 2:5. The ratio of nutrient to flux was chosen to be either 0.6 or 1.2. We also added 2% of powdered $YBa_2Cu_3O_{7-\delta}$ ceramic to the mixture in order to provide seeds for single crystal growth.

A crucible was loaded with appropriate amounts of the above mixture. These materials were in powder form, mixed in a agate mortar and compressed into the crucible by a pestle under finger pressure. The crucible was covered with a platinum lid and placed inside a muffle which was situated in the centre of the electrical furnace described in Chapter 3. The furnace was heated at the rate of about 150°C per hour up to 800°C and then held for 2 hours. The temperature was then raised by 50°C per hour up to 1000°C and the mixture soaked for 2-4 hours. Next. the temperature was decreased by 4-10°C per hour, until a temperature of 850°C was reached. Thereafter the power was turned off and the crucible was allowed to cool in the furnace.

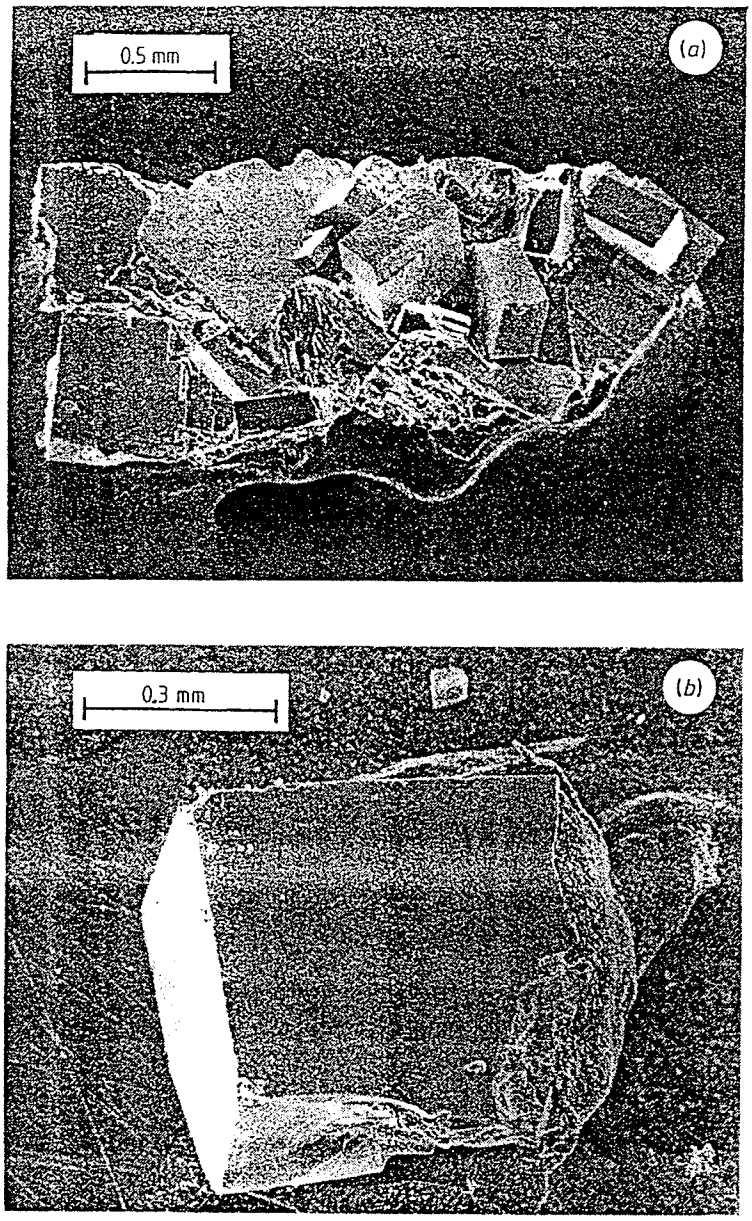

Figure 4.3: The SEM photographs of (a) single crystals of $YBa_2Cu_3O_{7-\delta}$ near the junction of the bottom and wall of the crucible and (b) one crystal separated by mechanical means.

Black crystals of $YBa_2Cu_3O_{7-\delta}$ in the shape of rectangular slabs or tablets formed both on the bottom and at the edge between the wall and bottom of the crucible; an example of the latter is shown in Fig. 4.3(a). The crystals were mechnically separated since a suitable solvent to assist separation was not found. The size of the crystals varied from about $0.5 \times 0.5 \times 0.2$ to $2 \times 2 \times 0.3$ mm^3; an example is shown in Fig. 4.3(b). EDAX analysis indicated that the ratio of Y : Ba : Cu in the single crystals was close to 1:2:3. Some needle-like CuO crystals with a length up to 2-3 mm and a square cross section were also found[43].

Various types of crucible, platinum, alumina and porcelain were tried. At high temperatures the porcelain crucible reacted with the mixture and hence is unsuitable. When a platinum crucible were used, EDAX showed the presence of Pt atoms in the single crystals. The best type of crucible appears to be the alumina ones. However a small amount of Al was also found to be incorporated into the crystals.

X-ray diffraction showed that the crystals are definitely orthorhombic with a=3.857(1), b=3.876(1), c=11.692(5)Å and a volume V=174.79 Å^3. Although the b-parameter is close to that found for ceramic $YBa_2Cu_3O_{7-\delta}$ the a- and c-parameters are appreciably larger than the reported value a=3.824 and c=11.667 Å for the polycrystalline materials[44]. Thus the single crystals are closer to tetragonal than the ceramic materials.

Measurements of the ac susceptibility showed that χ' becomes negative at about 86 K and full shielding is achieved at about 65 K. In these measurements groups of crystals were used since the sensitivity of the apparatus did not permit

the detection of signals from only one single crystal. The reduction of the onset of superconductivity 6-8°C below that for the best ceramics may imply that the oxygen contents are slightly different. Further, in other studies we have observed that a more tetragonal structure seems to decrease T_c. The larger width of transition may imply a lack homogeneity within one single crystal or a variation in oxygen content between different crystals.

In our technique the mixture is only partially melted, that is, a complete liquid does not form. The crystal growth mechanism is then more complicated than that for a solution. Many factors, including the ratio of nutrient to flux, the method used to mix the chemicals and the heating and cooling procedure, will influence the crystal growth.

4.3 Deterioration of the $YBa_2Cu_3O_{7-\delta}$ Superconductor in Various Ambient Environments

4.3.1 The Discovery of the Problems

Interest in high-T_c superconductors (T_c >90K) was twofold. On one hand, the origin of the superconductivity was of immense scientific interest. On the other hand, potential applications in the electronic and electrical-power industries were most exiting. However, stability of the materials in various environments is essential. Two chance observations indicated that the ceramic 123 superconductors quickly degrade on exposure to some conditions. These led us to investigate the deterioration of 123 superconductors more systematically.

The first indication of instability problems came from ac susceptibility mea-

surements. A two-day interruption occurred during which a pellet (density about 3 $g \cdot cm^{-3}$) was kept at room temperature in the sample holder of the low-temperature Dewar vessel. Upon resumption of the experiment, it was found that the diamagnetic signal had been significantly reduced. Inspection of the sample pellet revealed a white efflorescence on its surface. The probable cause of this change was assumed to be exposure to moisture that had condensed in the Dewar tail after the initial stage of the experiment. The reduction in the diamagnetic (shielding) properties was the result expected from erosion of the grian boundaries near the sample's surface; hence , the effective shielded volume was diminished.

The second observation related to attempts to grow single crystals by the flux technique as mentioned previously. After slowly cooling the molten mixture, the desired products are normally separated from the residual flux by boiling in an appropriate acid. For the fluxes used in our experiments, either acetic or nitric acids were employed. After several runs it was observed that the products also seemed to be dissolving. Therefore, it was decided to do a more detailed study of the envionmental stability of the $YBa_2Cu_3O_{7-\delta}$ compounds.

4.3.2 The Experiments in Various Ambient Environments

Experiments to test the resistance of the 123 material to attack by water at 20-80° C with reaction times 4–48 hours were made. Starting materials consisted both of pellets with varying densities and of fine-grained powders. All reactants and products were identified by powder x-ray diffraction. Changes in the suscep-

tibiliy of pellets were also investigated. In addition, the action of various acids was observed.

A solid pellet ($\sim$ 3.3 g $\cdot$ cm^{-3}) was reacted at 80° C for 4 hours in 80 mL of deionized water. About 20% of the pellet precipitated as fine-grained $BaCO_3$, and the residual pellet's surface was partially decomposed. No colour change was observed in the supernatant solution. Although the external appearance of the pellet was relatively unchanged, its composition had altered to about 60% CuO, 30% Y_2BaCuO_5, 10% $BaCO_3$ and 10% of the original $YBa_2Cu_3O_{7-\delta}$ (as estimated from powder x-ray diffraction patterns). The presence of $BaCO_3$ was attributed to dissolved CO_2 in the deionized water, as no carbonates were used in the synthesis of the starting materials; of course, an intermediate step involving hydroxide hydrates of BaO may well be involved. At lower temperatures, similar reactions occurred, but the rate was much slower.

One sample ($\sim$ 5.1 g $\cdot$ cm^{-3}, or about 80% of x-ray density) was heated in deionized water at 80°C in successive 1 hour steps. The susceptibility data after each heating are shown in fig. 4.4. Note that the diamagnetic susceptibility at 77 K has decreased by about 50% after heating for 5 hours. By comparison, a sample with smaller density ($\sim$ 3.1 g $\cdot$ cm^{-3}) heated for 4 hours in water at 80°C displays no diamagnetism at 77 K. Clearly the increased porosity leads to greater decomposition as expected. The width of the transition in fig. 4.4 does increase with heating time, but it is still considerably less than that for a pellet with smaller density. It follows that the reaction interface moves fairly uniformly into the sample after each heating. Then the size of the superconductor is reduced;

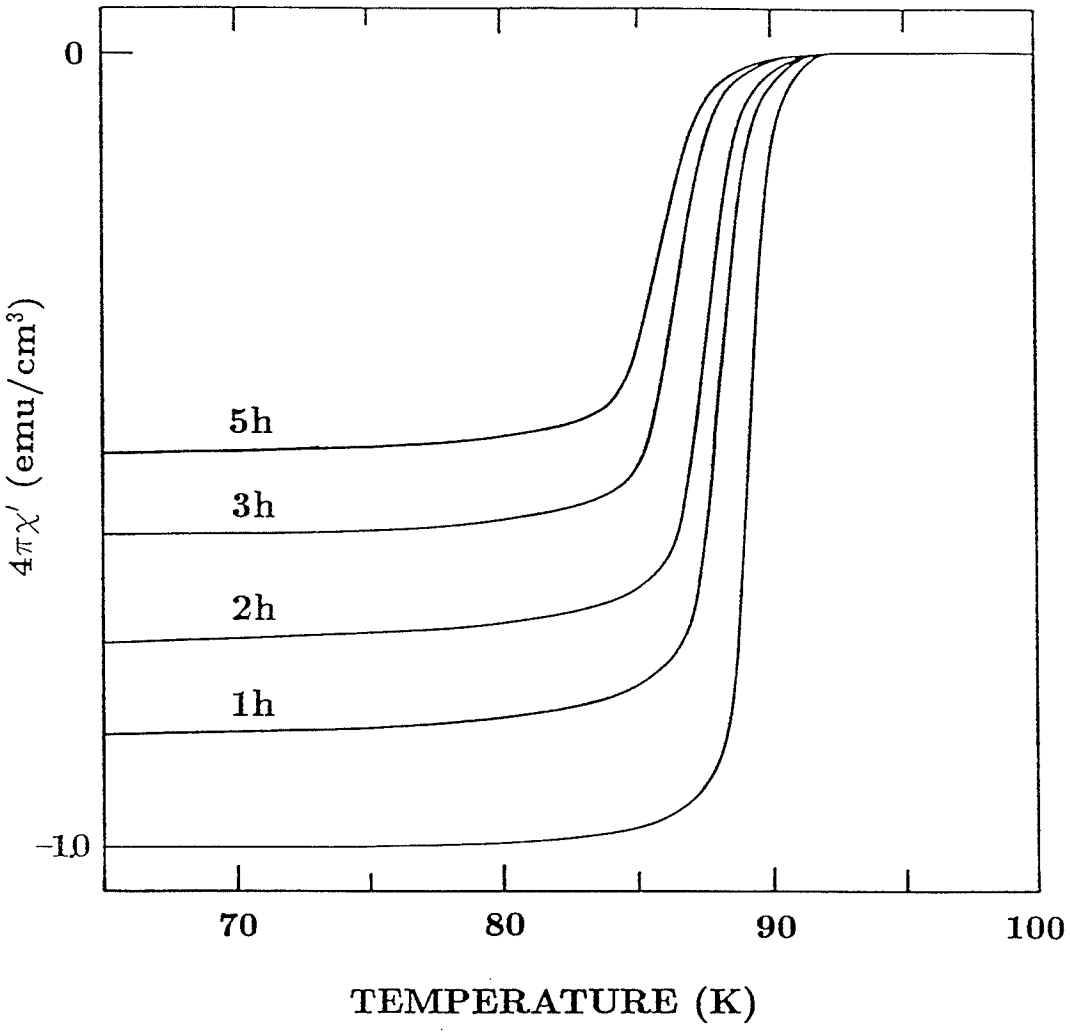

Figure 4.4: Susceptibility variation with time in water at 80°C; the lower curve represents the untreated sample. The data were taken at 3.7 kHz in a field strength of 0.12 Oe root mean square.

hence the full shielding is restricted to a smaller volume[45].

The reaction of various acids on the superconductor was observed; both concentrated and 10% solutions were used. The fastest dissolution occurred for HCl, followed by HNO_3, acetic and H_2SO_4 acids in decreasing order. The slow action of H_2SO_4 was undoubtly because $BaSO_4$ is formed, which does not dissolve in water. With acetic and HNO_3 acids, a blue colour was observed, probably a copper salt. For HCl, both a white and yellow powder were found; the yellow material may be a yttrium compound. Little reactivity was detected with NaOH.

These experiments show that the oxide supercoductors will deteriorate in environments that include water and acidic vapors; recently some other groups also reported that these materials degrade in humid air at 40°C [46,47,48]. These reactions will, of course, be much slower the lower the ambient temperature and the denser the materials used. The superconductors can be protected by various treatments including impervious coatings. However, the new superconducting 123 oxide may find limited use in application requiring long-term stability.

Chapter 5

The Structure of High Tc Superconductors

5.1 Perovskites

Ideal perovskites are described by the general formula ABX_3 and consist of cubes made up of three distinct chemical elements (A, B and X) that are present in a ratio 1:1:3. The A and B atoms are metallic cations and the X atoms are nonmetallic anions. The larger A cation lies at the centre of each cube, the smaller B anions occupy all eight corners and the X anions lie at the midpoints of the cube's twelve edges(Fig. 5.1).

All the corners and edges of each cube are shared with other cubes since each cube is surrounded on all its sides by other cubes. The contribution to the cube is 1/8 for each atom at the corners and 1/4 for each atom on the edges. So each cube is considered to have 1 A atom, 1 complete B atom and 3 complete X atoms. Thus each cube can be described by the formula ABX_3.

A great many elements can combine to form the hundreds of ideal or mod-

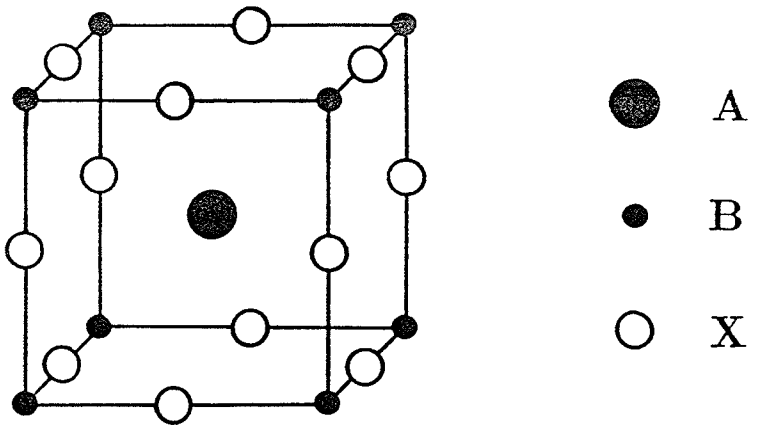

Figure 5.1: The perovskite structure.

ified perovskites now known. Calcium, barium, potassium and the rare-earth elements are typical of two dozen elements that can fill the A position. An astonishing total of almost 50 different elements, more than half of the stable entries in the periodic table, are known to adopt B sites. The X position can be taken up not only by oxygen but also by members of the halogen family of nonmetals: fluorine, chlorine or bromine [49].

Many perovskites are somewhat distorted because the central A cation is too small in relation to the B cations at the corners of the cube. This disparity causes the X atoms and sometimes the B atoms to move out of position. It is also possible that the A and B positions can fill with two or more type of cations. In the case of mixed cations *ordering*, or strictly alternations of position for A or B cation, may occur.

No matter how distorted or compositionally varied they are, all the per-

ovskites are stoichiometric. They have a total of two cations for every three anions, ABX_3. A variety of other perovskites or perovskite–related structures are nonstoichiometric: they deviate from ideal ABX_3 formula by having vacant sites where atoms would normally be.

5.2 The Structure of $YBa_2Cu_3O_{7-\delta}$

5.2.1 Oxygen Vacancy

We consider that the unit cell of $YBa_2Cu_3O_{7-\delta}$ consists of three basic perovskite cubes, called a triple-layer perovskite, in which the relatively larger Y and Ba atoms lie in A sites whereas the smaller copper atoms lie at the corners and the oxygen atoms lie on each of cube's edges. The yttrium cube is in the middle and the two barium cubes are on the top and bottom respectively. The ideal unit cell of such a structure should have 9 oxygen atoms at X sites, 3 atoms (Y and 2 Ba) at A sites and 3 copper atoms at B sites with the a formula $YBa_2Cu_3O_9$ (Fig. 5.2a).

This structure is tetragonal with three orthogonal axes (called a, b and c); one lattice constant c is considerably larger than the other two, a and b, which are equal (Fig. 5.2a). According to the charge balance rule there will be 5 to 8 oxygen atoms in the unit cell corresponding to copper in Cu^{1+} to Cu^{3+} states, respectively, since yttrium is in a Y^{3+} state and barium is in a Ba^{2+} state. That means there are some oxygen vacancies in the unit cell. Where are the vacancies? The experimental results [50,51,52] indicate that there are two principal sites for oxygen vacancies as compared to the ideal perovskite structure. One is in the

a-b plane of oxygen ions surrounding the yttrium cation and the other is the line of oxygen ions parallel to the a axis in the top and bottom planes (Fig. 5.2b). These vacancies alter the composition to $YBa_2Cu_3O_7$.

Our x-ray diffraction refinement deduced that the composition for a better quality yttrium-containing superconducting compound is $YBa_2Cu_3O_{6.92}$ [44]. That means 92 of every 100 unit cells contained 7 oxygen atoms whereas 8 contained only 6. The extra vacancy in these 8 unit cells is in the b-direction on the top and bottom copper planes. For the superconducting phase of $YBa_2Cu_3O_{7-\delta}$, the value of δ varies from 0 to 0.5 depending on the preparation procedure. It becomes a nonsuperconducting phase when $\delta > 0.5$ [53,54,55].

The oxygen vacancies also distort the structure slightly so that it just barely becomes orthorhombic with the two once equal lattice constants, a and b, now slightly different. Usually this kind of oxide is called an oxygen-deficient perovskite.

5.2.2 X-ray Diffraction Experiments

To do the structure analysis two samples were selected for detailed studies. Both samples were made by the standard ceramic method with chemicals Y_2O_3, CuO and BaO. Appropriate amounts of these compounds were mixed in a ball mill with acetone. For the first, designated sample(a), the mixture was pelletized into a disk 8 mm in diameter and about 2 mm in thickness, heated in air at about 900°C for 6 hours and then slowly cooled. For the second designated sample (b), the mixed powder was heated to 800°C for four hours under 1 atm oxygen pressure (1 atm =101 kPa), slowly cooled and reground. These powders were

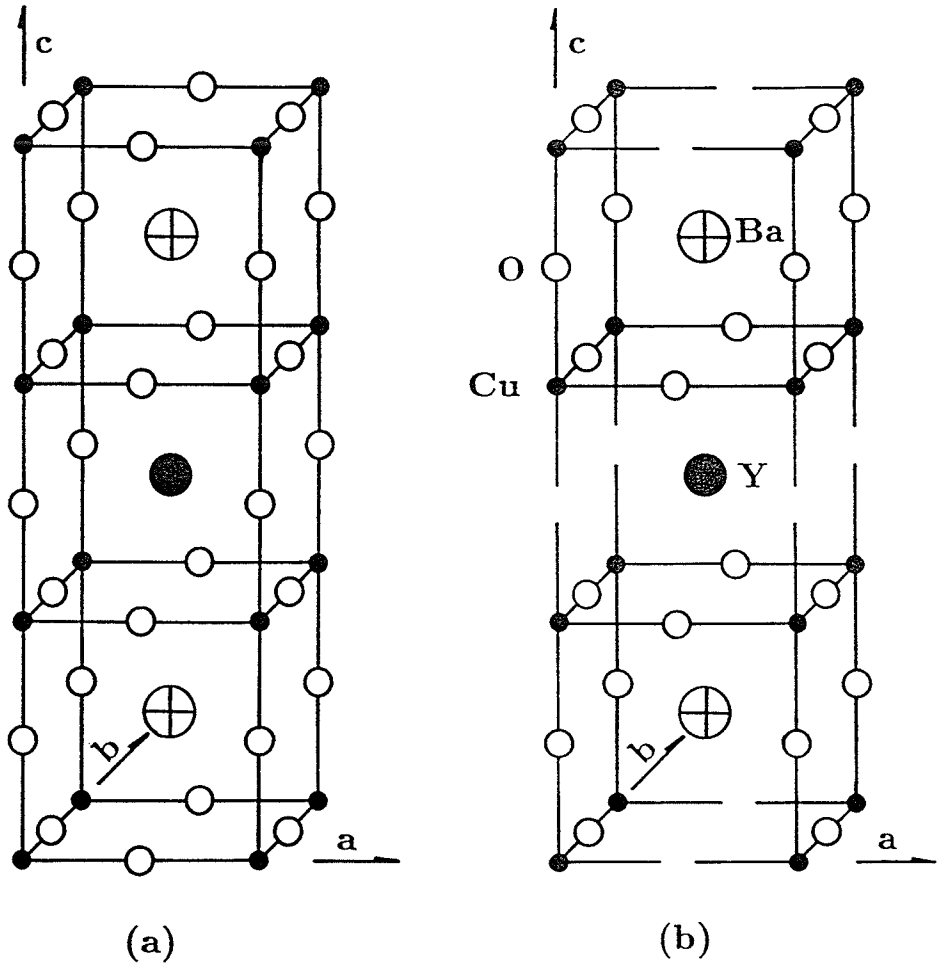

Figure 5.2: The ideal unit cell of triple-layer perovskite of $YBa_2Cu_3O_9$ without oxygen vacancies for (a) and with oxygen vacancies for (b).

then pelletized, fired at 970°C for six hours under 1 atm oxygen pressure and slowly cooled.

The second sample was mechanically much harder and denser than the first one; 4.2 $g.cm^{-3}$ as compared with 3.4 $g.cm^{-3}$. It is worth emphasizing that slow cooling is an essential step in producing samples with superior superconducting properties. It may allow the samples to absorb more oxygen.

X-ray diffraction experiments have been done on these two selected samples as follows. Samples were ground to a grain size of less than about 5-10 μm; this was essential in order to minimize preferred orientations parallel to the (001) plane, especially for the mechanically harder sample (b). The powdered material was side-drifted into a modified aluminium holder and mounted in a Philips PW 1050 diffractometer controlled by a PW 1710 automatic control system. Intensities were measured at 295 K at intervals 0.08° 2θ over a range 16–126° 2θ using graphite monochromated Cu Kα radiation and 1° divergence and receiving slits. The counting time at each step was 5 seconds. The x-ray diffraction pattern and data for sample (b) are shown in Fig. 5.3 and Table 5.1 respectively.

Structure refinement was done with a modified version of the Rietveld analysis program, DBW 3.2 [56,57,58]. Peak intensities were modelled with a 2θ-variable pesudo-Voigt function for four peak full-widths-at-half-maximum on either side of the peak centre; the background was refined as a third-order polynomial function in 2θ. Isotropic temperature parameters were fixed at values reasonable for x-ray crystal-structure refinements. Peaks from minor contaminating phases (CuO and Y_2BaCuO_5) were excluded from the refinement.

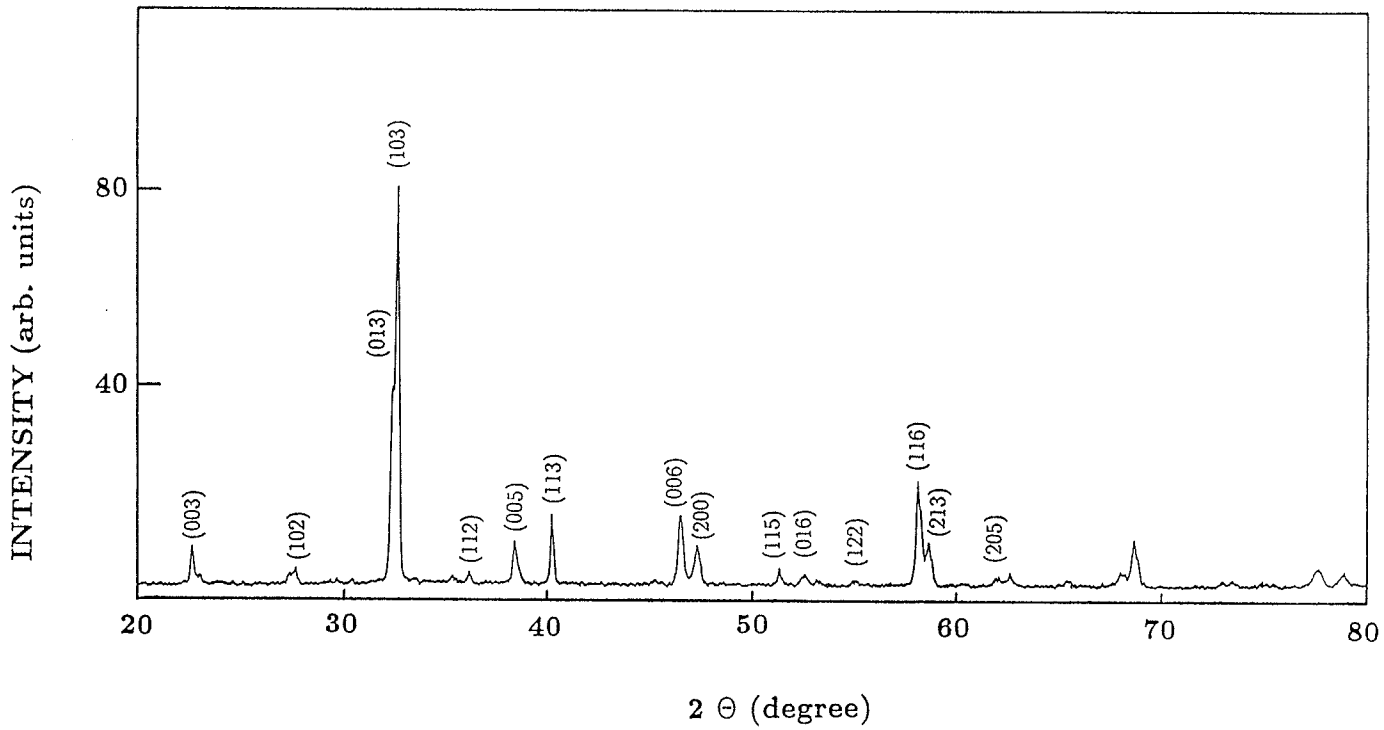

Figure 5.3: Powder x-ray diffraction pattern for $YBa_2Cu_3O_{6.92}$ with Cu Kα radiation.

Table 5.1: Powder x-ray diffraction lines for the phase $YBa_2Cu_3O_{7-\delta}$ (123). Patterns were obtained with filtered Cu Kα radiation. Orthorhombic unit cell a=3.8243(2), b=3.8862(3), c=11.667(1) Å.

h	k	l	2θ	d_{calc}	d_{obs}	I/I_0
0	0	2	15.15	5.844	5.844	5
0	0	3	22.87	3.886	3.885	10
1	0	0	23.25	3.822	3.823	5
0	1	2	27.60	3.230	3.230	5
1	0	2	27.86	3.196	3.200	6
0	1	3	32.60	2.745	2.745	50
1	0	3	32.85	2.725	2.724	100
1	1	0	32.82	2.723		
1	1	2	36.38	2.467	2.468	5
0	0	5	38.57	2.332	2.332	12
1	0	4	38.82	2.318	2.319	3
1	1	3	40.42	2.230	2.230	16
0	0	6	46.74	1.943	1.942	19
1	2	0	46.79	1.940		
2	0	0	47.56	1.911	1.910	12
1	1	5	51.54	1.771	1.772	5
0	1	6	52.64	1.737	1.737	2
0	2	3	52.70	1.736		
1	0	6	52.82	1.734	1.732	4
1	2	0	52.89	1.730		
2	0	3	53.39	1.715		
2	1	0	53.41	1.714	1.714	4
1	2	1	53.51	1.711		
1	2	2	55.36	1.658	1.658	1
1	1	6	58.32	1.581	1.581	27
1	2	3	58.35	1.580		
2	1	3	58.85	1.569	1.568	14
2	0	5	62.9	1.478	1.479	4

Table 5.2: Crystallographic data at 295K for the samples: (a) $YBa_2Cu_3O_{6.83}$; a=3.8259(2), b=3.8864(3), c=11.669(1)Å; and (b) $YBa_2Cu_3O_{6.92}$; a=3.8243(2), b=3.8862(3), c=11.667(1)Å. Space group: *Pmmm*.

Atom	Wyckoff Symbol	x	y	z	B(Å^2)*	Site occupancy
(a)Y	$1h$	1/2	1/2	1/2	0.8	1.0Y
(b)						1.0Y
(a)Ba	$2t$	1/2	1/2	0.1856(3)	0.8	1.0Ba
(b)				0.1846(3)		1.0Ba
(a)Cu(1)	$2i$	0.054(4)	0	0	0.7	1.0Cu
(b)		0.045(5)				1.0Cu
(a)Cu(2)	$2q$	0	0	0.3563(5)	0.7	1.0Cu
(b)				0.3570(6)		1.0Cu
(a)O(1)	$1e$	0	1/2	0	1.5	0.83(6)O
(b)						0.92(7)O
(a)O(2)	$2s$	1/2	0	0.380(2)	0.8	1.0O
(b)				0.378(2)		1.0O
(a)O(3)	$2r$	0	1/2	0.378(2)	0.8	1.0O
(b)				0.384(2)		1.0O
(a)O(4)	$2q$	0	0	0.160(3)	0.8	1.0O
(b)				0.160(3)		1.0O

* Isotopic temperature factor.

Table 5.3: Interatomic distance (Å) for samples (a) and (b).

Distance (Å)			
(a) Y–O(3)×4	2.38(1)	Cu(1)–O(4)×2	1.87(3)
(b)	2.34(2)		1.87(3)
(a) Y–O(2)×4	2.39(1)	Cu(1)–O(1)×2	1.9432(2)
(b)	2.41(2)		1.9431(2)
(a) Ba–O(4)×4	2.742(3)	Cu(2)–O(2)×2	1.933(3)
(b)	2.741(3)		1.928(3)
(a) Ba–O(1)×2	2.889(2)	Cu(2)–O(3)×2	1.959(3)
(b)	2.880(2)		1.968(4)
(a) Ba–O(3)×2	2.95(2)	Cu(2)–O(4)×1	2.283(3)
(b)	3.01(2)		2.30(3)
(a) Ba–O(2)×2	2.99(2)		
(b)	2.98(2)		

Angles (degrees)	
(a)O(2)–Cu(2)–O(3)	88.1(1)
(b)	88.8(1)
(a)O(2)–Cu(2)–O(4)	98.3(7)
(b)	97.4(7)
(a)O(3)–Cu(2)–O(4)	97.4(7)
(b)	99.1(8)

Refinement results are given in Tables 5.2 and 5.3.

Crystal-structure refinements of the orthorhombic superconducting phases of nominal composition $YBa_2Cu_3O_{7-\delta}$ by powder x-ray [50], neutron diffractions [51,52] and single-crystal x-ray diffraction [59] agree that the most likely space group is *Pmmm*. Refinement was initiated with all atomic sites fully occupied: Cu atoms at positions (0,0,0), Cu(1) and (0,0,z), Cu(2), Y atoms at (0.5,0.5,0.5), Ba atoms at (0.5,0.5,z), and O atoms at (0,0.5,0), O(1); (0.5,0,z), O(2); (0,0.5,z), O(3) and (0,0,z), O(4). The starting z coordinates were estimated from published structures.

Each position in turn was checked for the presence of vacancies by refining the site occupancy. Occupancies of the Cu(2), Y, Ba, O(2), O(3), and O(4) sites refined to values of essentially one or slightly higher. These were fixed at full occupancy for the final refinement. The O(1) site showed significant vacancies, refining to an occupancy of 0.83(6) for sample(a) and 0.92(7) for sample (b) (the one prefired in oxygen).

The occupancy of the potential fifth oxygen position at (0.5, 0, 0) reported by others [50,59] has been also checked, but the occupancy refined to a value not significantly different from zero. Significant vacancies were detected in the Cu(1) site (square planar coordination) with O(1) and O(4). Occupancies refined to 0.90(2) Cu for sample (a) and 0.88(2) for sample (b). As this is not likely, the Cu(1) vacancies were attributed to Cu disorder about the origin, which decreases the effective scattering at that site. Refinement of the structures with Cu(1) located at (x, 0, 0) not only caused the apparent Cu vacancies to vanish, but also

improved the results.

The structure obtained here (Fig. 5.4) is similar to the powder neutron diffraction structure reported by David and Beno [51,52] except for a slightly different oxygen-ordering scheme and Cu(1) disorder about their origin. The partial occupancy of the O(2) position(1/2,0,z) has not been observed while partial occupancies (0.83(6) and 0.92(7)) of the O(1) position(0,0.5,0) of sample (a) and (b) respectively were derived. The single crystal x-ray diffraction study reported partial occupancy of Cu(1) site (0.89(11)). It can be attributed to Cu disorder about the origin[44,59].

From the refinement results the refined compositions were $YBa_2Cu_3O_{6.83}$ for sample (a) and $YBa_2Cu_3O_{6.92}$ for sample (b). These compositions gave an average copper valence of 2.22 and 2.28 for sample (a) and (b), respectively. The short Cu(1)-O(4) bond length of 1.87(3)Å(Table 5.3) is similar to that found in alkali-metal cuprates such as $KCuO_2$ [60]. This may suggest that Cu^{3+} ions preferentially occupy the square planar, Cu(1), sites at (0,0,0) and Cu^{2+} ions the square pyramidal, Cu(2), sites at (0,0,z).

5.2.3 The Ordering of Atoms and Oxygen Vacancies

In the final refined structure the Y and Ba atoms are all in the A sites of a perovskite cube, but Y atoms always lie at the middle and Ba atoms on the top and bottom cubes of a unit cell. The Ba^{2+} coordination sphere consists of ten nearest neighbor oxygen atoms with distances ranging from 2.7Å for the oxygen atoms in the BaO plane to 3.0Å for the oxygen atoms in the CuO_2 plane. The

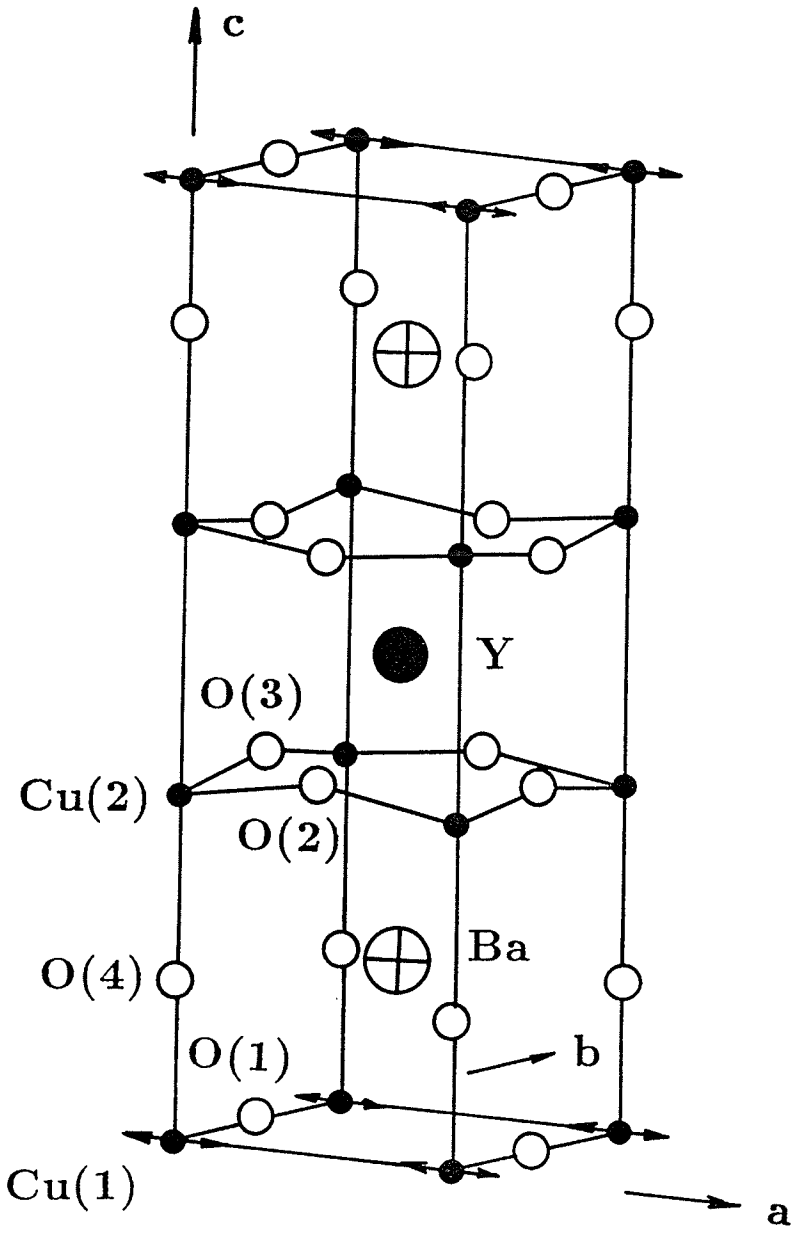

Figure 5.4: The final refined structure of $YBa_2Cu_3O_{7-\delta}$.

coordination sphere for the smaller and more highly charged Y^{3+} cation contains eight nearest neighbor O atoms with distance of 2.4 Å. This structure leads to crystallographically distinct sites for Y and Ba; this structure is ordered.

The oxygen vacancies in $YBa_2Cu_3O_{7-\delta}$ only occur in the a-b plane surrounding yttrium cations and the one line parallel to the a axis in the top and bottom copper planes. This oxygen vacancy ordering results in two characteristics of the structure. Firstly, the Cu(2) atom surrounded by five oxygen atoms is in a square pyramidal site and each oxygen atom at the corners of the square planar is shared with the other. They form a two dimensional Cu–O_2 plane parallel to a-b planes above and below the yttrium atom plane. Secondly, Cu(1) atoms are surrounded by four oxygen atoms in the square planar site. A one-dimensional Cu-O chain along the b axis is formed (Fig. 5.5). The oxygen vacancies on the top and bottom edges also cause the structure to transfer from tetragonal to orthorhombic.

From the structural point of view, what is responsible for the high-T_c superconductivity? The Cu-O_2 plane or the Cu-O chains? The orthorhombic or the tetragonal structure? Some researchers suggest that the orthorhombic structure and the copper-oxygen chain are responsible for the high-T_c superconductivity based on experimental results when the oxygen content is varied from 7 to 6.5 in $YBa_2Cu_3O_{7-\delta}$ or when some elements are substituted for Cu[53]. Then the structure transforms gradually from orthorhombic to tetragonal and the copper-oxygen chain is destroyed. Simultaneously, the superconducting transition temperature T_c is reduced from 92K to zero [53,55,61]. This suggests that the Cu-O chain or

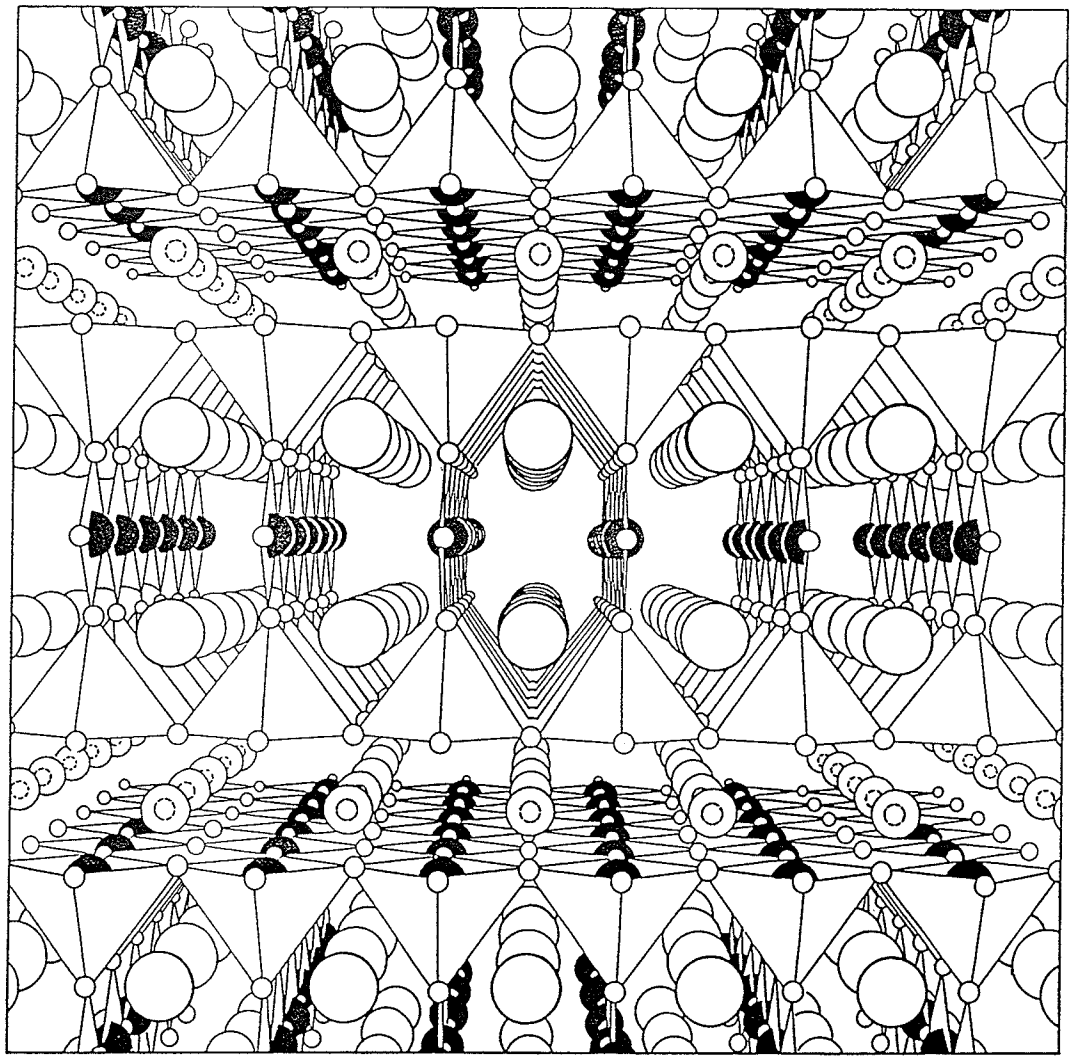

Figure 5.5: The square pyramidal and square planar sites in the orthorhombic structure of $YBa_2Cu_3O_{7-\delta}$.

the oxygen vacancy order is essential to high-T_c and any loss or damage to the Cu-O chain will affect the superconductivity detrimentally. This was the point of view that prevailed for awhile.

Later on, the experiments in which Cu is substituted by M(=Zn, Ga, Co, and Al) in $YBa_2(Cu_{1-x}M_x)_3O_{7-\delta}$ indicated that small dopings by Ga induce an orthorhombic to tetragonal structural transition but the T_c's are still as high as 81 K [62], whereas $YBa_2(Cu_{1-x}Zn_x)_3O_{7-\delta}$ retains the same orthorhombic structure as the parent compound, but with a highly depressed T_c. It was also shown that Ga and Zn atoms preferentially substitute on Cu(1) and Cu(2) sites, respectively[62], which suggests that the Cu-O_2 plane is responsible for the high-T_c and that the Cu-O chain plays a much less important role. Discovery of BiCaSrCuO and TlCaBaCuO superconducting systems show that the Cu-O_2 planes are essential for high-T_c's and that the Cu-O chains are not necessary for high-T_c's among the cuprates since these new compounds have no Cu-O chains.

It is worth noting that the Cu-O_2 plane responsible for the high-T_c does not conflict with the fact that T_c correlates with the number of oxygen anions along the Cu-O chains. The oxygen defficiency effectively reduces the carrier densities and possible coupling between the Cu-O_2 planes. The role of the chains may be to act as a hole carrier reservoir coupling the planes [63] or to act as a metallic layer lying between the Cu-O_2 planes to enhance superconductivity in the $YBa_2Cu_3O_{7-\delta}$ materials [64].

5.3 The Structure of the Tl-Ca-Ba-Cu-O System

In the Tl-Ca-Ba-Cu-O system there are two phases, $Tl_2CaBa_2Cu_2O_8$ (hereafter referred to as the 2122 phase) and $Tl_2Ca_2Ba_2Cu_3O_{10}$ (hereafter referred to as the 2223 phase) that possess transition temperatures 110K and 125K, respectively. Both of them have similar structures except there are additional Cu-O and Ca layers in the 2223 phase.

5.3.1 The 2122 Phase

An x-ray powder diffraction pattern of the 2122 sample was obtained with Cu Kα radiation at room temperature and shown in Fig. 5.6(a); the procedure used is the same as that for the YBaCuO system. The results reveal a pseudotetragonal unit cell with a=3.8526(6) Å, and c=29.239(8) Å [65,66,67]. The positions and intensities of the powder lines are shown in Table 5.4. A prominent powder line(002), corresponding to $d \simeq 14.7$ Å ($2\theta \simeq 6°$ with Cu radiation), is useful for diagnostic purposes.

The distribution of atoms in the unit cell is shown in Fig. 5.7(a). Each basic building block contains two formula units of $Tl_2CaBa_2Cu_2O_8$ which have a relative shift on the a-b plane. The crystallographic asymmetric unit consists of four kinds of cations, Tl^{3+}, Ca^{2+}, Ba^{2+} and Cu^{2+}, and three unique oxygen anions all on special positions (Table 5.5). The distance between the ions are listed in Table 5.6. It can be seen clearly from Fig. 5.7(a) that each formula unit consists of three perovskite cubes similar to the 123 phase except that calcium replaces

Table 5.4: Powder x-ray diffraction lines for the phase $Tl_2Ca_1Ba_2Cu_2O_8$ (2122). The pattern was obtained with filtered Cu Kα radiation.

h	k	l	2θ	d_{calc}	d_{obs}	I/I_0
0	0	2	6.02	14.62	14.67	11
0	0	4	12.05	7.309	7.318	2
0	0	6	18.19	4.873	4.921	3
1	0	5	27.70	3.217	3.218	60
1	0	7	31.56	2.832	2.833	100
1	1	0	32.85	2.724	2.724	80
1	1	2	33.43	2.678	2.678	15
1	0	9	36.14	2.484	2.484	9
0	0	12	36.863	2.436	2.437	20
1	1	8	41.28	2.184	2.186	13
0	0	14	43.32	2.088	2.087	9
1	1	10	45.48	1.993	1.993	10
1	0	13	46.79	1.942	1.940	9
2	0	0	47.15	1.926	1.926	34
1	1	12	50.22	1.816	1.815	23
2	1	5	55.55	1.653	1.653	22
2	1	7	57.86	1.5931	1.592	32
1	0	17	58.95	1.570	1.569	12

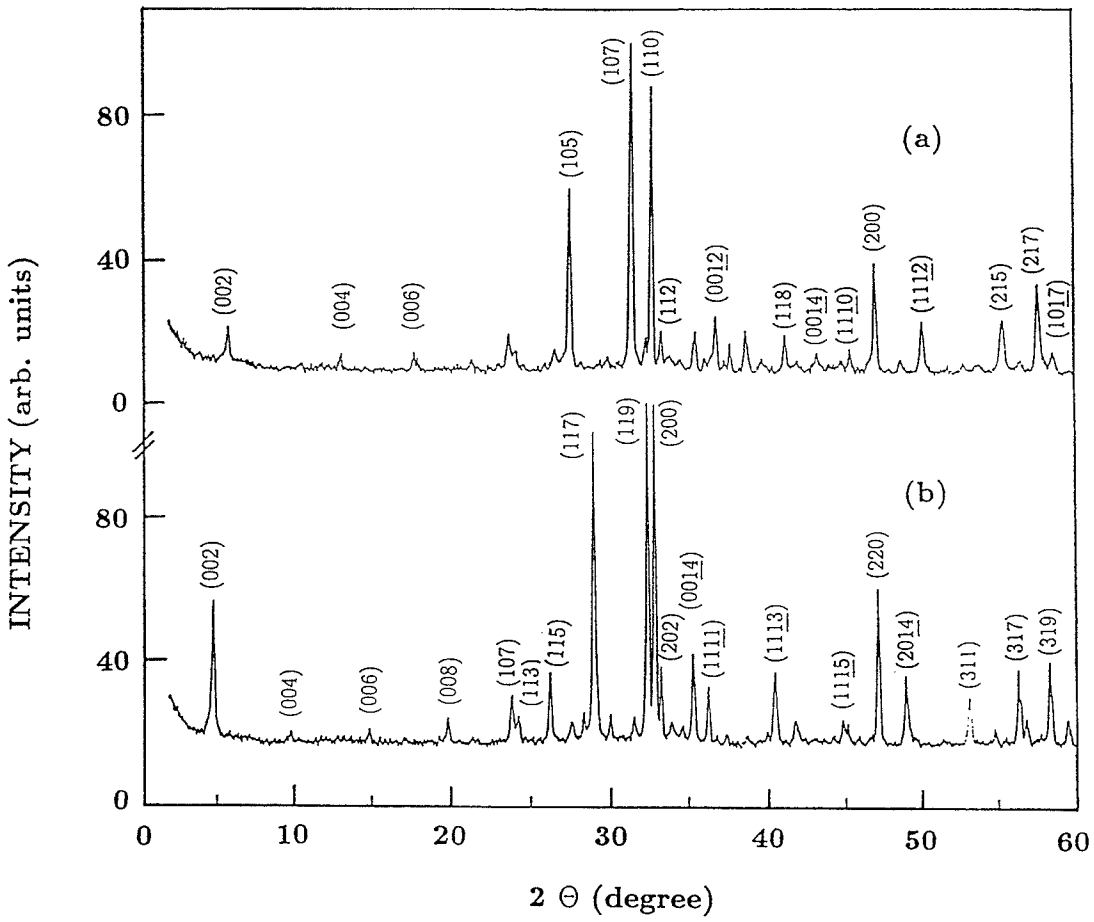

Figure 5.6: The powder x-ray diffraction patterns of (a) $Tl_2CaBa_2Cu_2O_8$ phase and (b) $Tl_2Ca_2Ba_2Cu_3O_{10}$ phase.

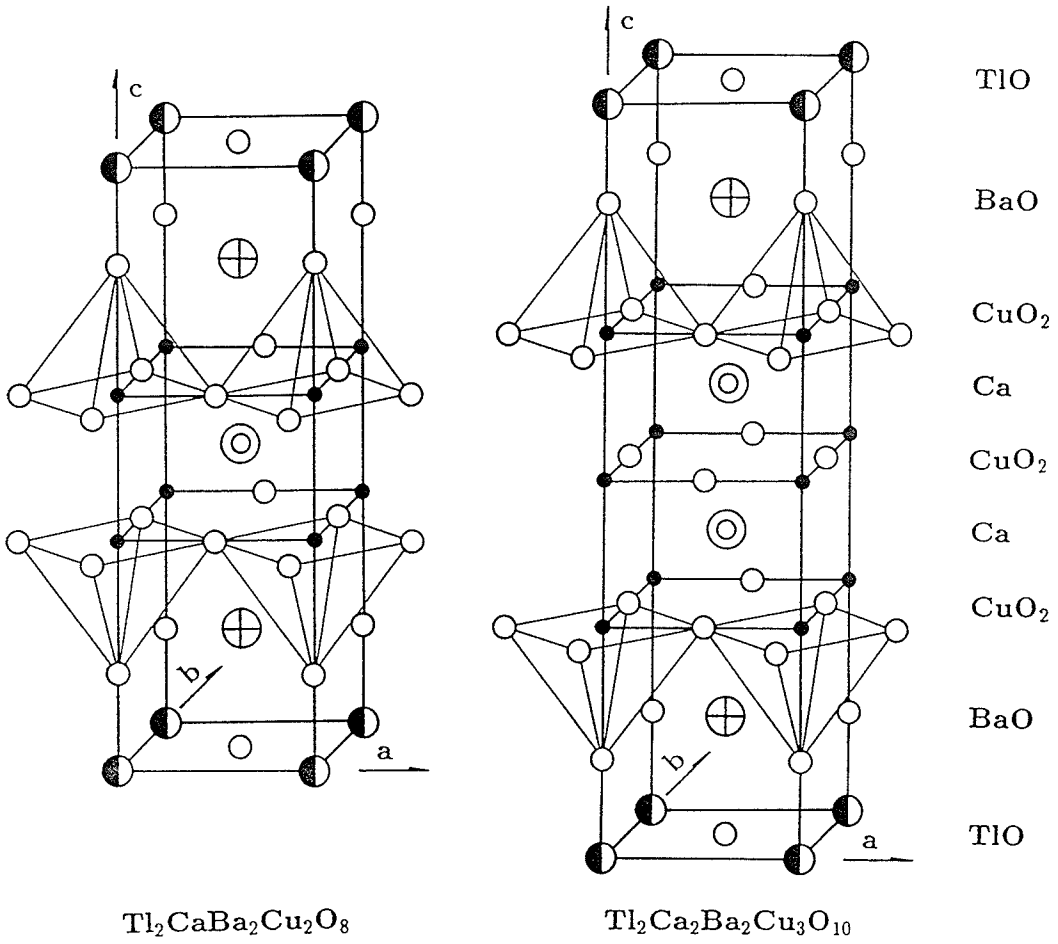

Figure 5.7: The distribution of atoms in the half unit cell of (a) $Tl_2CaBa_2Cu_2O_8$ and (b) $Tl_2Ca_2Ba_2Cu_3O_{10}$.

Table 5.5: Crystallographic data at 295K for $Tl_2CaBa_2Cu_2O_8$; a=3.8526(6), c=29.239(4) Å. Space group: $I4/mmm$.

Atom	Wyckoff Symbol	x	y	z	B(Å^2)
(a)Tl(1)	4e	1/2	1/2	0.21359(2)	1.7(1)
(a)Ba(1)	4e	0.00	0.00	0.12179(3)	0.8(1)
(a)Cu(1)	4e	0.50	0.50	0.0540(1)	0.4(1)
(a)Ca(1)	2a	0.00	0.00	0.00	0.6(1)
(a)O(1)	8g	0.00	0.50	0.0531(2)	0.8(1)
(a)O(2)	4e	0.50	0.50	0.1461(3)	1.5(2)
(a)O(3)	16n	0.604(9)	0.50	0.2185(7)	3.9(11)

yttrium and thallium replaces Cu(1) atoms.

In the crystal structure of 2122, double sheets of corner-sharing square-planar Cu-O_4 groups are oriented parallel to the (001) plane (Fig. 5.7(a)). Cu-O bond distances within the sheets are 1.928Å. There are additional oxygen anions located above and below the double Cu-O_2 sheets at a distance of 2.70Å from the copper cations to form a square-pyramidal site. There are no oxygen anions between the double Cu-O_2 sheets. The sheets are separated by 3.2Å (Cu-Cu distance) by calcium ions which have eight oxygen nearest neighbors; the Ca-O distance is 2.48Å (cubic Ca). The structural features described above are also present in the 123 superconductor except that yttrium replaces calcium.

Barium ions reside just above and below the Cu–O_2 double sheets and are coordinated with nine oxygens. The Ba-Cu-Ca-Cu-Ba slabs in the 2122 phase are sandwiched between two thallium oxygen sheets, giving a layer repeat sequence of ...Tl-Ba-Cu-Ca-Cu-Ba-Tl... along the c direction. The second half unit cell is

Table 5.6: Interatomic distance(Å) for a sample of $Tl_2CaBa_2Cu_2O_8$; a=3.8526(6), c=29.239(4) Å. Space group: $I4/mmm$

	Distance (Å)		
Cu(1)–O(1)×4	1.92773(3)	Tl(1)–O(2)×1	1.978(10)
Cu(1)–O(2)×1	2.699(10)	Tl(1)–O(3)×1	2.031(21)
Cu(1)–Cu(1)(inter-sheet)	3.166(3)	Tl(1)–O(3)×2	2.462(22)
Ba(1)–O(1)×4	2.788(4)	Tl(1)–O(3)×2	3.027(28)
Ba(1)–O(2)×4	2.818(3)	Ca(1)–O(1)×8	2.478(4)
Ba(1)–O(3)×1	2.864(21)		
	Angles (degrees)		
O(1)–Cu(1)–O(1)	178.4(4)	(×2)	
Cu(1)–O(1)–Cu(1)	178.4(4)	(×1)	
O(1)–Cu(1)–O(1)	89.99(1)	(×4)	
O(1)–Cu(1)–O(2)	90.8(2)	(×4)	

displaced by (a/2 and b/2) perpendicular to the c axis. The thallium bonds to six oxygen anions in a distorted octahedral arrangement (Fig. 5.7(a)). It can be seen clearly that there is only one site for Cu, a square pyramidal one. The Cu atoms and surrounding oxygen atoms form two corner sharing two-dimensional Cu-O_2 planes separated by calcium atoms. The Cu-O chains do not exist any more.

5.3.2 The 2223 Phase

X-ray powder diffraction patterns of the 2223 phase were obtained with Cu Kα radiation at room temperature by using the same procedure as that for the YBaCuO system. The pattern reveals a tetragonal unit cell with a=5.4509(9)Å and c=35.59(1)Å. The positions and intensities of the powder lines are shown in Table 5.7. The powder x-ray diffraction pattern is shown in Fig. 5.6(b). The

Table 5.7: Powder x-ray diffraction lines for $Tl_2Ca_2Ba_2Cu_3O_{10}$ (2223). Patterns were obtained with filtered Cu Kα radiation.

h	k	l	2θ	d_{obs}	d_{calc}	I/I_0
0	0	2	4.9	18.02	17.78	40
0	0	4	9.9	8.927	8.899	3
0	0	6	14.9	5.941	5.932	5
0	0	8	19.9	4.458	4.449	10
1	0	7	23.9	3.720	3.718	14
1	1	3	24.3	3.663	3.666	8
1	1	5	26.3	3.391	3.389	23
1	1	7	29.0	3.073	3.072	87
1	1	9	32.4	2.762	2.760	100
2	0	0	32.8	2.725	2.725	80
2	0	2	33.2	2.694	2.694	22
0	0	14	35.3	2.543	2.543	25
1	1	11	36.2	2.479	2.478	16
1	1	13	40.4	2.232	2.228	20
1	1	15	44.8	2.021	2.020	7
2	2	0	47.1	1.927	1.926	45
2	0	14	48.9	1.859	1.859	20
3	1	1	53.1	1.723	1.722	14
3	1	7	56.3	1.632	1.632	22
3	1	9	58.4	1.580	1.580	24
3	1	10	59.5	1.552	1.551	7

presence of a strong (002) powder line corresponding to d$\simeq$ 18 Å ($2\theta \simeq 5°$ with Cu Kα radiation), obviously different to that for the 2122 phase, is a useful diagnostic feature of the 2223 phase [65,68].

The 2223 structure is similar to the 2122 one except that now one additional Cu-O layer and one extra Ca layer are present. Therefore, Ba-Cu-Ca-Cu-Ca-Cu-Ba slabs in the 2223 phase, which replace the Ba-Cu-Ca-Cu-Ba slabs in the 2122 phase, lie between two Tl layers, giving the repeat sequence of ...Tl-Ba-Cu-Ca-Cu-

Ca-Cu-Ba-Tl... along the c direction (Fig. 5.7(b)). The second half unit cell, as in the 2122 phase, is displaced by (a/2 and b/2) perpendicular to the c axis. Since the T_c of the 2223 phase is higher than that of the 2122 phase, it follows that the additional Cu-O layer must also be involved in the superconducting mechanism.

Chapter 6

Resistivity and ac Susceptibility

It is well known that superconductors have two diagnostic characteristics: one is perfect conductivity, namely the resistivity equals zero below T_c and the other is perfect diamagnetism, namely the Meissner effect. In order to distiguish a superconductor from other materials, we have to determine these two characteristics.

6.1 Resistivity

When we measure the resistance of a material, some leads are required in order to connect the sample. This will introduce a certain contact resistance at the joints. For superconductors, contact resistance has to be considered since their resistance is zero in the superconducting state. This problem is circumvented by using the standard four probe technique which eliminates contact resistance[69]. Therefore this technique was chosen to measure the resistance of our samples.

The resistivity as a function of temperature was measured in the homemade stainless steel cylinder and a liquid nitrogen glass dewar discribed in Chapter 3.

The disk pellets, usually 8 mm in diameter, or the bars, usually $8 \times 3 \times 1.5$ mm^3, cut from the pellet were used for the measurements. Four silver points, 0.8 mm diameter, were evaporated onto the surface of the sample as the pads and the four leads were connected to the pads by using indium as a solder. Typical resistivity versus temperature curves of $YBa_2Cu_3O_{7-\delta}$, $Tl_2CaBa_2Cu_2O_8$ and $Tl_2Ca_2Ba_2Cu_3O_{10}$ in the range of 77 K to room temperature are shown in Fig. 6.1 and Fig. 6.2, respectively.

It can be seen clearly from Fig. 6.1 that for the $YBa_2Cu_3O_{7-\delta}$ sample, the resistivity decreases linearly between room temperature, 295 K, and onset temperature, T_{onset}=93 K, as the temperature lowered; this is a metallic behavior. A steep decrease of resistance appears at about 93 K and the resistivity becomes zero at 89 K. The width of transition from the normal to superconducting state, starting at 90% of the resistivity at the onset temperature, is about 1 K. We also found that the transition width and the zero-resistivity temperature change from sample to sample and depend on the heating procedure which produces different oxygen contents.

The same technique was used for the TlCaBaCuO system. A typical result was shown in Fig. 6.2. The profile of the R-T curve is similiar to that for the YBaCuO system except that Tl-system has a higher transition temperature, with T_{onset} = 110K and T_{zero} = 105K for $Tl_2CaBa_2Cu_2O_8$ and T_{onset} = 120K and T_{zero} = 115K for $Tl_2Ca_2Ba_2Cu_3O_{10}$. The measurements of resistivity indicate that $YBa_2Cu_3O_{7-\delta}$, $Tl_2CaBa_2Cu_2O_8$ and $Tl_2Ca_2Ba_2Cu_3O_{10}$ are high-temperature superconductors.

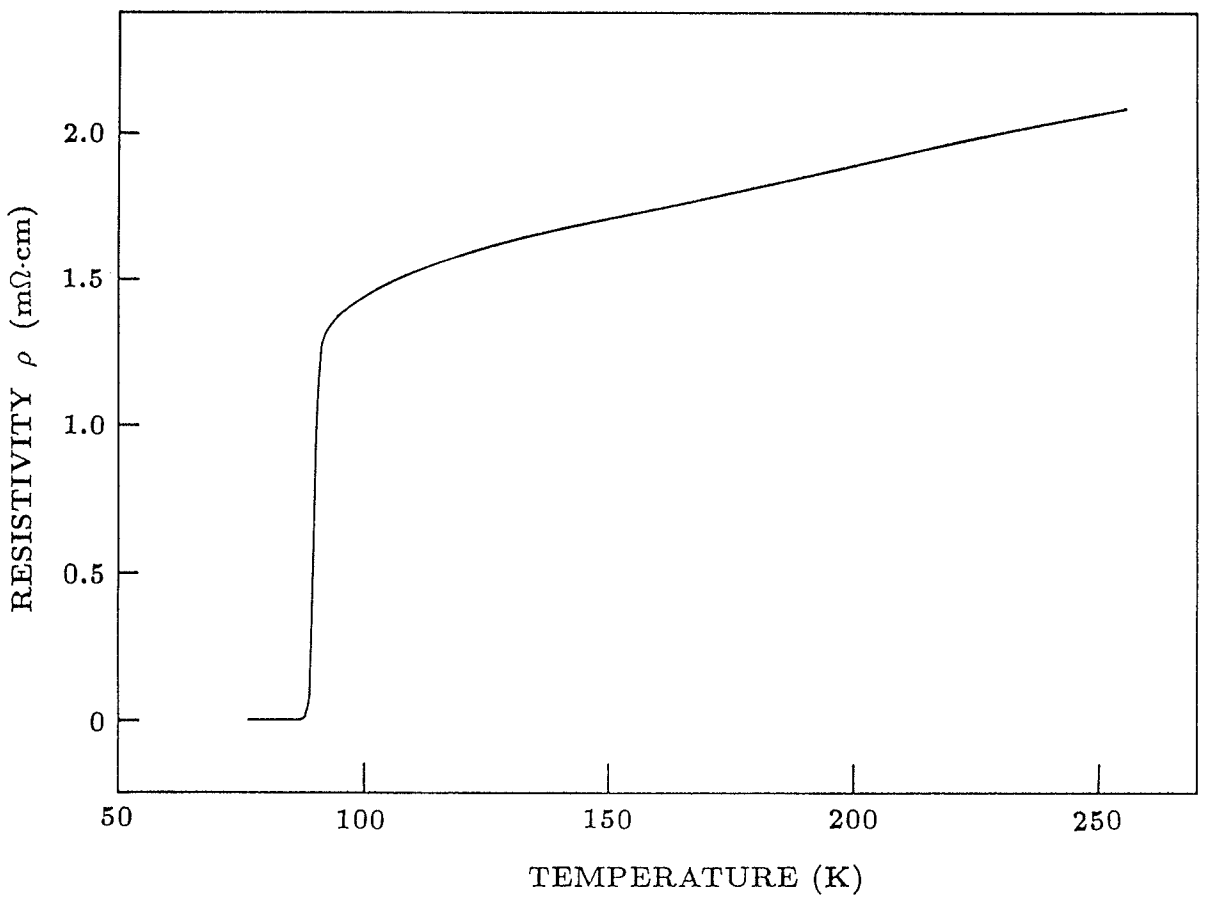

Figure 6.1: The resistivity versus temperarure of $YBa_2Cu_3O_{7-\delta}$.

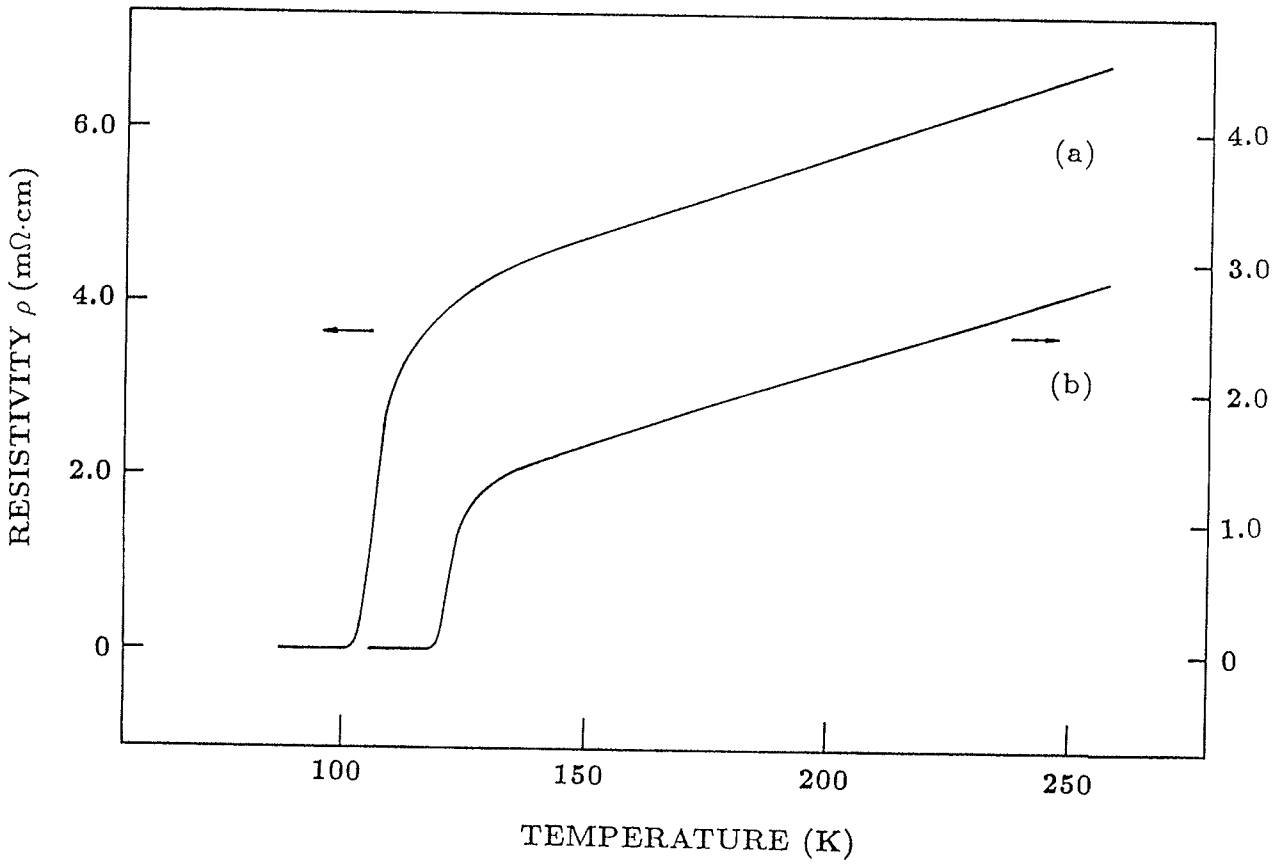

Figure 6.2: The resistivity versus temperarure of (a) $Tl_2Ca_1Ba_2Cu_2O_8$. and (b) $Tl_2Ca_2Ba_2Cu_3O_{10}$.

6.2 ac Susceptibility

There are various methods, such as ac susceptibility [70], dc magnetization [71], SQUID [72] and so on, that are used to measure the magnetic properties and to determine the superconducting transition. Among these, the ac susceptibility technique became popular due to both experimental simplicity and versatility with regard to sample size and shape. It also possesses a distinguishing trait, namely the real component, χ', and the imaginary component, χ'', of the complex χ represent different physical quantities. Thus we can examine the superconducting nature from different viewpoints. As is well known, the change of χ' relative to temperature is caused by the Meissner shielding effect and indicates the phase transition between the normal and superconducting states. Meanwhile, χ'' is proportional to the energy dissipation in a sample located in a periodically varying magnetic field.

If the measurements are performed without an externally applied dc magnetic field, H_{app}=0, the complex quantity measured is the initial magnetic susceptibility denoted by $\chi(T) = \chi'(T) + i\chi''(T)$. When an applied dc magnetic field, H_{app}, is present and if H_{app} is parallel to h_o, where h_o is the ac field, the quantity measured is the differential ac magnetic susceptibility denoted by $\chi_H(T) = \chi'_H(T) + i\chi''_H(T)$. Then $\chi'_H(T)$ and $\chi''_H(T)$ give different information on the magnetic properties of materials.

6.2.1 Complex Susceptiblity of Conventional Superconducting Materials

In 1963, Maxwell and Strongin first measured the complex ac magnetic susceptibility, $\chi = \chi' + i\chi''$, of the conventional superconductor Sn and found that the real part χ' of χ decreases monotonically from a small value in the normal state to $-1/4\pi$ in the superconducting state as the temperature is lowered; χ' has a sharp drop at T_c. The imaginary part χ'' of χ monotonically goes from its level in the normal state to essentially zero in the superconducting state or has a maximum at the midpoint of the transition which depends on the structure of the materials. An average-conductivity filamentary model was proposed by Maxwell and Strongin to explain these results [70] and is generally accepted by many other authors [73,74,75]. This model is based on the behavior of the complex susceptibility of a normal metal. For a cylindrical rod of metal with an applied ac magnetic field $h = h_o e^{-i\omega t}$ parallel to the rod axis the susceptibility is given by [76]

$$\begin{aligned} \chi &= \chi' + i\chi'' \\ &= 1/4\pi \left[-1 + \frac{2J_1(ka)}{kaJ_o(ka)} \right] \end{aligned} \tag{6.1}$$

where a is the cylinder's radius, k=(1 + i)/δ, and δ is the skin depth related to the electrical conductivity σ as $\delta = c/\sqrt{2\pi\sigma\omega}$. $J_0(ka)$ and $J_1(ka)$ are Bessel functions. Therefore χ'' exhibits a maximum for $a/\delta \simeq 1.8$ (Fig. 6.3).

This model suggested that when a/δ increases then χ'' increases and has a

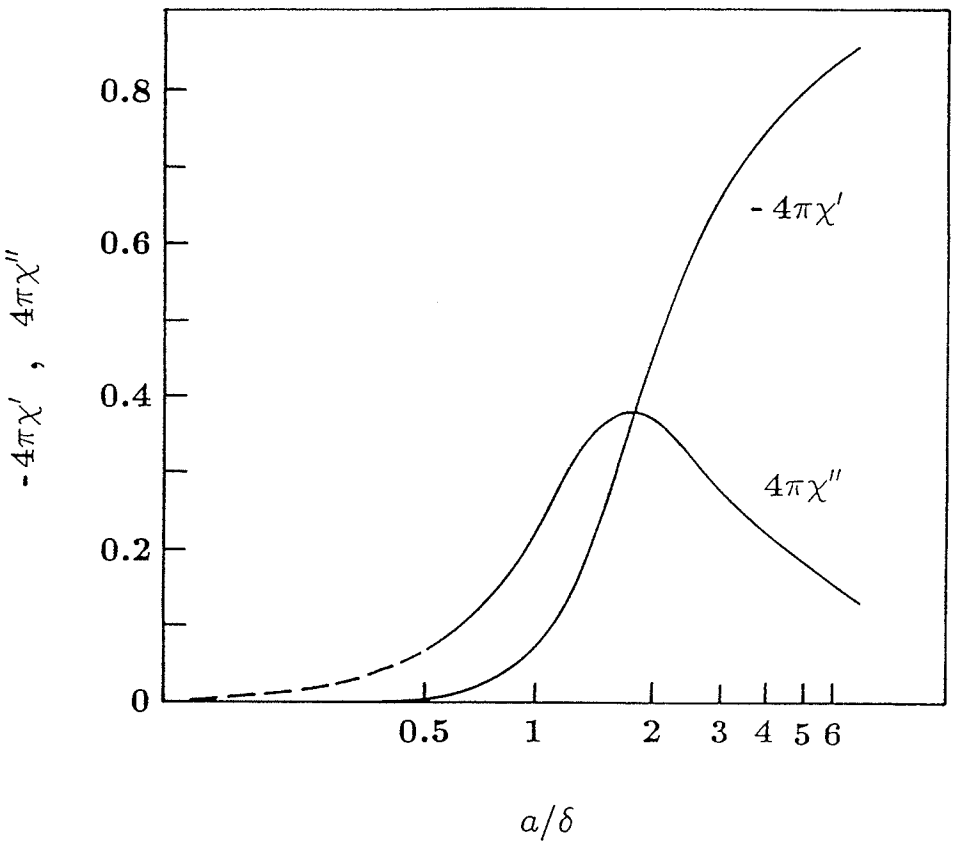

Figure 6.3: Susceptibility, $4\pi\chi'$ and $4\pi\chi''$, as function of a/δ for a normal conducting cylinder of infinite length and radius a. δ is the normal state skin depth.

maximum at a/δ=1.8. On lowering the temperature, the physical picture is that some grains become superconducting, the increased average current then results in increased dissipation, that is χ'' increases. When the temperature is lowered further eddy-current shielding becomes dominant, resulting in a decreased χ''. Thus, these two competing mechanisms produce a maximum in χ'' at the midpoint of the transition in the filamentary structure.

After Maxwell and Strongin's work[70], many investigations of the ac magnetic response of superconductors were carried out[73,77]. Most of them were mainly focused on the response to a small low-frequency ac field, $h(t) = h_o \sin\omega t$. It has been revealed that the ac susceptibility strongly depends on the amplitude h_o of the ac field. The superconducting transition width of χ' is appreciably broadened as h_o increases, but the onset temperature of the transition does not change significantly. Although χ'' has an asymmetric shape in the χ'' versus T curve the peak is located at close to the inflection point of χ' but moves to the lower temperature side as h_o is increased. To understand these results, several models were proposed such as surface and boundary effects [78], weak coupling due to a multiconnected Josephson network [79] a BCS approach [80], and so on.

The BCS model indicates that the average conductivity model is not able to explain the observed χ'' behavior. Physically, the peak of χ'' results from two competing processes. The first one is the great ability of the supercurrent to be accelerated and is favoured when $\lambda >> a$ (where λ is the penetration depth and a is the radius of cylindrical material). The second one is the Meissner effect which reduces the field amplitude in the superconducting material. The appearance of

the χ'' peak at T_c does not depend on the presence of defects or impurities and is only associated with the bulk superconducting transition.

All of these models have their own successes and shortcomings. The average conductivity model is capable of accounting for several facets of the zero-field ac susceptibility data, i.e. $\chi'(T)$ and $\chi''(T)$, but appears incapable of explaining frequency and h_o effects on the loss peaks in χ''. The BCS model indicates that the peak of χ'' is associated with the bulk superconducting transition, but it can not interpret some cases where there is no peak in the χ'' versus T curve.

The discrepecies among these models are mainly in the interpretation of the peak of χ'' and whether or not the zero-field magnetic susceptibility data can be used as a criterion to discriminate between bulk and non-bulk superconductivity or to distinguish between filamentary and nonfilamentary structure [81]. The experimental results show the mechanism responsible for the loss is not well understood at least for some samples.

6.2.2 AC Susceptibility of High-T_c Superconductors

The complex ac susceptibility was measured for samples of both the YBaCuO system and the TlCaBaCuO system at 3.7 kHz in a field of 0.12 Oe root-mean-square (rms) as a function of temperature. In the YBaCuO system two samples were chosen. One of them was only heated once at 900°C for six hours and is denoted as sample (a). The other one was heated twice at 800°C for four hours and at 970°C for six hours and is denoted as sample (b). Both of them were furnance cooled under 1 atmosphere oxygen pressure. The real component χ' and imaginary component χ'' in the temperature range of 65-100K are shown in Fig.

6.4(A) and (B), respectively.

The χ' scale (in unit of $1/4\pi$ emu/cm^3) of Fig. 6.4(A) has been normalized to the diamagnetic response expected for full shielding of an ac field by a superconducting disk measured along its diameter. The diameter-to-thickness ratio of the disk is 6 for sample (a) and 5 for sample (b). The calibration is expected to be accurate to within 5% or better. The imaginary components are uncalibrated recorder tracings.

It is clearly seen from Fig. 6.4(A) that the real part χ' monotonically decreases from nearly zero in the normal state to its limiting value $-1/4\pi$ in the superconducting state as the temperature goes down; there is a sharp drop at T_c for sample (b). The double-step nature of the transition to the superconducting state seen in sample (a) is characteristic of all samples prepared similarly. Sample (b) has such a narrow transition that the two steps have essentially merged in the recorded data, although under suitable measuring conditions they can be resolved. The first step may correspond to the bulk, that is, within the grains and the second step to the grain boundaries[82].

The imaginary component χ'' for sample (a) (Fig. 6.4(B)) shows that when the temperature decreases the maximum loss occurs at the temperature corresponding to the inflection point of χ'. The peak of χ'' for sample (b) is more sharp and narrow than that for sample (a). It is also at a higher temperature than for sample (a). The ac susceptibility of samples of the TlCaBaCuO system have the same feature.

The variation of χ' and χ'' for sample $YBa_2Cu_3O_{7-\delta}$ as the magnitude of the

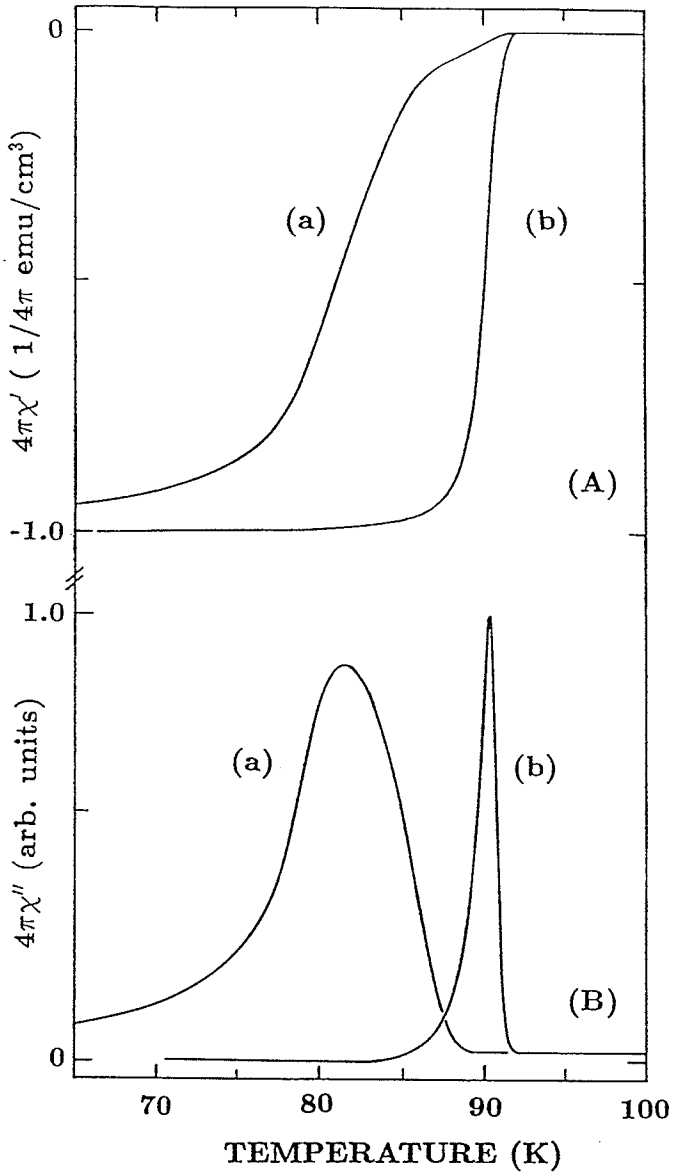

Figure 6.4: (A) the real part and (B) the imaginary part of the ac susceptibility at 3.7 kHz and 0.12 Oe rms for samples (a) and (b) as indicated in the figure.

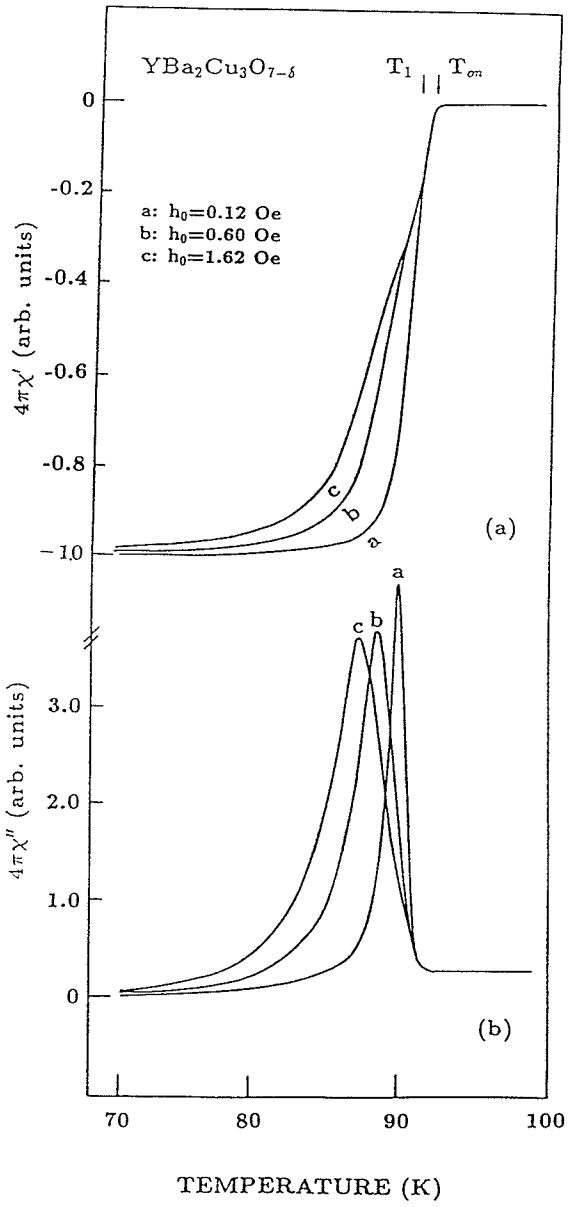

Figure 6.5: The dependence of ac susceptibility, of (a) $4\pi\chi'$ and (b) $4\pi\chi''$, on magnetic field h_0 for $YBa_2Cu_3O_{7-\delta}$.

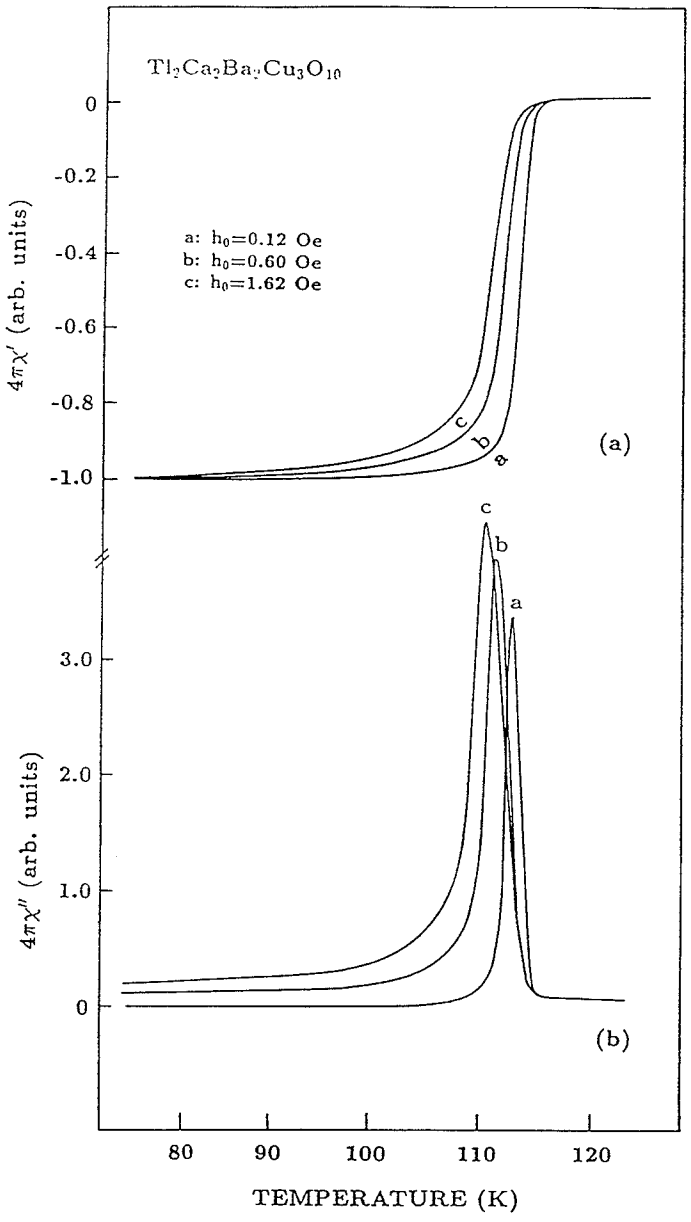

Figure 6.6: The dependence of ac susceptibility, (a) $4\pi\chi'$ and (b) $4\pi\chi''$, on magnetic field h_0 for $Tl_2Ca_2Ba_2Cu_3O_{10}$.

ac magnetic field, h_o, changes is shown in Fig. 6.5(a) and (b) respectively. Both χ' and χ'' are sensitive to the amplitude of the ac field h_o. The transition width of χ' is broadened but the onset temperature of χ', T_{on}, remains almost a constant as h_o is increased. If we carefully examine Fig. 6.5(a), it can be found that the high temperature part of χ' during the transition, between T_{on} and T_1, is basically independent of h_o whereas the low temperature part of χ', below T_1, is sensitive to h_o and increases as h_o increases. The onset temperature of χ' is approximately equal to or a little lower than the T_0 at which the resistance becomes zero. Similar results have been reported by others [83,84]. This means that there are very few parts of the superconductor where the magnetic flux is expelled from the sample above T_0. This suggests that the supercurrent is flowing through some filamentary circuits at T_0 along the boundaries and surfaces of the grains. Below T_0 three-dimensional networks are gradually formed with decreasing temperature and give rise to the decrease of χ'.

The position of the χ'' peak moves toward the lower temperature side and the value of the maximum decreases as h_o increases for the samples in Fig. 6.5(b). The same features, in the variations of χ' and χ'' with the ac magnetic field h_0, can be seen for samples of $Tl_2Ca_2Ba_2Cu_3O_{10}$ in Fig. 6.6(a) and (b), except that now the value of the χ'' peaks increase as the temperature is lowered in this sample.

These characteristics of χ' and χ'' suggest that the high-T_c superconductors most likely are characterized by the weak-link model, that is, they consist of two parts even when the materials are a single phase[79]. In one part χ' and χ'' are independent of h_o, possibly inside the grains of the materials. In the other

part, χ' and χ'' are sensitive to h_o and may relate to the boundaries or surfaces of the grains which form a weak-link network multiply connected via Josephson junctions. The contribution of the network to χ' and χ'' lies mainly in the lower temperature range. These considerations agree with the weak-coupling model [79].

The common features that χ' and χ'' are sensitive to the ac field h_0 and that the peak of χ'' broadens and moves to lower temperatures as h_0 is increased in high-temperature superconductors, have been seen in some conventional superconductors. These features result from a weak-link structure in which the shielding current flows in a loop which includes Josephson junctions. For large h_0, the magnetic flux passes the Josephson junction every cycle and an effective resistance results. This may be the origin of χ'' [85].

To confirm this idea, comparison of the ac susceptibility between pellets and powdered samples was made. The bar sample (about $6 \times 1.5 \times 2$ mm) used to measure χ' and χ'' as shown in figs. 6.5 and 6.6 was ground twice. It was first coarsely crushed in an agate mortar by pestle and the particles were put into a teflon tube, 2 mm in diameter. After the ac susceptibility measurements were made the coarse powder was ground again in the agate mortar to a fine powder with particle sizes ranging from 3 to 30 μm; most were 10 to 20 μm. The powders were again put into the teflon tube and the susceptibility was measured.

The χ' and χ'' of the coarse powder for $YBa_2Cu_3O_{7-\delta}$ varies with temperature and various h_o are shown in Fig. 6.7(a) and (b) respectively. The magnitude of χ' is smaller than the bar sample and deceases as h_0 increases. The peak of

χ'' become smaller and still depends on h_0. But the onset temperature has no significant change. Many of the grains are separated on coarse crushing but some grain clusters remain. The weak-coupling network between the grains was only partially destoryed in the coarse grinding.

Fig. 6.8(a) and (b) show the χ' and χ'' versus temperature at various h_0 for finely-powdered $YBa_2Cu_3O_{7-\delta}$ sample, respectively. It can be clearly seen this time that the χ' of the finely-powdered sample is essentially independent of h_o over the whole temperature range, but the magnitude is about 10 times smaller than for the bar sample. The onset temperature remains nearly the same as that of the bar sample. The transition width is broadened. The peak in the χ'' versus T curve completely disappears [86].

We suppose that in the finely powdered sample not only most grains are separated from each other but also the grain size is reduced. Hence the weak coupling between the grains is completely destroyed. The reduction of grain size also causes a decrease in χ'.

Similar experiments have been done for $Tl_2Ca_2Ba_2Cu_3O_{10}$. The same results have been obtained and shown in Fig. 6.9. The similar property has been observed by others [87].

The results of powdered samples are now compared with the susceptibility of our single crystals. The ac susceptibilities, χ' and χ'', of a single-crystal $YBa_2Cu_3O_{7-\delta}$ are shown in Figs. 6.10(a) and (b), respectively. They are similar to the finely-powdered samples; both have a smaller magnitude and broadened transition in χ'. The peak of χ'', usually seen in the pellet samples, now disap-

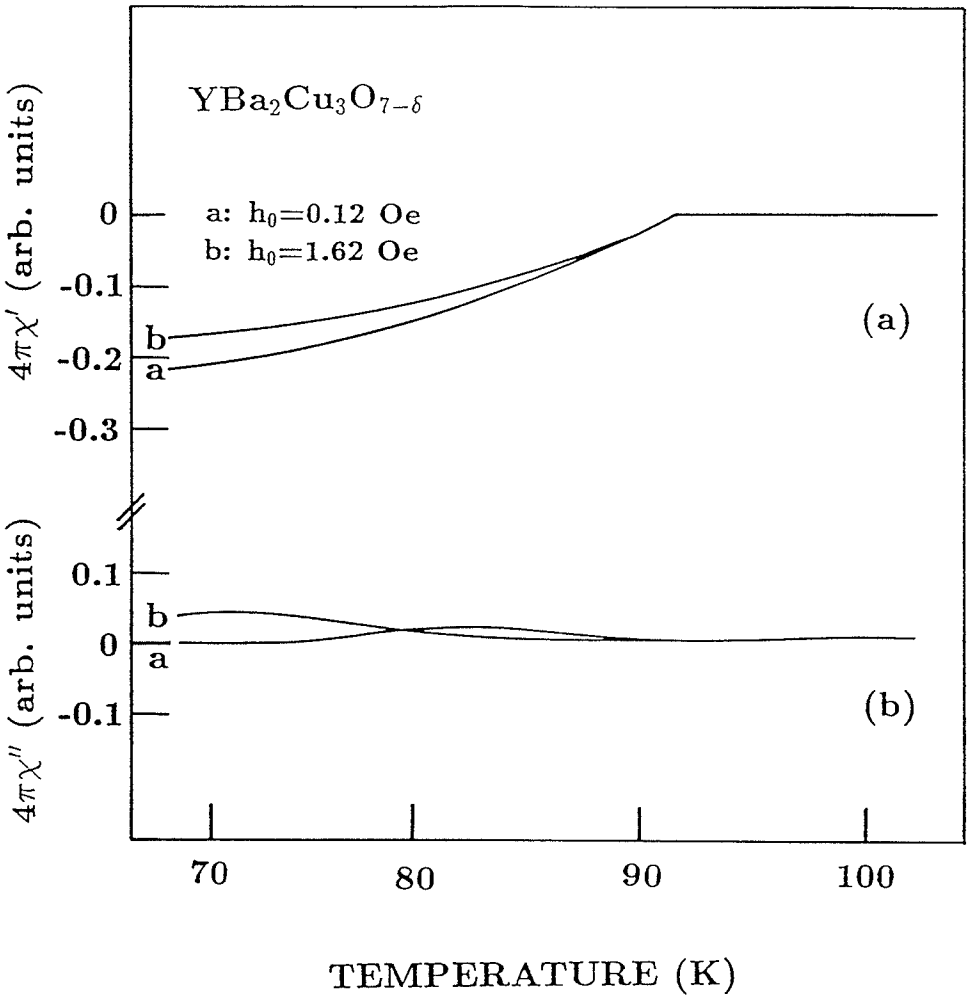

Figure 6.7: Susceptibility, (a) $4\pi\chi'$ and (b) $4\pi\chi''$, versus temperature for the coarse powdered sample of $YBa_2Cu_3O_{7-\delta}$.

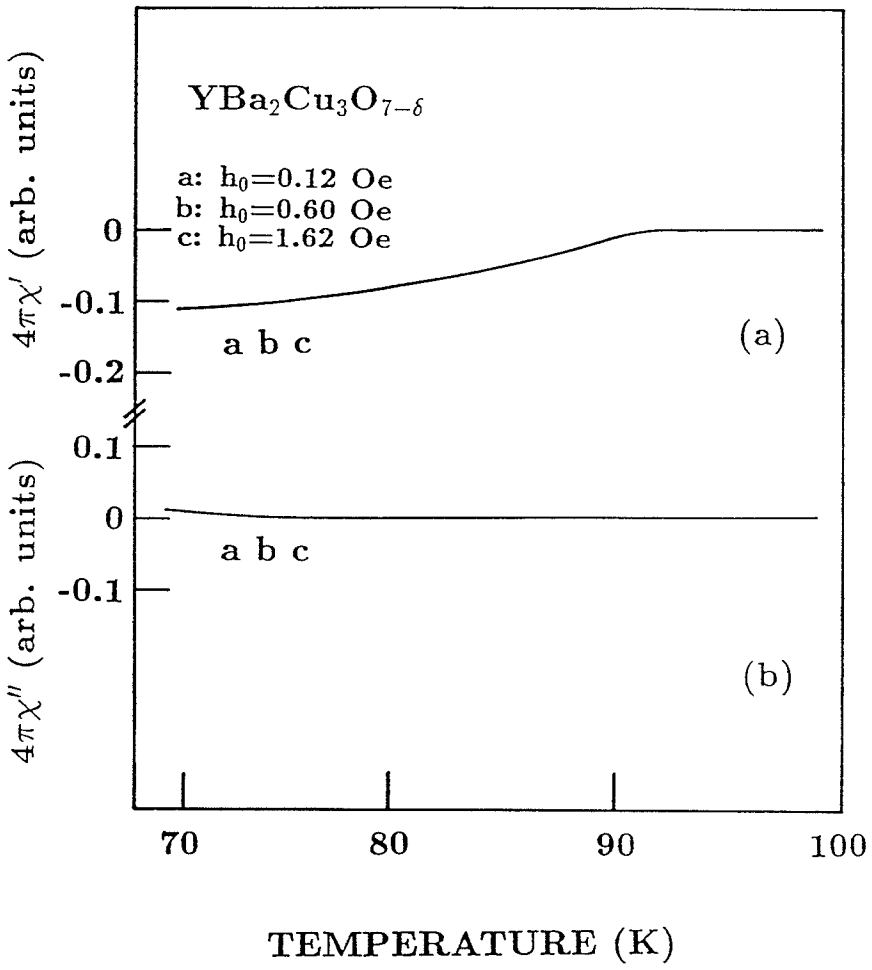

Figure 6.8: Susceptibility, (a) $4\pi\chi'$ and (b) $4\pi\chi''$, versus temperature for the finely-powdered sample of $YBa_2Cu_3O_{7-\delta}$.

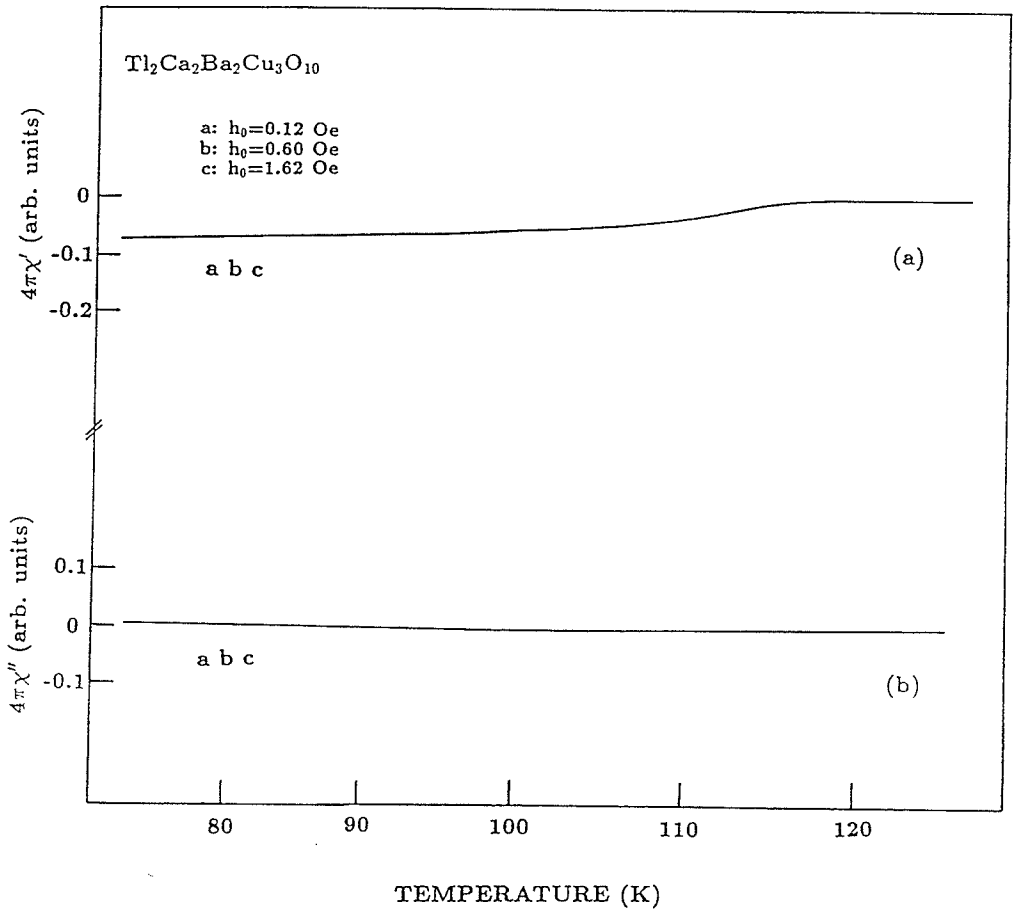

Figure 6.9: Susceptibility, (a) $4\pi\chi'$ and (b) $4\pi\chi''$, versus temperature for finely-powdered sample of $Tl_2Ca_2Ba_2Cu_3O_{10}$.

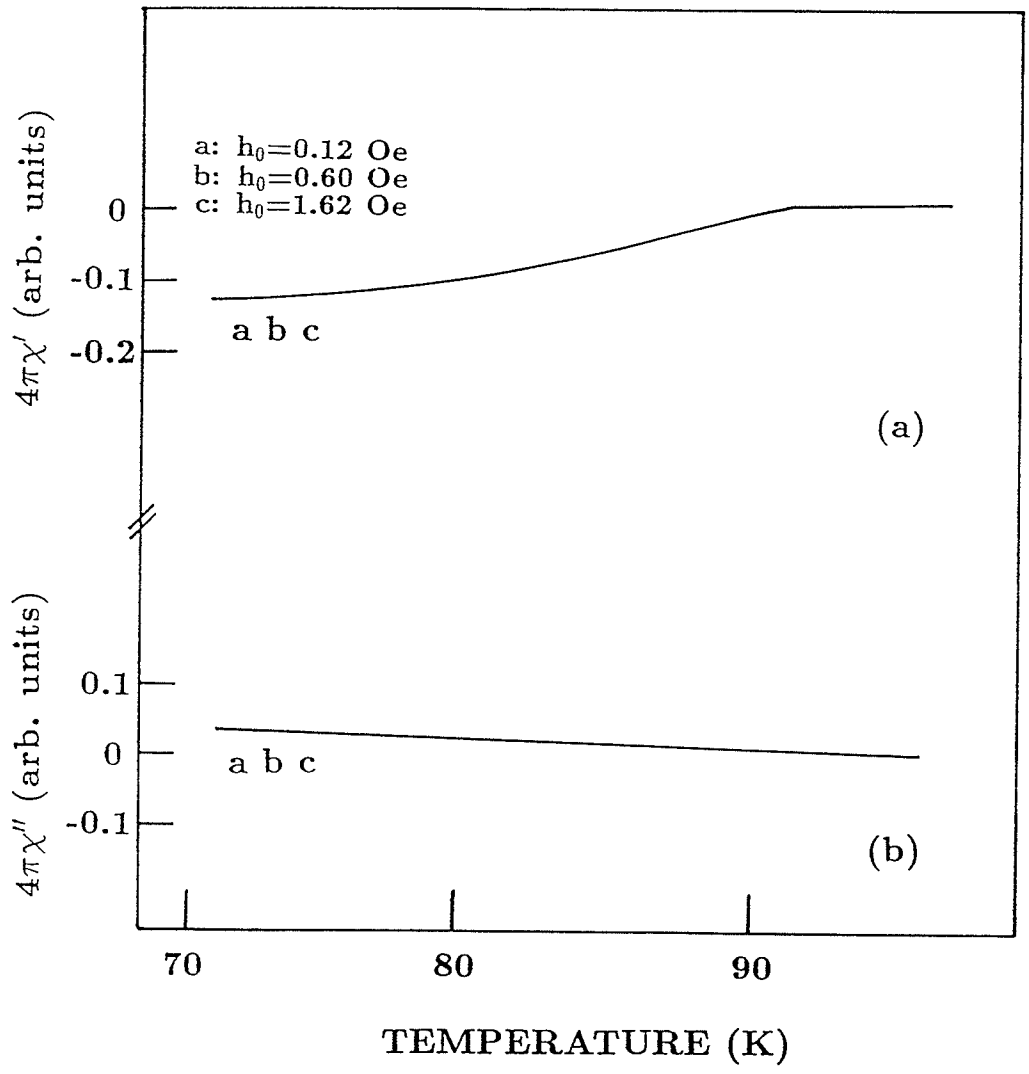

Figure 6.10: Susceptibility, (a) $4\pi\chi'$ and (b) $4\pi\chi''$, versus temperature for single crystal of $YBa_2Cu_3O_{7-\delta}$.

pears. As expected, the single crystals separate from each other, that is, there is no coupling between the single crystals.

These results strongly support the above discussion, that is the larger diamagnetic signal associated with a bar sample is sensitive to h_o and the peak of χ'' is to be attributed to the grain boundaries which form a weak coupling via Josephson junctions. After powdering, this weak coupling is destroyed and only the intrinsic bulk superconducting grains are left. The Meissner effect is only present in the individual particles and therefore the magnitude of χ' for a powdered sample becomes smaller than for a bar sample. Thus, the grain boundaries play a important role in this kind of superconductor. Improvements in the boundary conditions may enhance the critical current.

6.2.3 Summary

The experimental data presented here reveal that high-T_c materials and conventional superconductors are both perfect conductors and perfect diamagnets. They have many susceptibility characteristics in common. High-T_c superconductors have magnetic properties similar to those of conventional superconductors. Therefore, it is reasonable to attribute these properties to the same origin. Results on powdered high-T_c samples reveal that grain boundaries play an important role in determining χ' and χ'' during the superconducting transition. As a consequence, low critical currents may be usually expected for high-T_c superconductors.

Chapter 7

Mössbauer Studies

Mössbauer spectroscopy has been known as one of the very useful tools in fundamental solid state physics. The main Mössbauer parameters obtained from the spectra are the isomer shift, the quadrupole splitting, the magnetic hyperfine field and the recoil-free fraction. The electronic structure of a relevant atom is deduced from the value of the isomer shift and in the usual ionic case the valency state can be determined unambiguiously. If a magnetic hyperfine splitting is observed, it is very helpful in confirming the existence of magnetic order. From the temperature dependence of the hyperfine field the magnetic transition temperature can be estimated. Based on the recoil-free fraction and the structure parameters the site occupancy by the atoms in the compounds can be assigned, at least in principle.

To take Mössbauer spectra of high-temperature superconductors, we have to introduce a small amount of ^{57}Fe into the lattice as microscopic local probe since there is no Mössbauer isotope in the material in most cases. The Mössbauer parameters obtained from ^{57}Fe doped superconductors provide some information

about the valence, site occupancy and effect of doped ^{57}Fe atoms on T_c, magnetic ordering at low temperature and so on. This information complements some other experimental results (x-ray diffraction and susceptibility). Also these data may shed light on the valencies and electronic structure of the copper and oxygen ions. In addition, the coexistence of magnetic ordering and superconductivity may help in arriving at the mechanism operating in high-$T_c$materials. Mössbauer experiments have been done from room temperature down to the pumped liquid helium for both the 123 and the TlCaBaCuO systems.

7.1 YBaCuO System

7.1.1 Absorber

To make Mössbauer absorbers of $YBa_2(Cu_{1-x}Fe_x)_3O_{7-\delta}$, 93% and 45% ^{57}Fe enriched Fe_2O_3 were used for x=0.015 and x=0.05, x=0.10, respectively. For economic reasons and the small amount of Fe_2O_3 in the materials, the starting chemicals were mixed in a mortar by pestle instead of ball milling. The mixture was pelletized into disks 8 mm in diameter and about 1.5 mm in thickness, preheated at 900°C for 8 hours, reground and heated at 920°C for 6 hours, then furnace cooled under flowing oxygen. To avoid the effect of unexpected factors, samples with various x were heated in the same batch.

X-ray diffraction patterns indicated that all the samples are mainly single phases. Usually the impurity phases were Y_2BaCuO_5 and CuO. The lattice constants a and b change as x increases, when x=0.1, the basal plane lattice constants become a=b. As is clear from Fig 7.1, the ac susceptibility measurements show

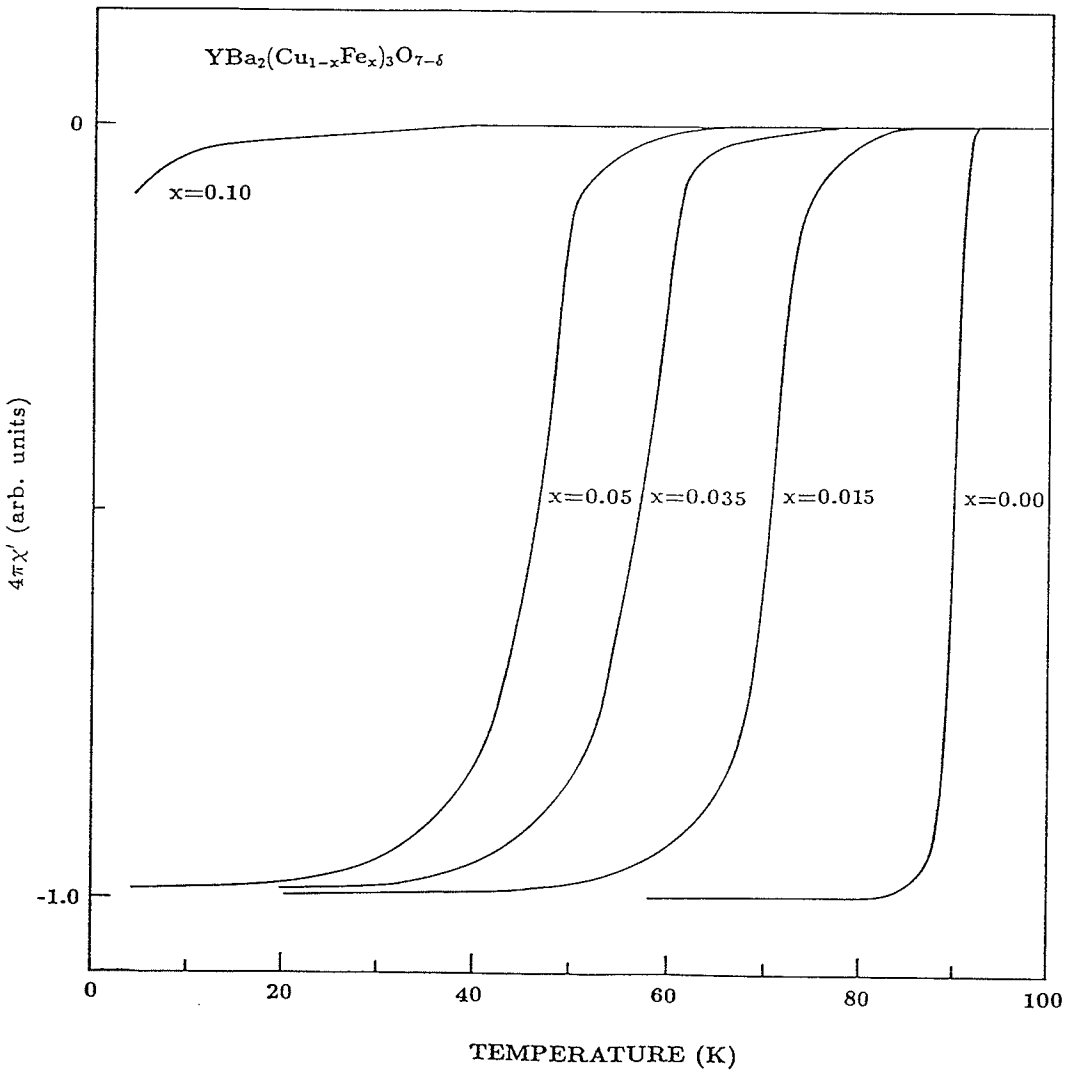

Figure 7.1: The real part of the ac susceptibility at 3.7 kHz and 0.12 Oe rms as a function of temperature for $YBa_2(Cu_{1-x}Fe_x)_3O_{7-\delta}$.

that the transition temperature decreases and the transition width broadens as x increases.

Powders of about 60 mg each were ground from the pellets, mixed with about 400 mg of Benzophone ($(C_6H_5)_2CO$, melting point, 48°C), and heated together at about 60°C. Then the homogeneous mixture was fixed into a copper ring, 19 mm in inner diameter and 21 mm in outer diameter, by a die in a press, this ring fitted the sample holder in the Mössbauer spectrometer. This absorber is easy to handle for both room and low-temperature measurements.

7.1.2 Mössbauer Spectra at Room Temperature

Room-temperature transmission Mössbauer spectra of $YBa_2(Cu_{1-x}Fe_x)_3O_{7-\delta}$ for x=0.015, 0.05 and 0.10 were taken using a conventional constant-acceleration Mössbauer spectrometer; they are shown in Fig. 7.2 by the dots. The solid curves in the figure are the computer fits. Similar spectra have been reported by others [88,89,90,91]. The spectra clearly show the presence of electric-quadrupole interactions. A satisfactory fit can be obtained in terms of three quadrupole doublets which we enumerate according to decreasing areas for the x=0.015 spectrum. Mössbauer parameters obtained from computer fits are listed in Table 7.1.

Because of the similarity of the electric configuration and atomic size, Fe is most likely to go into Cu sites rather than Y or Ba sites. In the structure of $YBa_2(Cu_{1-x}Fe_x)_3O_{7-\delta}$ there are two kinds of Cu sites, Cu(1) chain sites and Cu(2) planar sites. If Fe atoms substitute for Cu ions randomly among the Cu(1) and Cu(2) sites, the Mössbauer spectrum would be a superposition of two quadrupole doublets with an area ratio about 1:2, assuming equal recoilless fractions. That is,

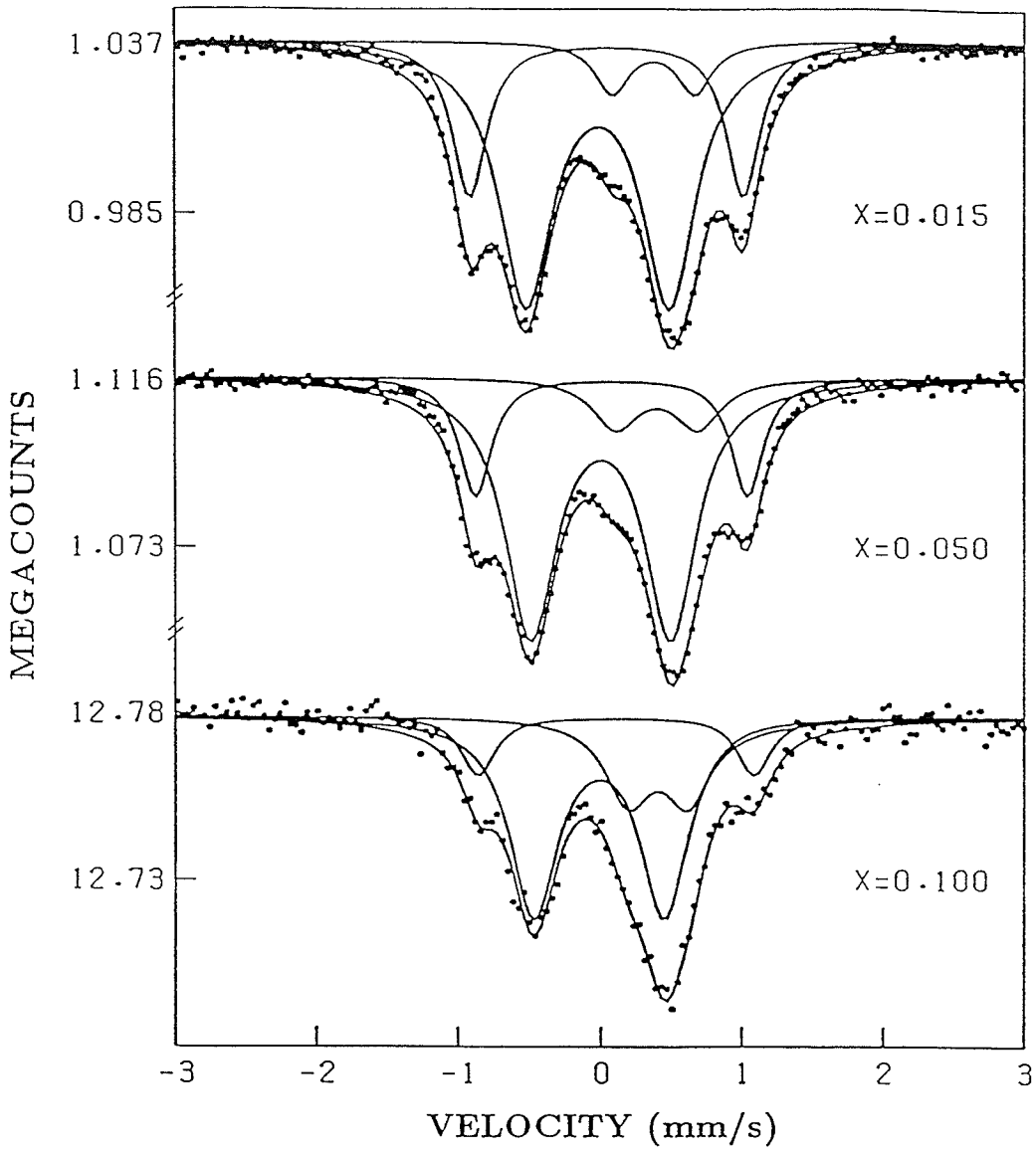

Figure 7.2: Room temperature Mössbauer spectra of $YBa_2(Cu_{1-x}Fe_x)_3O_{7-\delta}$ for (a) x=0.015, (b) x=0.05 and (c) x=0.10.

Table 7.1: Isomer shifts, δ, relative to α-Fe, quadrupole splitting, Δ, linewidth(Γ), all in mms^{-1}, and relative areas(A), for doublet 1, 2 and 3 of the room temperature Mössbauer spectra of $YBa_2Cu_3O_{7-\delta}$. The errors in δ are ± 0.03, in Δ, ± 0.03, in Γ, ± 0.02 and in A, ± 2.

doublet	X=0.015				X=0.05				X=0.10			
	δ	Δ	Γ	A	δ	Δ	Γ	A	δ	Δ	Γ	A
1	-0.0	1.00	0.45	66	-0.01	0.97	0.43	68	-0.03	0.91	0.40	62
2	0.04	1.93	0.29	25	0.07	1.90	0.29	23	0.09	1.94	0.28	13
3	0.36	0.58	0.29	9	0.36	0.57	0.28	9	0.38	0.42	0.39	25

one half as many Fe atoms would occupy the chains as the planes. Now the spectra in Fig. 7.2 show the presence of at least three doublets with different quadrupole splittings. For each value x, the spectra comprise three symmetric Lorentzian doublets, with quadrupole splittings of form by $\Delta = (1/2)eQ|V_{zz}|\sqrt{1+\eta^2/3}$. Here Q is the nuclear quadupole moment of the exited state of ^{57}Fe, V_{zz} is the principal component of the electric field gradient and $\eta = (V_{xx} - V_{yy})/V_{zz}$ is the asymmetry parameter. Doublet 1 accounts for close to two-thirds of the spectral area in all three compounds which appears to imply that it is associated with Fe in the square-pyramidal coordination of Cu(2) sites. In turn, doublets 2 and 3 would seem to be associated with the square-planar, Cu(1) sites. The splitting $\Delta_3 \simeq 0.6 mms^{-1}$ is typical of octahedrally coordinated Fe^{3+}, implying that doublet 3 may correspond to Cu(1) sites at which all nearest neighbour sites are occupied including those oxygen sites that are normally vacant in $YBa_2Cu_3O_{7-\delta}$.

Thermogravimetric measurements of $YBa_2(Cu_{1-x}Fe_x)_3O_{7-\delta}$ by Tarascon et al[89] indicated that the substitution of Fe for Cu most likely occurs on both copper sites and that at large x the substitution preferentially takes place on the

Cu(2) sites. This result supports our site assignment. The substitution of Fe for Cu could introduce extra oxygen into the O(5) site, normally vacant in the superconducting phase. It would also cause a change of the occupancy on the O(1) sites and the oxygen vacancy ordering in substituted samples then will be distorted. The degree of disorder of the vacancies results in a much lower T_c. By contrast, in the orthorhombic-tetragonal transition of $YBa_2(Cu_{1-x}Fe_x)_3O_{7-\delta}$, the total oxygen content does not fall below 7 and appears to become slightly greater than 7 for the larger x [90]. This makes the octahedral coordination of Fe in substituted samples more likely.

Simple point-charge calculations of the electric field gradients for various oxygen configurations surrounding Fe in Cu(1) and Cu(2) sites[92] showed that the quadrupole splitting of Fe in Cu(2) sites should be only about half of the splitting of Fe in the Cu(1) sites. The average values of the quadrupole splitting for Cu(1) sites with 3 oxygen configurations (zero, one or two extra oxygens in the plane) and for Cu(2) sites are 1.95 mms^{-1} and 1.10 mms^{-1} respectively [93]. This calculation agrees with the above site assignment.

Mössbauer studies of Fe-doped $YBa_2(Cu_{1-x}Fe_x)_3O_{7-\delta}$ have been reported by several research groups. Each group obtains slightly different spectra and present somewhat different interpretations. The discrepancies amongst them are mainly in the relative intensities of the doublets. Probably the different preparation procedures used, which determine the oxygen content, are the source. However, the quadrupole splitting values of the three doublets agree with each other [91,94,95,96]. Different site assignments have also been suggested. Some use 2

doublets[95] or 4 doublets[97,98] to fit the spectra, and some propose that Fe only occupies the Cu(1) sites [99].

The difference in the quadrupole splittings between the main doublets 1 and 2 can be attributed to Fe atoms with different nearest neighbours. Further experiments and other techniques are needed to clarify the various proposed site assignments.

The isomer shift of doublet 3 ($\simeq$0.37 mm s^{-1}) is typical of high-spin Fe^{3+} with octahedral coordination. The value for doublets 1 and 2 can be regarded as low spin Fe^{2+}, high spin Fe^{4+} or low spin Fe^{3+} [100]. However, the oxidizing synthesis conditions used makes the presence of Fe^{2+} very unlikely [93].

The quadrupole splitting of doublet 2, $\Delta_2 \simeq 1.9$ mm s^{-1}, is unusually large for high-spin Fe^{3+}, therefore Δ_2 can be attributed to Fe^{3+} situated in the highly atypical (for Fe^{3+}) coordination of the chain Cu(1) sites. To test this hypothesis, a theoretical estimate of the magnitude of the quadrupole splitting that would be experienced by a high-spin Fe^{3+} ion at the Cu(1) and Cu(2) sites was performed using a simple point-charge model [93]. In the calculation, we assumed that the valence-electron contribution is negligible, so that the electrical field gradient (EFG) at a given site may be attributed to the charges on the surrounding ions. The unit cell dimensions and ionic positional parameters used were those determined from the sample used for structure analysis. Following [51] we assumed that all Cu(2) ions were the in the Cu^{2+} state while the Cu(1) ions were 30% in Cu^{2+} and 70% in Cu^{3+} states. For simplicity, the presence of oxygen vacancies was neglected. Summations were performed within a sphere of radius 35Å centered at

the reference ion. The following estimates of the EFG principal components, expressed in the crystallographic coordinate system, were obtained. For the planar Cu(1) site V_{xx}=(0,-0.31,0), V_{yy}=(0,0,-0.92), V_{zz}=(1.23,0,0), all in electron Å^{-3}. For the pyramidal Cu(2) site V_{xx}=(-0.30,0,0), V_{yy}=(0,-0.37,0), V_{zz}=(0,0,0.67), again all in electron Å^{-3}. It is apparent that the quantity $|V_{zz}|\sqrt{(1+\eta^2/3)}$, where η is the asymmetry parameter, at the Cu(1) site is about 1.9 times greater than at the Cu(2) site, in good agreement with the observed Δ_1 and Δ_2 values in Table 7.1. Thus it seems reasonable to assign a trivalent state to Fe doped into $YBa_2Cu_3O_{7-\delta}$. The suggestion that the Fe must be in the unusual Fe^{4+} valence state would appear to be unnecessary. The results of an x-ray-absorption spectroscopy study of the Fe site in $YBa_2(Cu_{1-x}Fe_x)_3O_{7-\delta}$ [101] indicates that the valence state of substitutional Fe is mainly 3+. Neither variation of the lattice parameters with composition nor the phase transition has any significant influence on the valence of the Fe site.

7.1.3 Mössbauer Spectra at Various Temperatures

Transmission Mössbauer spectra of $YBa_2(Cu_{1-x}Fe_x)_3O_{7-\delta}$ for x=0.015 and x=0.05 were recorded at a number of temperatures down to 1.5 K. The x=0.015 sample showed signs of magnetic order below 5.1 K(Fig. 7.3). Between room temperature and 15 K there was little change in the spectra, other than the usual increase in total absorption area due to the temperature dependence of the Mössbauer recoil-free fraction (Fig. 7.4). In the Debye model, the recoil-free fraction f is related to the Debye temperature Θ_D and the nuclear recoil energy

E_R via the expression [102]

$$f = exp\left[-\frac{3}{2}\frac{E_R}{k_B\Theta_D}\left(1+4\frac{T^2}{\Theta_D^2}\int_0^{\Theta_D/T}\frac{xdx}{e^x-1}\right)\right]. \tag{7.1}$$

Assuming that a single recoil-free fraction may be associated with the Fe in the sample, the fitted curve shown in Fig. 7.4 was obtained, with $\Theta_D \simeq$ 455 K. This is not a particularly high Debye temperature, and may be interpreted as evidence that if the superconductive mechanism were of a conventional BCS nature, the electron-phonon interaction would need to be unusually strong [103].

The x=0.05 spectra (Fig. 7.5) display an onset of order at around 12 K. Appreciable broadening and asymmetry is apparent in the 8.9 K spectrum, and below about 5 K, distinct hyperfine field splitting is observed. Such spectra are typical of relaxation effects. Attempts to interpret the spectra in terms of the Blume relaxation model [104], using a Mössbauer fitting program written by Q. Pankhurst were made. In Blume's model a general solution for the line shape of radiation emitted was calculated by a system whose Hamiltonian jumps at random as a function of time between a finite number of possible forms. Two examples of a Mössbauer line shape were also calculated. In one, a nuclear hyperfine magnetic field fluctuates along the z axis. In the second one, a nucleus is in an electric-field gradient that jumps at random between the x, y, and z axes.

A number of restrictions were imposed in the fitting process. First, it was assumed that the low-temperature spectra were composed of three components, assigned to the pyramidal (Cu(2)), planar (Cu(1)) and octahedral sites (Cu(1)) in the room-temperature spectra. Further, it was assumed that the quadrupole

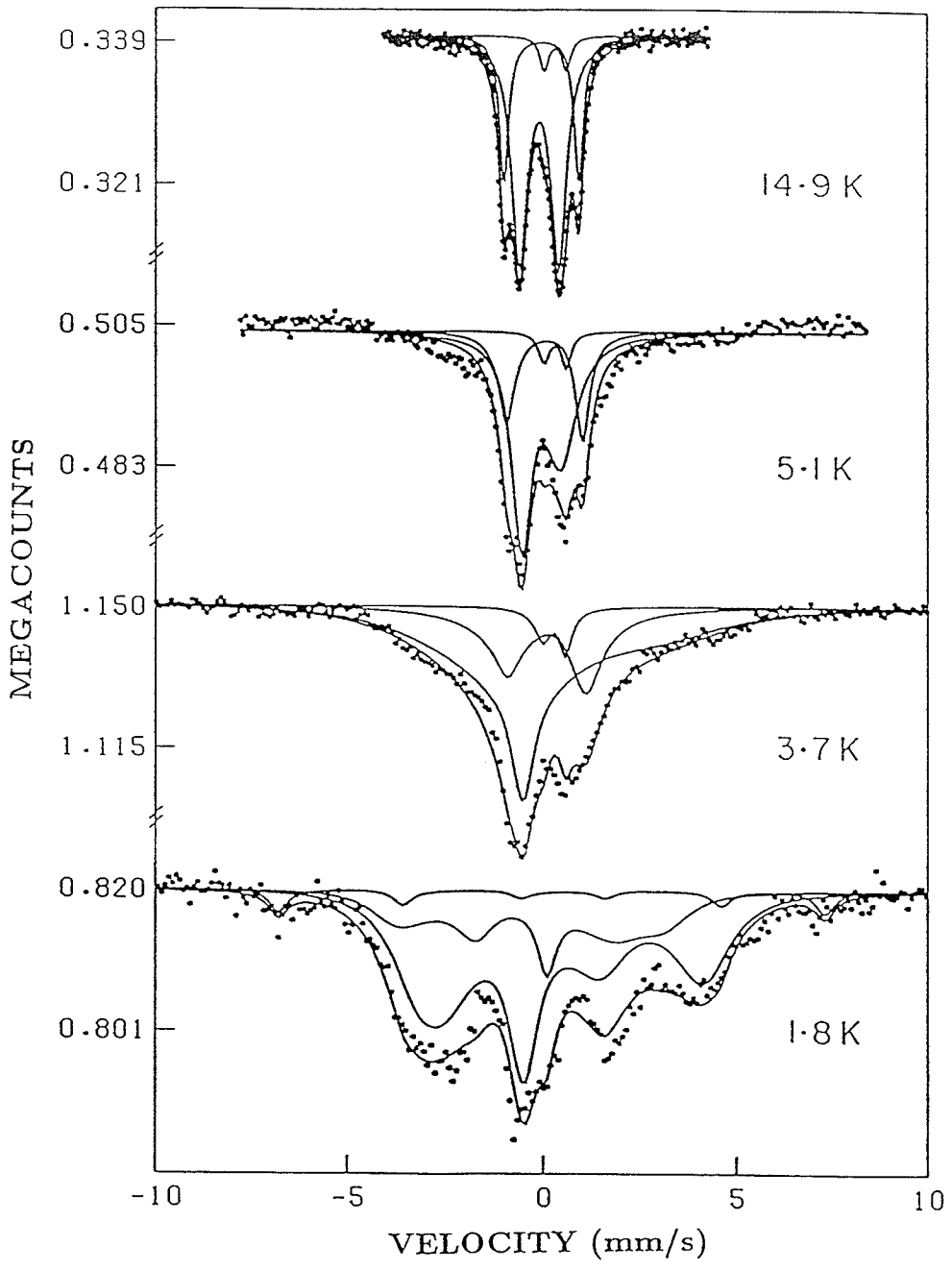

Figure 7.3: Mössbauer spectra of $YBa_2(Cu_{0.985}Fe_{0.015})_3O_{7-\delta}$ at various temperatures as indicated in the figure.

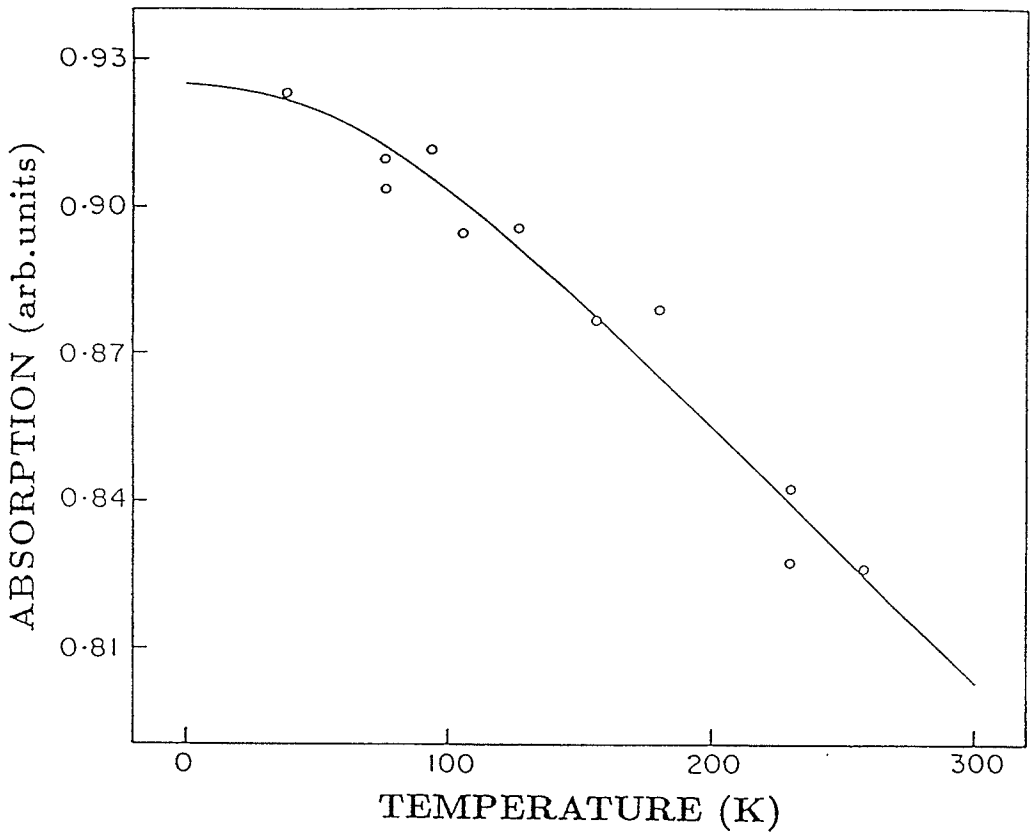

Figure 7.4: Temperature dependence of the total absorption area of the Mössbauer spectra of $YBa_2(Cu_{0.985}Fe_{0.015})_3O_{7-\delta}$.

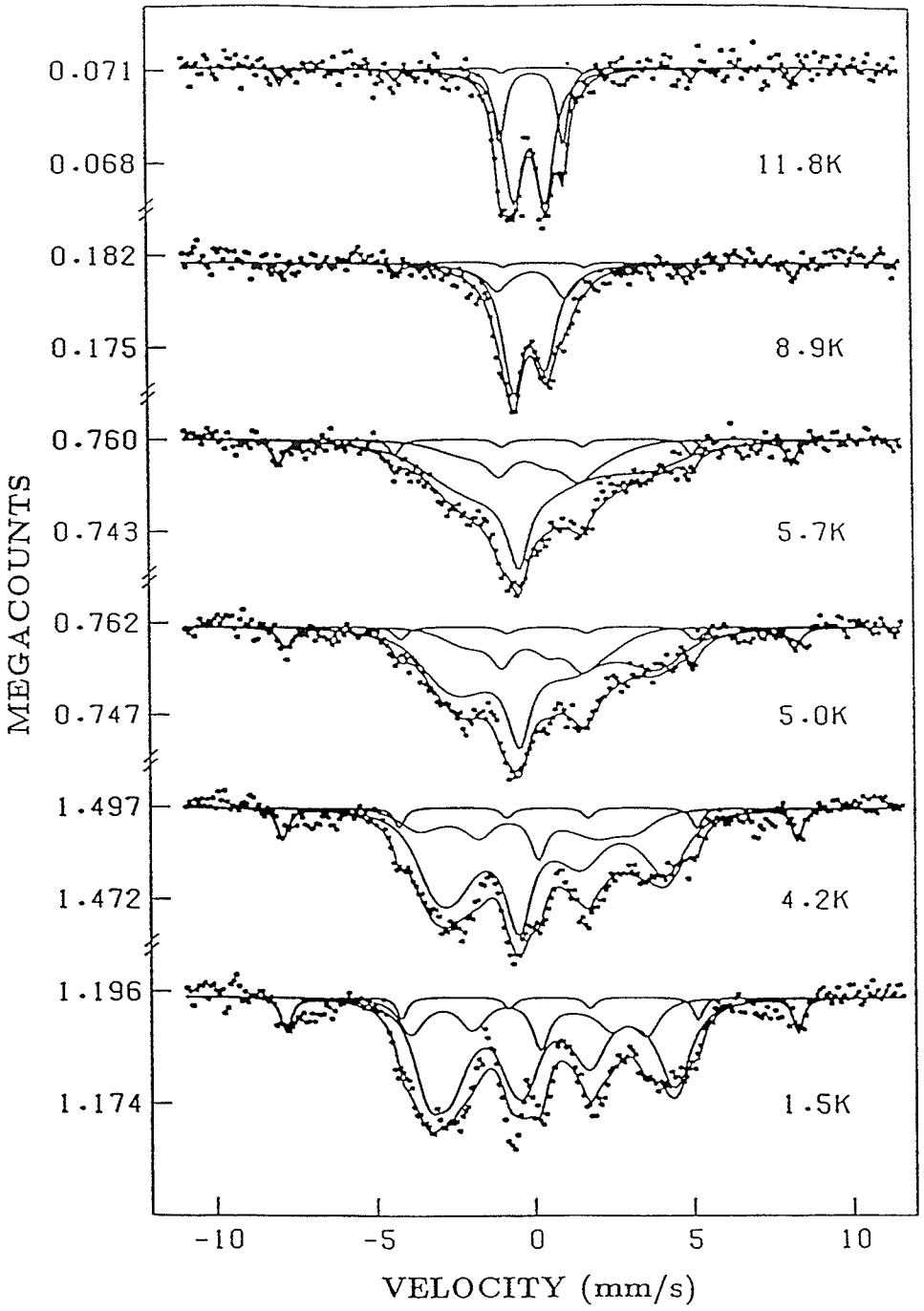

Figure 7.5: Mössbauer spectra of $YBa_2(Cu_{0.95}Fe_{0.05})_3O_{7-\delta}$ at various temperatures as indicated in the figure.

splitting and relative spectral area of each component were the same as those at 77 K (these parameters changed only slightly between room temperature and 77 K). Next, the asymmetry and orientation of the EFG at each site were taken to be those determined in the theoretical calculations. For the relaxing hyperfine fields, it was assumed that the easy axes at each site were parallel to each other and parallel to one of the crystallographic axes. Finally, it was assumed that the hyperfine fields relaxed from their *up* state to their *down* state at the same rate as the *down* to *up* fluctuations.

The theoretical spectra(Fig. 7.5) were subject to two other assumptions: one, that the spins were aligned with the crystallographic c axis and two, that the sign of V_{zz} was positive for all sites. Fits of similar quality were obtained with the spins parallel to the b axis and with negative value of V_{zz}, whereas all other combinations gave substantially poorer fits. However, the existence of negative values of V_{zz} contradicts the EFG calculations; hence the latter model was discarded.

As is evident in Fig. 7.5, octahedrally coordinated Fe appears as a magnetically split sextet in all spectra. It has a hyperfine field of $B_{hf} \simeq 50T$ and a relaxation rate of $R \simeq 0$. Since this sextet was not evident in a spectrum recorded at liquid-nitrogen temperature, the octahedral iron apparently orders between 77 and 12 K. This is clearly much higher than at the pyramidal and planar sites, leading to the suspicion that the octahedral Fe is situated in distinct regions of the sample–possibly in the form of an *impurity* phase with stoichiometry $YBa_2(Cu_{1-x}Fe_x)_3O_8$ on those surfaces that were directly exposed to oxygen

Table 7.2: Hyperfine fields, B_{hf}, relaxation rate, R, and linewidth, Γ, of Fe in the pyramidal and planar Cu sites of $YBa_2(Cu_{0.95}Fe_{0.05})_3O_{7-\delta}$. Asterisks denote parameters that were not allowed to vary.

	Pyramidal			Planar		
T(K)	B_{hf}(T)	R(MHz)	$\Gamma(mms^{-1})$	B_{hf}(T)	R(MHz)	$\Gamma(mms^{-1})$
11.8	0*	0*	0.69	0*	0*	0.39
8.9	14.2	291.8	0.67	13.8	28.4	0.26
5.7	22.8	17.9	0.54	15.1	14.1	0.26
5.0	22.4	11.5	0.46	13.8	10.3	0.26
4.2	23.3	8.0	0.32	20.2	8.3	0.26
1.5	24.3	5.8	0.26	21.5	4.4	0.26
4.2†	24.3	7.8	0.26	21.0	6.9	0.26

†In an applied field of 5T.

annealing. Such a possibility may be important when coupled with the suggestion that even in single-phase $YBa_2Cu_3O_{7-\delta}$ the superconductivity only occurs in shells surrounding normal grains [105]. The fitted hyperfine fields, relaxation rates, and linewidths of the pyramidal and planar components are given in Table 7.2.

The fields increased as the temperature was lowered, tending towards saturation values of order 25 and 22 T respectively and the relaxation rates at both sites followed approximately logarithmic temperature dependences. The linewidths measured for the pyramidal component were significantly larger than the experimental natural linewidth, $\Gamma_0 \simeq 0.26 mms^{-1}$, whereas those of the planar component were close to Γ_0. If line broadening were to be attributed to sample inhomogeneity affecting the local environments of Fe ions, the Γs of both sites should have been larger than Γ_0.

In general, the fits shown in Fig. 7.5 are of sufficiently good quality that the

model of relaxing spins aligned with the c axis remains valid. Significant misfit is only apparent at 1.5 K in the central portion of the spectrum. In this case, the linewidths at all the Fe sites were close to Γ_0 and we can attribute the misfit to sample inhomogeneity, giving rise to a distribution in the local hyperfine fields and relaxation rates.

In an attempt to determine the nature of the magnetic order in $YBa_2(Cu_{0.95}Fe_{0.05})_3O_{7-\delta}$ a field of 5 T was applied in a direction parallel to the incident γ-ray beam. The spectrum thus obtained is shown in Fig. 7.6 along with the zero-field 4.2 K spectrum. If the order is antiferromagnetic, we would anticipate a sizeable increase in linewidth and a slight increase in the mean effective field $\overline{B}_{eff}$ (the vector sum of the hyperfine and applied fields). On the other hand, if the order is ferromagnetic, we would expect a significant increase in $\overline{B}_{eff}$ and a diminution in the relative intensities of lines two and five of the magnetic sextets.

It is clear from Fig. 7.6, and from the fitted $\overline{B}_{eff}$, R and Γ parameters included in Table 7.2, that neither of above cases was observed. The applied field did not have a major effect on the spectrum apart from causing a slight slowing of the relaxation rates. This result is most probably due to the superconducting nature of the sample which prevents the applied field from penetrating into the bulk of the absorber. The sub-spectrum of the octahedrally coordinated Fe, did show a small increase in linewidth (0.26→0.30 mms^{-1}); however this is an inconclusive indication of antiferromagnetic order.

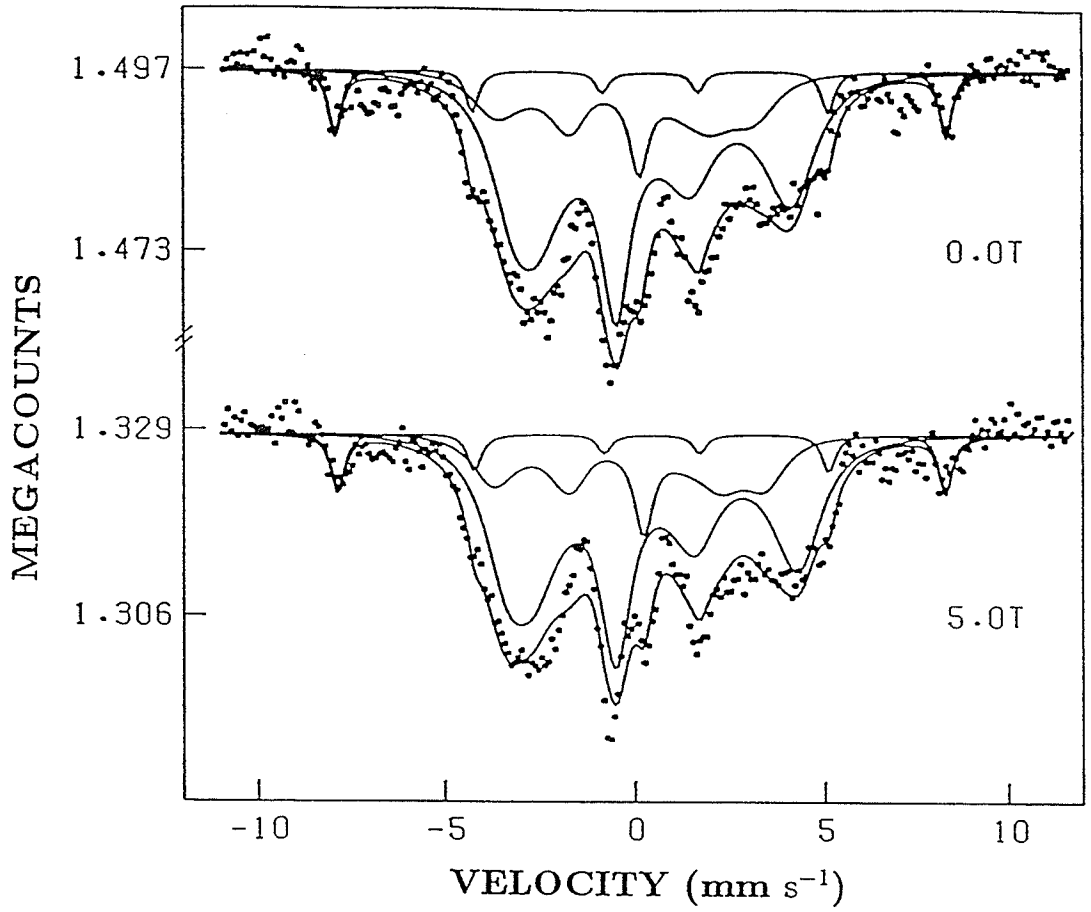

Figure 7.6: Spectra of $YBa_2(Cu_{0.95}Fe_{0.05})_3O_{7-\delta}$ at 4.2K in the presence of 0 and 5 T applied fields.

7.2 TlCaBaCuO System

7.2.1 Samples

As mentioned previously, the 2122 and 2223 phases usually coexist in a sample and are very sensitive to the manufacturing procedure. It is , of course, important to use a single phase in Mössbauer studies. The details for making single phase samples in the TlCaBaCuO system have been described in Chapter 4.

The phase purity in the samples $Tl_2CaBa_2(Cu_{1-x}Fe_x)_2O_{8+\delta}$ and $Tl_2Ca_2Ba_2(Cu_{1-x}Fe_x)_3O_{10+\delta}$ were examined by using x-ray diffraction patterns with Cu Kα radiation. The diffractograms of the 2122 and 2223 samples for various x are almost same as that of the x=0 samples (see Fig. 5.7). Only a trace of the 2223 phase appears in the 2122 samples. In the 2223 samples a small amount of 2122 phase appears that increases with iron concentration. In addition, for x=0.05 and 0.10, an extra line appears at $2\theta \simeq 30.2°$ that may correspond to a $Tl_2Ba_2CuO_{6-\delta}$ phase. Nevertheless, we consider that the samples are 90%, if not better, single phase compounds in both 2122 and 2223 samples. In order to eliminate, as far as possible, small manufacturing differences, the samples of the 2122 and 2223 phase with different x were made in the same batch.

The samples were also characterized by resistance and ac susceptibility measurements. Dependence of the resistance on the temperature for the 2122 samples are shown in Fig. 7.7. Obviously T_c is lowered and the resistance above onset is increased as x is increased. As compared to the 123 system, the change in T_c is smaller. For example, for x=0.10 $T_c \simeq 81K$ for the 2122 phase and $T_c \simeq 100K$

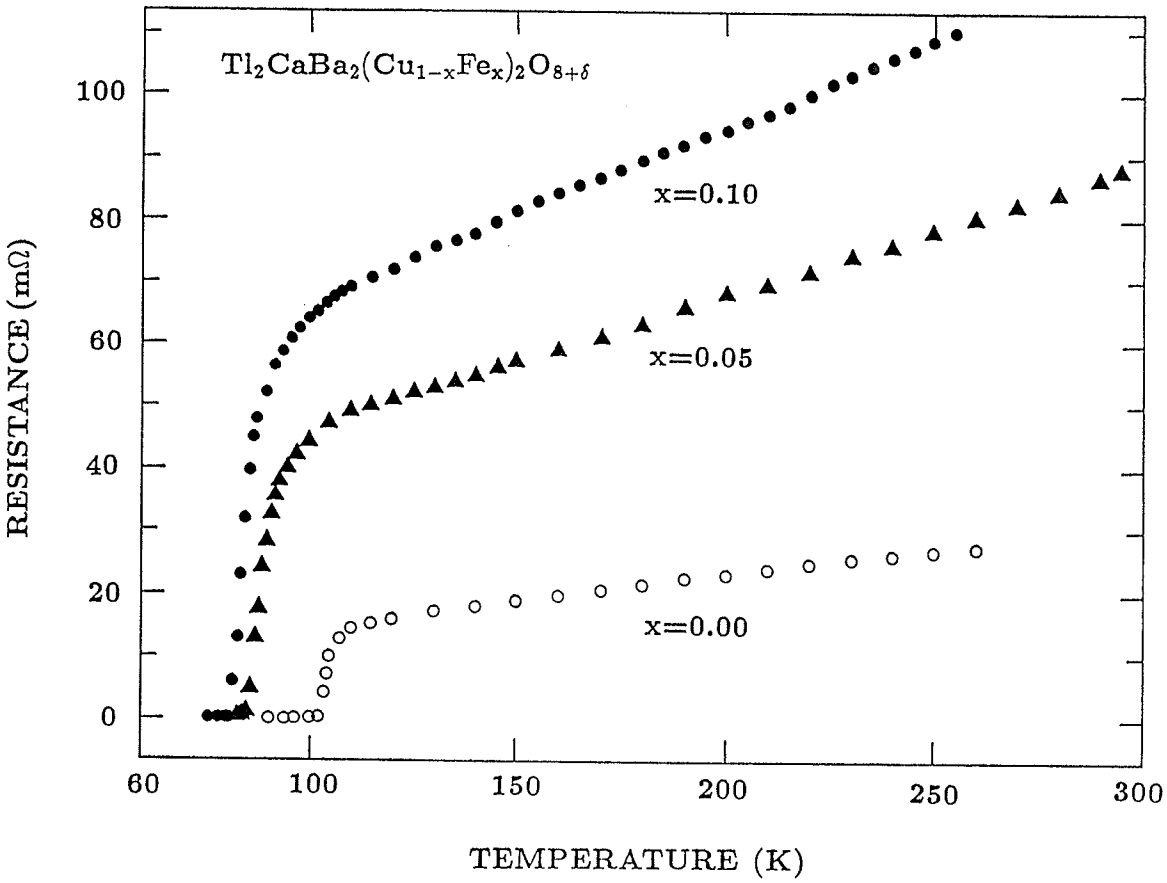

Figure 7.7: Electric resistance versus temperatures for $Tl_2CaBa_2(Cu_{1-x}Fe_x)_2O_{8+\delta}$. The values of x are indicated.

for the 2223 phase whereas T_c is only about 31 K for the 123 compound with the same doping[106].

The ac susceptibility, χ', was measured at 3.7 kHz in a magnetic field with an amplitude of 0.12 Oe root-mean-square (rms). The data recorded for a temperature range above pumped liquid nitrogen are shown in Fig. 7.8. for the 2122 phase and in Fig. 7.9 for the 2223 phase.

The onset in the decrease of the susceptibility commences close to the temperature for zero resistance. The shielding (ac Meissner effect) decreases with increasing iron concentration.

7.2.2 Mössbauer Spectra of the 2122 Phase

Mössbauer absorbers were made by powdering the same pellets used in the resistance and susceptibility measurements. These powders were immobilized in benzophenone; our usual careful precautions were followed to ensure that the absorbers were as homogenous and isotropic as possible. Spectra were obtained at various temperatures from 2.3 K (pumped liquid helium) to room temperature in an Oxford cryogenic system. The source was ^{57}Co in a rhodium host. A constant acceleration drive in a sine and triangular mode was used for the 2122 and 2223 sample, respectively. Each spectrum was folded.

Mössbauer spectra of $Tl_2CaBa_2(Cu_{1-x}Fe_x)_2O_{8+\delta}$ for x=0.05 and 0.10 at various temperatures are shown in Figs. 7.10 and 7.11 respectively.

The spectra at 77 K are similar, although slightly broader, than those at room temperature. If these spectra consist of only one doublet, it is clearly asymmetric. An asymmetric doublet can have two possible sources [107]. One

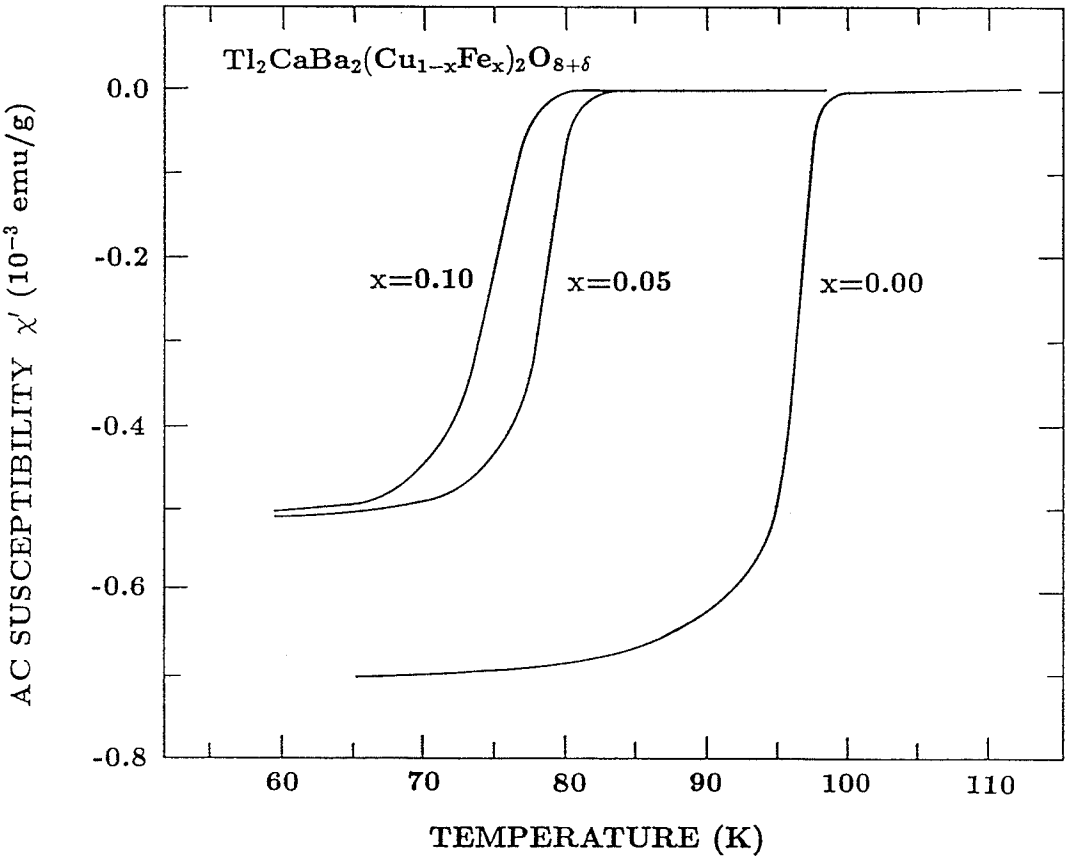

Figure 7.8: The real part of the ac susceptibility at 3.7 kHz and 0.12 Oe rms versus temperatures for sample $Tl_2CaBa_2(Cu_{1-x}Fe_x)_2O_{8+\delta}$.

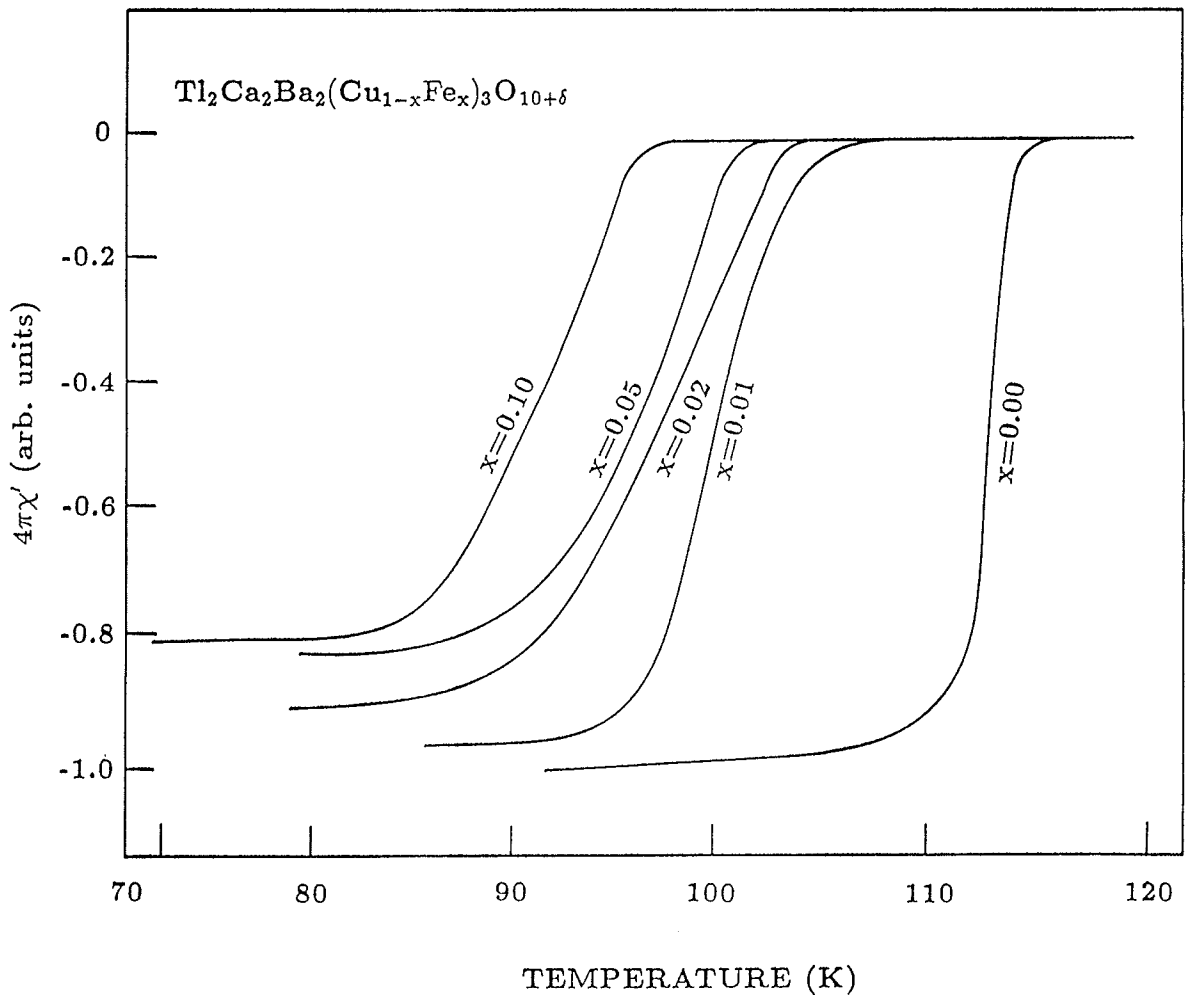

Figure 7.9: The real part of the ac susceptibility at 3.7 kHz and 0.12 Oe rms versus temperatures for sample $Tl_2Ca_2Ba_2(Cu_{1-x}Fe_x)_3O_{10+\delta}$.

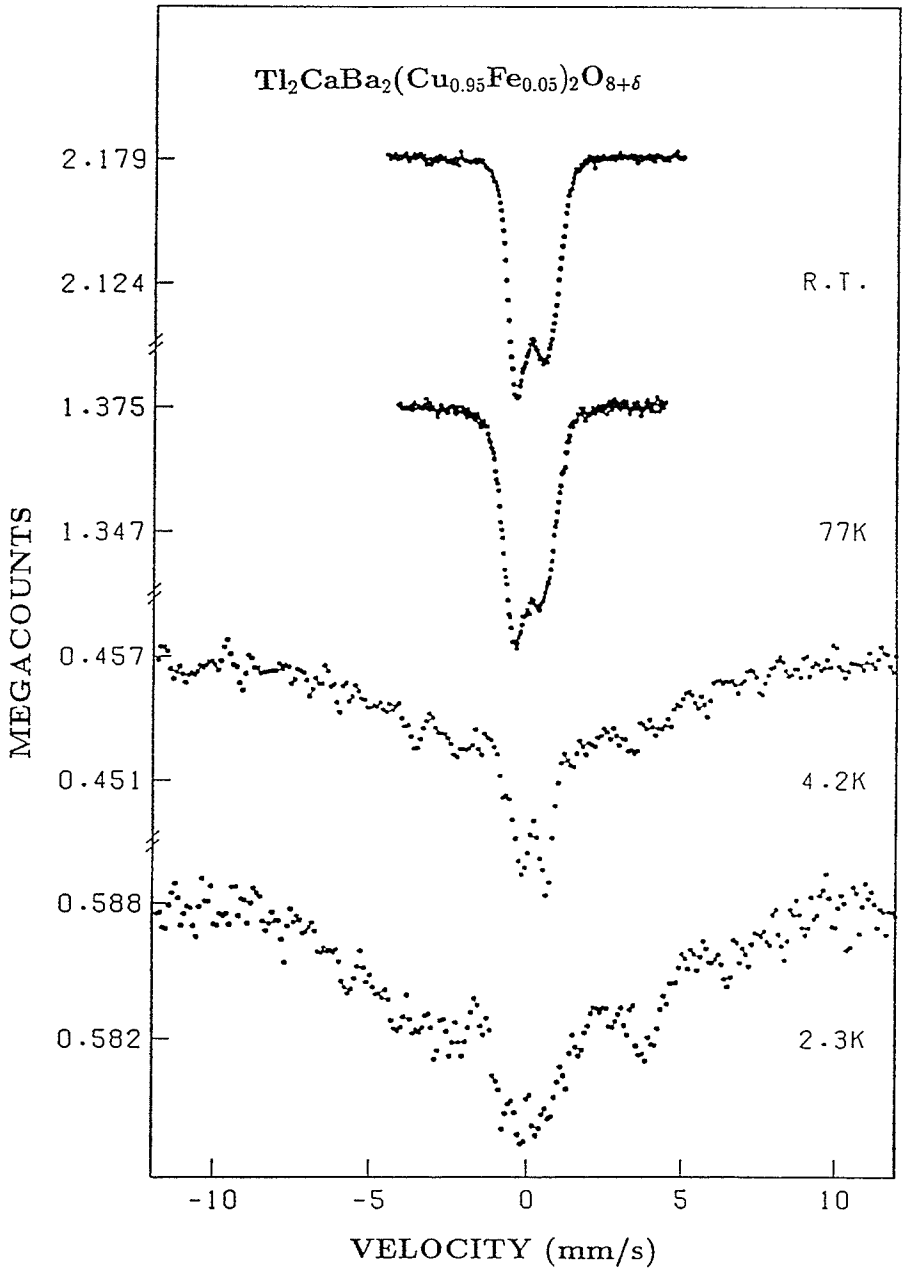

Figure 7.10: Mössbauer spectra of $Tl_2CaBa_2(Cu_{0.95}Fe_{0.05})_2O_{8+\delta}$ at various temperatures.

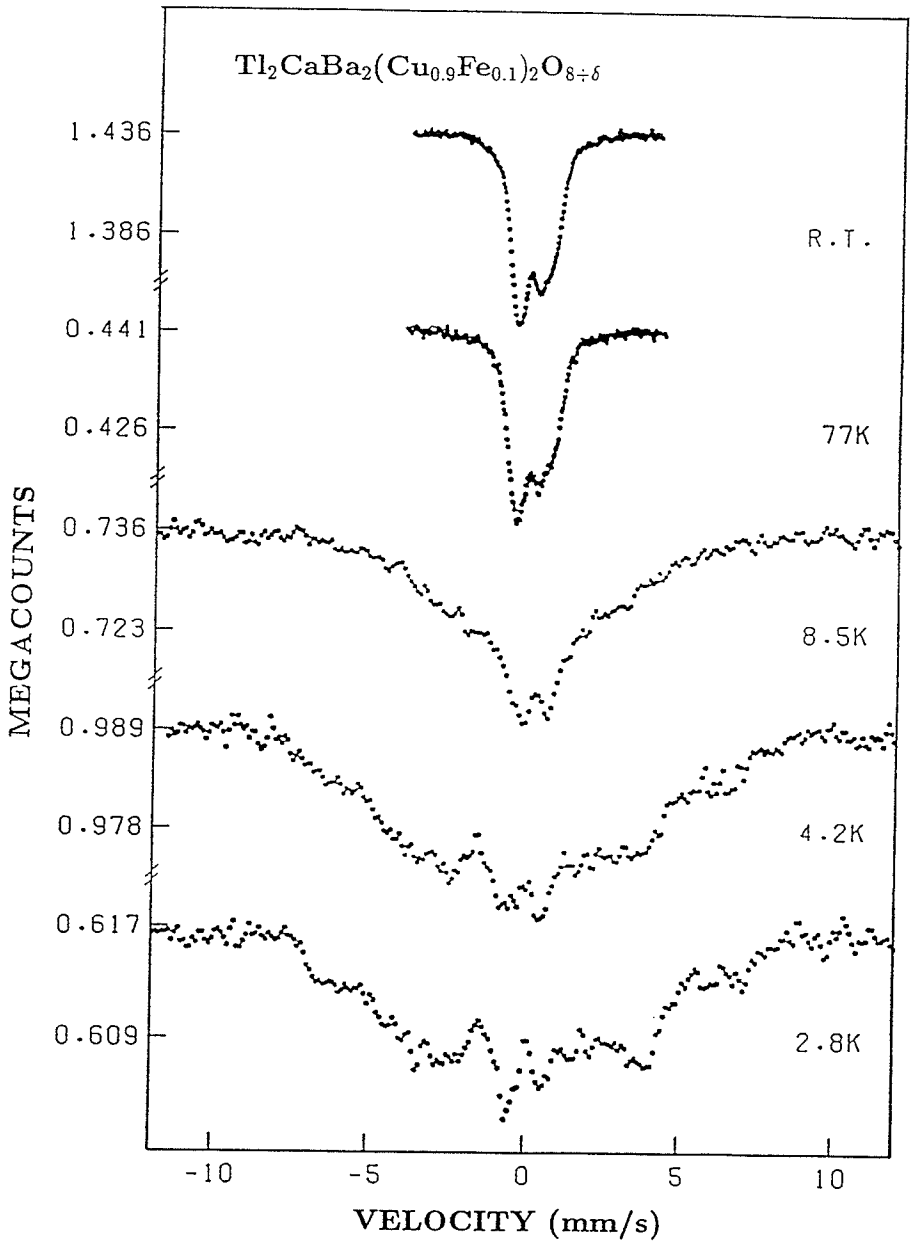

Figure 7.11: Mössbauer spectra of $Tl_2CaBa_2(Cu_{0.90}Fe_{0.10})_2O_{8+\delta}$ at various temperatures.

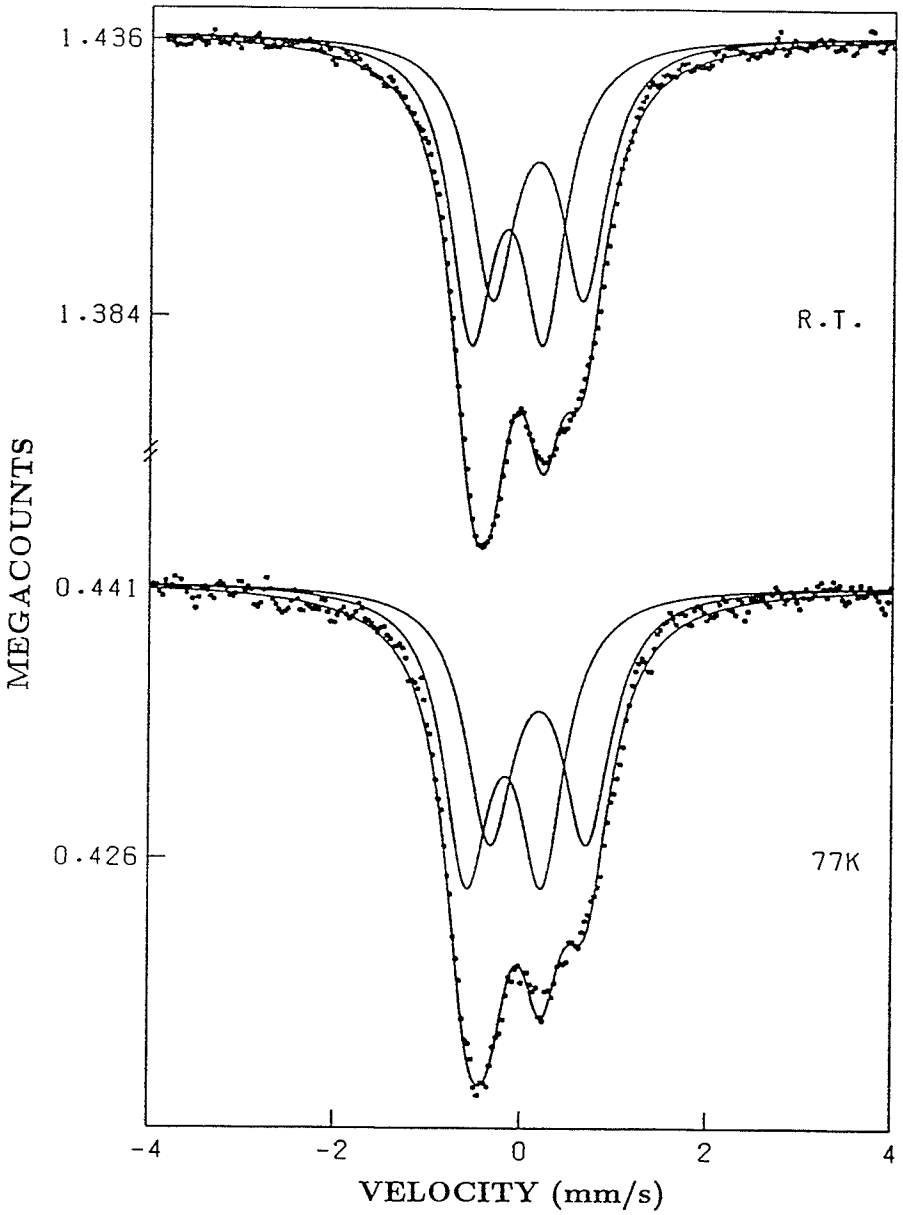

Figure 7.12: Mössbauer spectra of $Tl_2CaBa_2(Cu_{0.90}Fe_{0.10})_2O_{8+\delta}$ at room temperature and 77 K fitted by two doublets.

Table 7.3: Quadrupole splittings, Δ, and isomer shifts relative to α-Fe, δ, for $Tl_2CaBa_2(Cu_{1-x}Fe_x)_2O_{8+\delta}$ at room temperature in units of mm s^{-1}.

x	Δ_1	δ_1	Δ_2	δ_2
0.05	0.60	-0.04	1.27	0.10
0.10	0.59	-0.60	1.25	0.07

is the texture effect, wherein the particles of the absorber are not isotropically distributed. Then the electric-field gradient has some preferred orientation. The other possibility is the Karyagin-Goldanskii effect, wherein a dynamic anisotropy in the recoilless fraction occurs in the absorber. Since rotating the absorber from 90 to 45° with respect to the γ-ray direction led to an identical spectrum, the texture effect can be ruled out. The increase in the asymmetry with increased iron content, together with the complexity of the spectra in liquid-helium range, would seem to make the Karyagin-Goldanskii effect unlikely.

Therefore, two doublets have been used to fit the room-temperature spectra. Even then, an ambiguity exists. Either two doublets, each with small isomer shifts, or two doublets with larger isomer shifts of opposite sign, provide satisfactory fits. Since there is only one copper site in the 2122 structure we have chosen the first possibility, viz-two doublets with a large amount of overlap.The hyperfine parameters obtained are listed in Table 7.3. The computer fitted curves for $Tl_2CaBa_2(Cu_{0.90}Fe_{0.10})_2O_{8+\delta}$ are shown in Fig. 7.12.

The Mössbauer spectra below room temperature will be considered now. The absence of a significant change in the spectra $Tl_2CaBa_2(Cu_{1-x}Fe_x)_2O_{8+\delta}$ at 77 K suggests that no structural change occurs during the superconducting tran-

Table 7.4: Quadrupole splittings, Δ, and isomer shifts relative to α-Fe, δ, of $Tl_2Ca_2Ba_2(Cu_{1-x}Fe_x)_3O_{10+\delta}$ at room temperature in units of mm s^{-1}.

x	Δ_1	δ_1	Δ_2	δ_2	Δ_3	δ_3
0.01	0.65	0.25	0.59	-0.17	1,32	0.15
0.02	0.65	0.25	0.69	-0.11	1.37	0.14
0.05	0.64	0.24	0.73	-0.06	1.42	0.13
0.10	0.67	0.24	0.67	-0.06	1.40	0.14

sition; nevertheless, a small change in the lattice parameters is not ruled out.

Below 10 K the spectra have the same general appearance observed for the 123 phase. At 8.5 K, the spectrum for the x=0.10 sample is clearly broadened and *wings* are discernable in the outer regions. The magnetic hyperfine splitting continues to increase as the temperature is lowered below 4.2 K; the shape of the spectra still possess relaxation characteristics at 2.8K. It is usual to assume that the low-temperature spectra imply that antiferromagnetic ordering of the iron has taken place.

7.2.3 Mössbauer Spectra of the 2223 Phase

The Mössbauer spectra obtained for the $Tl_2Ca_2Ba_2(Cu_{1-x}Fe_x)_3O_{10+\delta}$ with x=0.01, 0.02, 0.05, and 0.10 at room temperature by using an expanded velocity scale are shown in Fig. 7.13. Although two doublets can provide a respectable fit at x=0.01 and 0.02, the spectra for x=0.05 and 0.10 clearly show that three doublets are required. Therefore all four spectra of Fig. 7.13 were fitted with three doublets; the hyperfine parameters obtained are listed in Table 7.4.

Mössbauer spectra for the Fe substituted 2223 phase at various tempera-

tures, from 4.2 K to room temperature have been taken and special precautions have been paid to the temperature range of 100-120 K, just above the superconducting transition. The shape of Mössbauer spectra in $Tl_2Ca_2Ba_2Cu_{2.94}Fe_{0.6}O_{10+\delta}$ in the temperature range 77-250 K are similar to that at room temperature and are shown in Fig. 7.14.

The dependence of the total spectral areas, A, on temperature is shown in Fig. 7.15. It can be seen that A increases as the temperature decreases. As for the YBaCuO system, the curve in Fig. 7.15 is the computer fit for the Debye model, equation (7.1), with $\Theta_D \simeq 342$ K. Obviously, the Θ_D deduced in the TlCaBaCuO system is lower than in the YBaCuO system. If the materials are still BCS or BCS-like in nature, the higher T_c for the TlCaBaCuO system implies that a stronger electron-phonon interaction, $N(E_F)V_0$, exists (see equation 2.22).

There is a small step in the spectral area in Fig. 7.15 at T$\simeq$ 120 K. This may be related to the lattice softening which has been observed in the 123 phase [108,109]; however the data do not permit a definite conclusion to be made.

The dependences of the quadrupole splitting, Δ, and the spectral shift, δ, on temperature are shown in Fig. 7.16. When the second-order Doppler effect is included, the spectral shift, δ, can be expressed as [110]

$$\delta = \delta_{I.S.} - \frac{9k_B\Theta_D}{16Mc}\left[1 + 8\left(\frac{T}{\Theta_D}\right)^4 \int_0^{\Theta_D/T} \frac{x^3 dx}{e^x - 1}\right] \qquad (7.2)$$

were $\delta_{I.S.}$ is the isomer shift at room temperature relative to α-Fe, k_B is Boltzmann's constant, M is the mass of the Fe nucleus and c is the velocity of light. The second term of equation (7.2) is the second-order Doppler effect. The calcu-

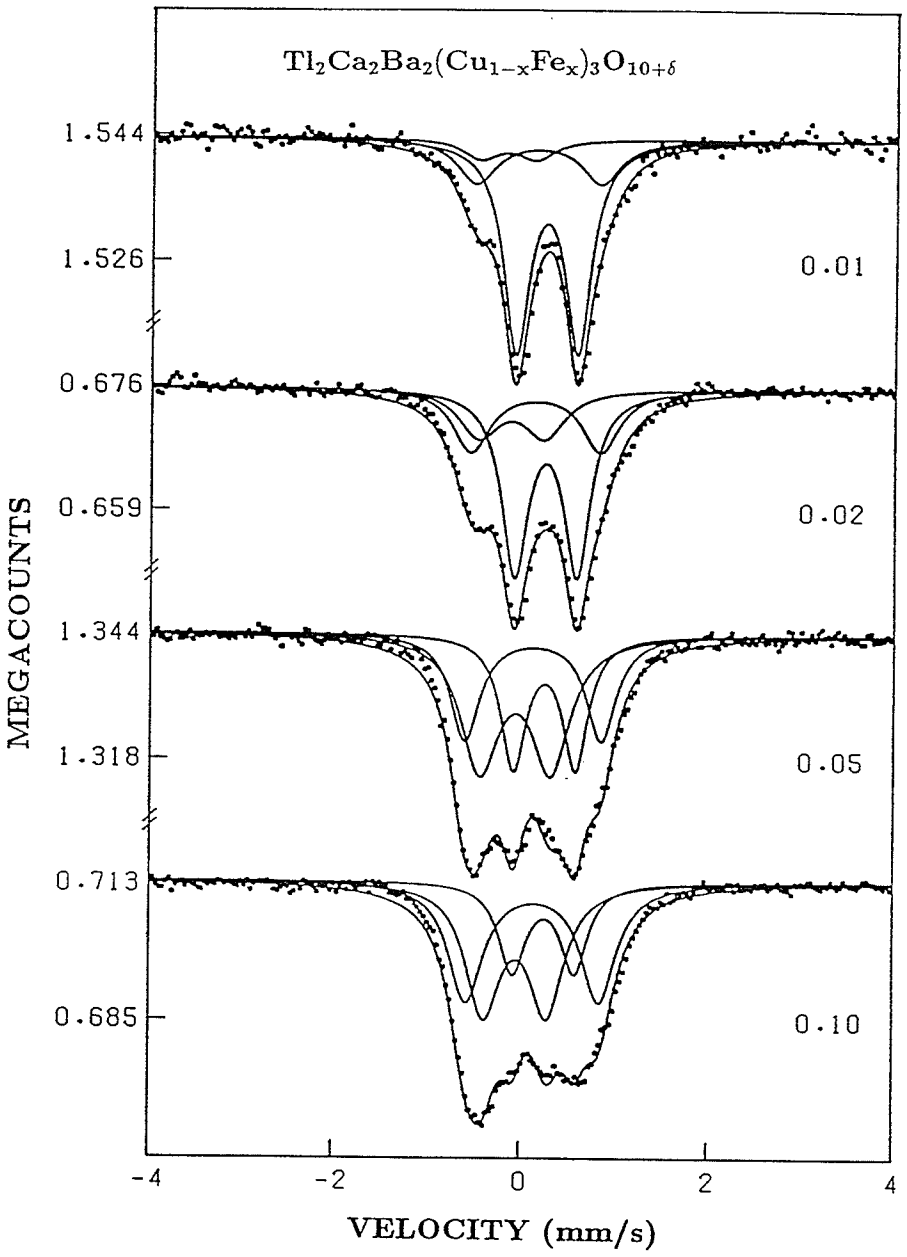

Figure 7.13: Mössbauer spectra of $Tl_2Ca_2Ba_2(Cu_{1-x}Fe_x)_3O_{10+\delta}$ at room temperatures for x=0.01, 0.02, 0.05 and 0.10.

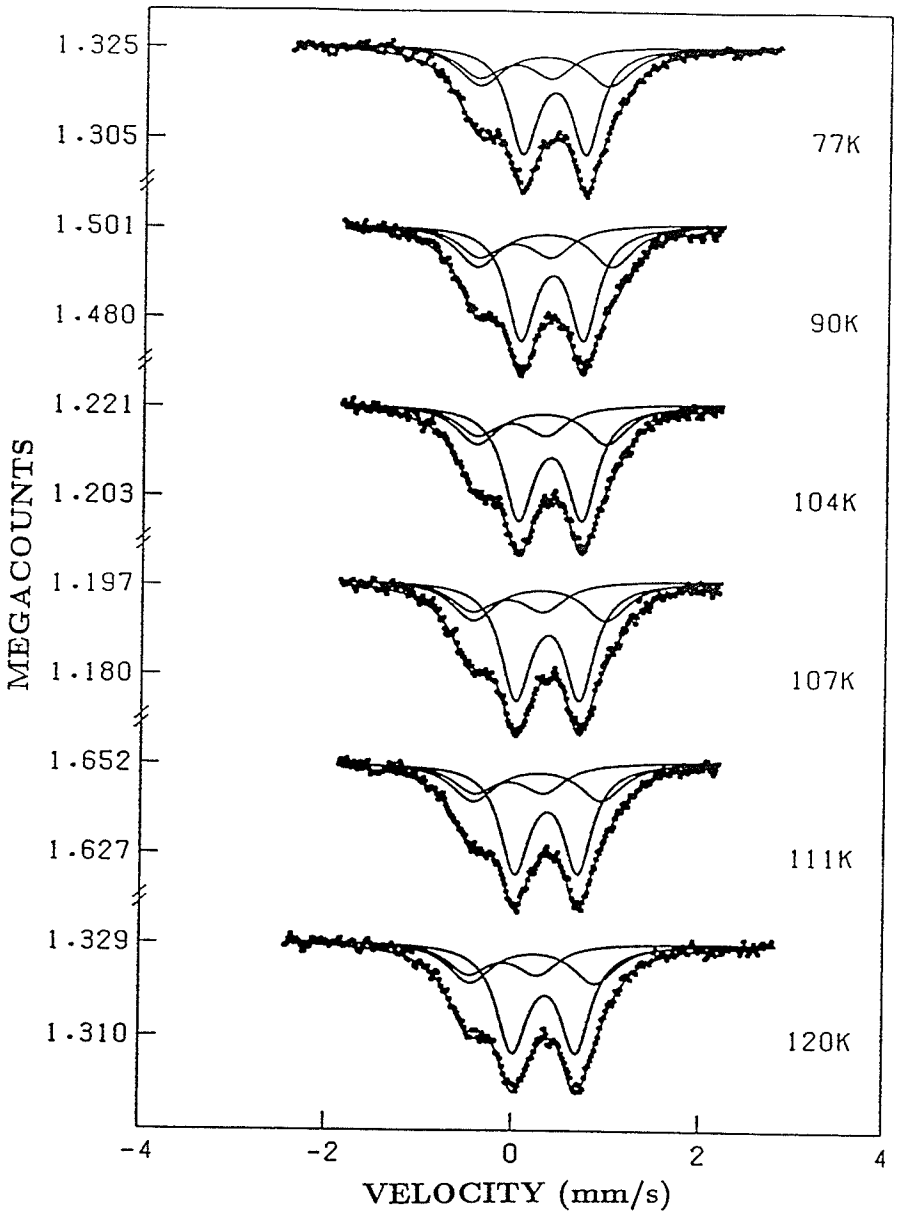

Figure 7.14: Mössbauer spectra for $Tl_2Ca_2Ba_2(Cu_{0.98}Fe_{0.02})_3O_{10+\delta}$ at various temperatures.

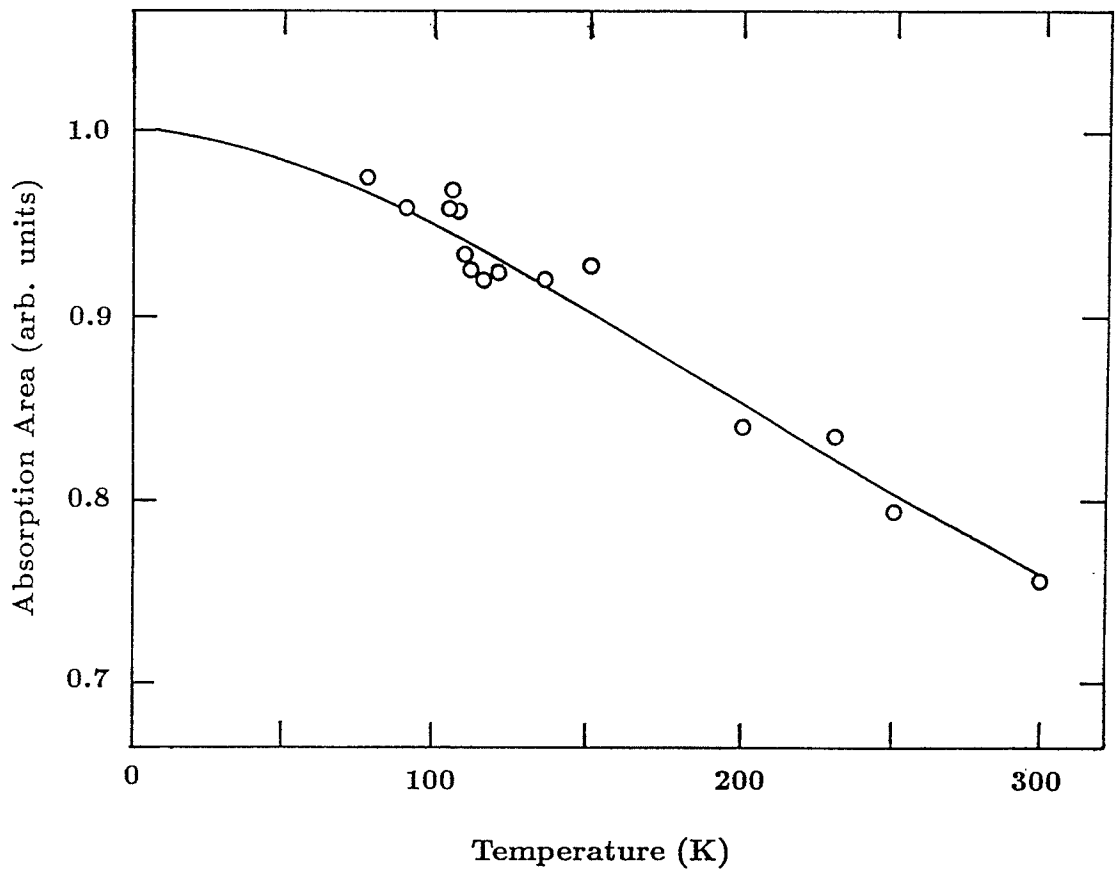

Figure 7.15: Temperature dependence of the total spectral areas of the Mössbauer spectra for $Tl_2Ca_2Ba_2Cu_{2.94}Fe_{0.06}O_{10+\delta}$.

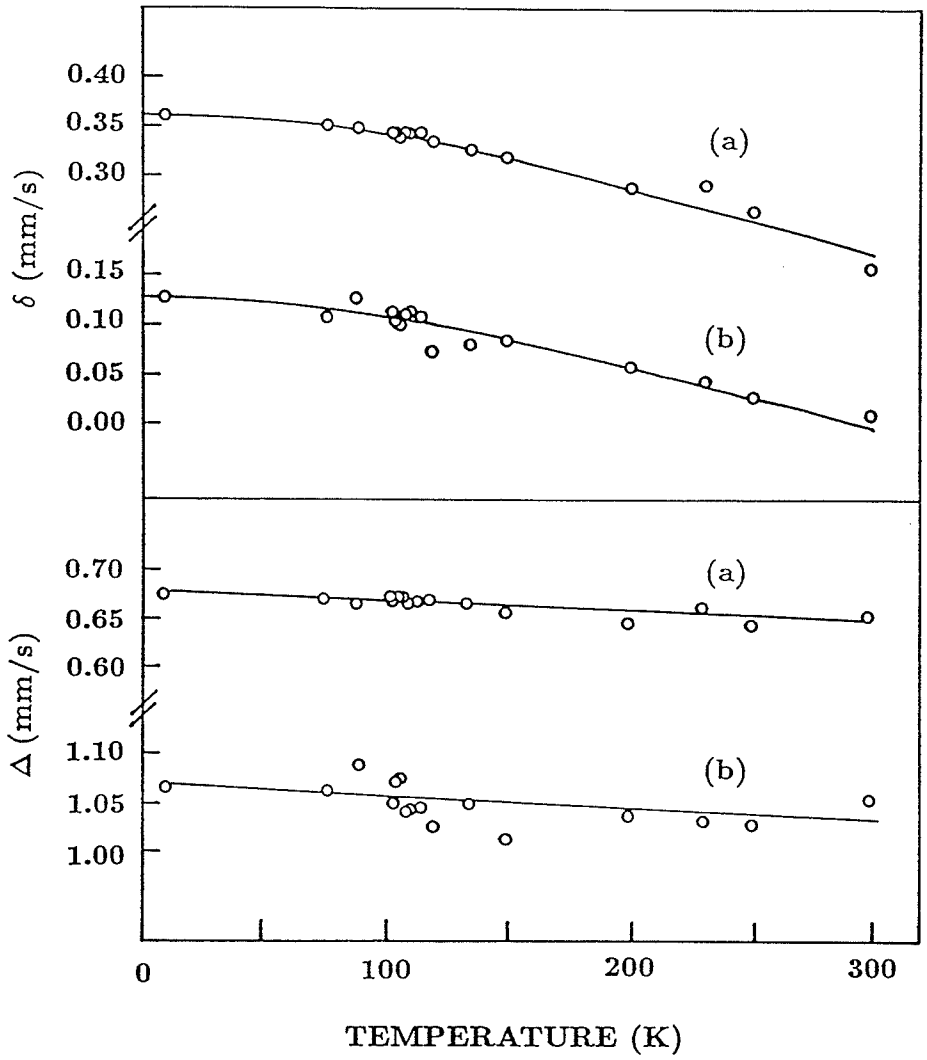

Figure 7.16: Dependence of the quadrupole splitting, Δ, and the spectral shift, δ, on temperature for $Tl_2Ca_2Ba_2Cu_{2.94}Fe_{0.06}O_{10+\delta}$ (a)for square-pyramidal sites, (b) for middle-planar sites.

lated curve of δ in Fig. 7.16 fits the experimental results well with $\delta_{I.S.} \simeq -0.025$ mms^{-1}. Thus, changes of the spectral shift with temperature are mainly and perhaps entirely from the second-order Doppler effect.

Mössbauer spectra of $Tl_2Ca_2Ba_2(Cu_{1-x}Fe_x)_3O_{10+\delta}$ for x=0.02, 0.05 and 0.10 at 10 K and 4.2 K are shown in Figs. 7.17 and 7.18, respectively. At 10 K the spectra have no significant changes for x=0.02 and 0.05, but are a little broader for x=0.10 as compared with 77 K. At 4.2 K, the spectrum for x=0.02 is essentially the same as that at 10 K except a small broadening near the baseline. An obviously broadened *wing* appears on the spectrum for x=0.05. Hyperfine splitting with magnetic relaxation can be seen clearly from the spectrum for x=0.10.

7.2.4 Discussion

Of the two Mössbauer sub-patterns for the 2122 compound, it is possible that one is associated with iron in an another phase. In view of the small amount of impurities present, the iron would have to have a strong preference for the impurity to account for the area of the absorption pattern. Hence, we discount this possibility.

It is also possible that some iron ions occupy interstitial positions in the 2122 lattice; for example there is a large space available in the Ca planes. However, consideration of the size and possible configuration of the iron ions, they are more likely to substitute for Cu in Cu-O_2 planes. Since there is only one Cu site, a square pyramid, how can there be two Mössbauer sub-patterns? Since the valency of the iron ions probably is higher than that of the copper, extra oxygen may be present in the lattice; this is the reason for the δ that we have

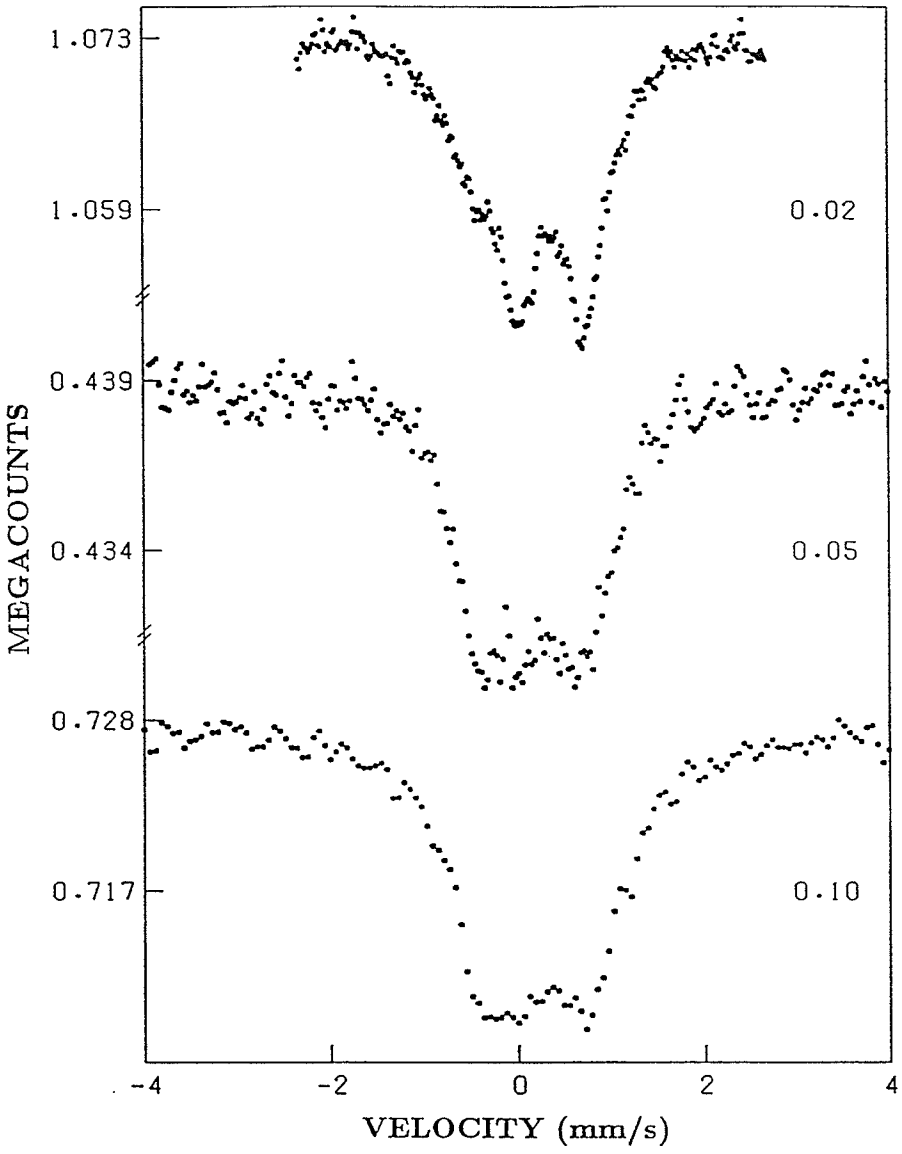

Figure 7.17: Mössbauer spectra of sample $Tl_2Ca_2Ba_2(Cu_{1-x}Fe_x)_3O_{10+\delta}$ at 10 K for various x.

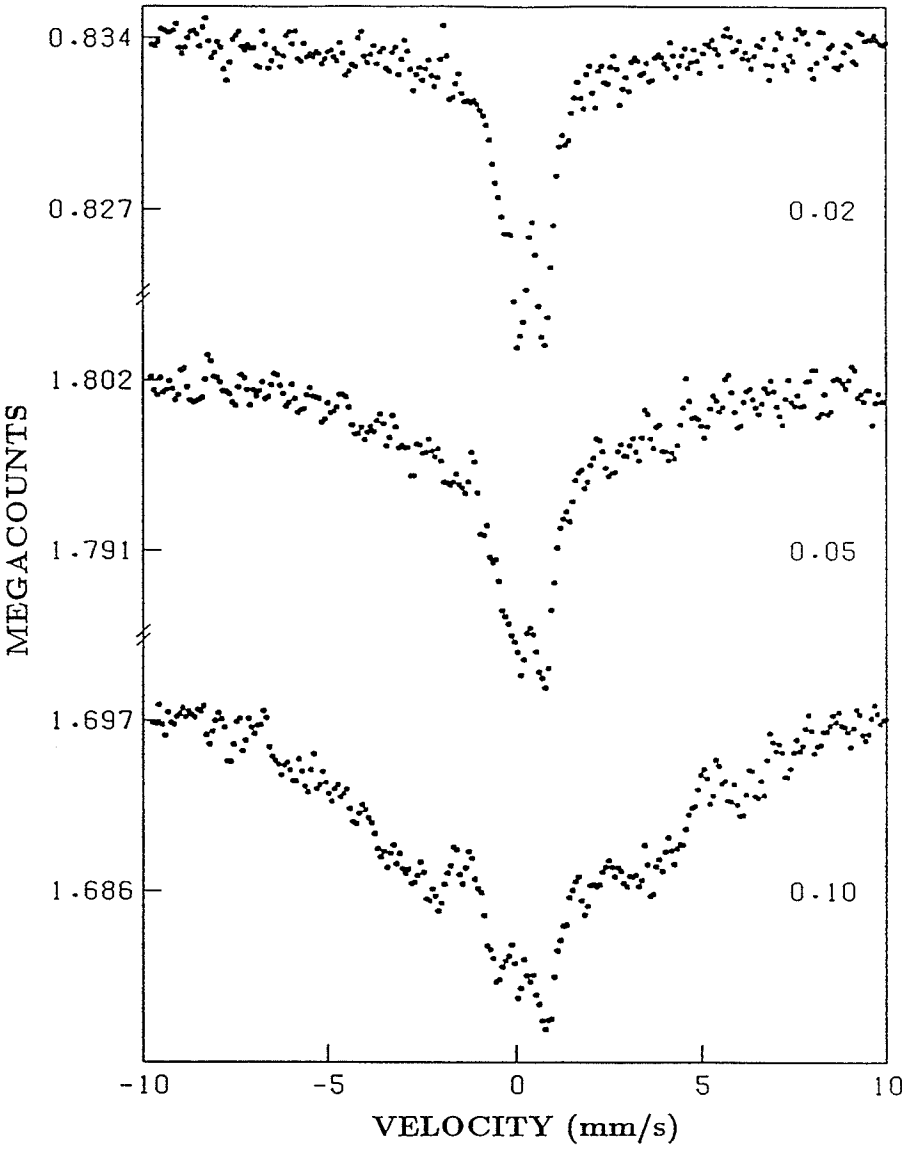

Figure 7.18: Mössbauer spectra of sample $Tl_2Ca_2Ba_2(Cu_{1-x}Fe_x)_3O_{10+\delta}$ at 4.2 K for various x.

written in the chemical formula. This oxygen would probably tend to go into the Ca plane[111]. Hence the oxygen coordination number for some of the iron ions would be increased and lead to an additional, slightly displaced, doublet.

The three doublets in the fit to the 2223 spectra then would have a natural origin. Doublet 1, with $\Delta \simeq 0.65 \text{mms}^{-1}$ and $\delta \simeq 0.25 \text{mms}^{-1}$ (Table 7.4), corresponds to iron located in the middle Cu-O_2 layer whereas doublets 2 and 3 correspond to Fe in the square-pyramidal Cu-O_2 layers. As based on the relative areas of the patterns in Fig. 7.13, iron prefers the middle Cu-O_2 layer for small x, as concluded earlier [112], and it prefers the square-pyramidal sites for larger x (0.05 and 0.10).

It is of interest to compare spectra of $Tl_2Ca_2Ba_2(Cu_{1-x}Fe_x)_3O_{10+\delta}$, $Tl_2CaBa_2(Cu_{1-x}Fe_x)_2O_{8+\delta}$ and $YBa_2(Cu_{1-x}Fe_x)_3O_{7-\delta}$[93] at 4.2K for the same x. The biggest change of the spectrum relative to that at room temperature occurs for the 123 phase; the smallest change is for the 2223 phase. These simply correspond to the highest T_c for the 2223 phase and the lowest T_c for the 123 phase. The drop of T_c as x increase is fastest for the 123 phase and slowest for the 2223 phase.

The magnetic-ordering temperature depends on the amount of substitution, x. When x is small, such as x=0.02, there is no magnetic splitting in the spectrum down to 4.2 K. This strongly suggests that the magnetic ordering for large x is to be attributed to interactions between the iron ions. When x is larger the magnetic interaction between the iron ions becomes stronger; hence the magnetic ordering temperature becomes higher.

In conventional superconductors, very small amounts of magnetic impurities suffice to destroy the superconductivity completely. The coexistence of magnetic-ordering and superconductivity involving the same crystallographic sites in the high-T_c compounds may well imply that the mechanisms operating have similiarities.

Chapter 8

Summary and suggestion for further work

8.1 Summary

Three phases of high-T_c superconductors, $YBa_2Cu_3O_{7-\delta}$, $Tl_2CaBa_2Cu_2O_8$, and $Tl_2Ca_2Ba_2Cu_3O_{10}$, have been successfully prepared by a ceramic technique. Resistivity and ac susceptibility measurements have shown that they are both perfect conductors and perfect diamagnets. They have superconducting transitions above liquid nitrogen temperature and many properties in common with conventional superconductors. The ac susceptibility results of powdered samples show that the nature of the grain boundary has a strong effect on the magnetic properties.

X-ray diffraction experiments verified that $YBa_2Cu_3O_{7-\delta}$ is a orthorhombically distorted perovskite with the space group Pmmm. The ordering of oxygen vacancies forms two structural characteristics, Cu-O chains and Cu-O_2 planes. The properties of this material strongly depend on the oxygen content. It becomes a non-superconductor when $\delta \geq 0.5$. The phases of $Tl_2CaBa_2Cu_2O_8$ and

$Tl_2Ca_2Ba_2Cu_3O_{10}$ have tetragonal or pseudotetragonal structure with space group I4/mmm. Structural analysis of this system reveals that the Cu-O_2 planes which commonly exist in the cuprate are essential for high-T_c superconductors. T_c rises as the number of Cu-O_2 layers in a unit cell increases.

Substitution of iron for Cu led to a decrease in the transition temperature. Magnetic ordering has been observed in ^{57}Fe-doped samples at low temperature in Mössbauer effect experiments. The Debye temperature of high-T_c superconductors, Θ_D, deduced from the relation between the recoil-free fraction and the temperature, is not particularly high which implies that a stronger electron-phonon interaction must exist in high-T_c superconductors as compared to conventional superconductors if the materials are still BCS or BCS-like in nature.

In conventional superconductors very small amounts of magnetic impurities suffice to destroy the superconductivity completely. The coexistence of magnetic ordering and superconductivity in the high-T_c compounds suggests that the origin responsible for superconductivity may differ from the electron-phonon interaction.

High-T_c superconductors have a T_c above 90 K in $YBa_2Cu_3O_{7-\delta}$ and above 120 K in $Tl_2Ca_2Ba_2Cu_3O_{10}$. Hence, liquid nitrogen can be used as the refrigerant. From the application point of view, the discovery of high-T_c compounds is a milestone in superconductivity. On the other hand such high T_c's make suspect the traditional BCS theory based on weak coupling between electrons and phonons. Many new models based on strong coupling have been proposed for the new materials. From a scientific point of view the discovery of high-T_c materials has presented a lot of new goals for physics and material science.

8.2 Suggestions for Further Work

Mössbauer spectra of ^{57}Fe-doped $YBa_2Cu_3O_{7-\delta}$ show some complications since there are two different Cu sites, square planar and square pyramidal sites. The oxygen content is very sensitive to the procedure used to make this compound. The analysis and interpretation of the spectra from different groups do not agree with each other. There is only one Cu site, a pyramidal one in the 2122 phase. If iron ions only substitute for Cu then the Mössbauer spectra should be relatively simple for the 2122 phase. Further study for this compound may give a better understanding for the complex spectra of $YBa_2(Cu_{1-x}Fe_x)_3O_{7-\delta}$.

Mössbauer spectra of $YBa_2(Cu_{0.95}Fe_{0.05})_3O_{7-\delta}$ in the temperature range from 11.8 to 77 K (fig. 7.4) shown that a magnetically split sextet appears in all spectra. This sextet does not appear at 77 K. It may be worthwhile to take more spectra between 12 and 77 K to find the ordering temperature more accurately for this site. This information will be helpful in the goal to understand the nature of magnetic ordering in high-T_c superconductors.

The ac susceptibility measurements of powdered polycrystalline samples have revealed that grain boundaries have a significant effect on the superconducting properties. Anisotropy of the superconducting properties have been observed in single crystals[113,114]. Millimeter sized single crystals of $YBa_2Cu_3O_{7-\delta}$ have been grown in our laboratary. If some measurements can be performed on single crystals it may give more information about the role of grain boundaries.

The ac susceptibility measurements have shown that the amplitude of the ac magnetic field, h_0, has a significant effect on χ' and χ''. It may be worthwhile

to look at the dependence of χ' and χ'' on the frequency of ac magnetic field with and without a dc external field.

It is exciting that T_c is above liquid nitrogen temperature in high-T_c superconductors. At the onset of the discovery of high-T_c materials it was hoped that high-T_c superconductors might give rise to an industrial revolution. Actually, the ceramic nature of these materials greatly limited their applications. Low critical currents, low critical fields and deterioration in the ambient environment of the $YBa_2Cu_3O_{7-\delta}$ superconductor are other shortcomings. It is therefore worthwhile to investigate these problems. On the one hand it is possible that some techniques will be found to overcome these shortcomings, such as thin films, doping with extra elements, improved procedures and so on. On the other hand it is also possible to search for a high-T_c superconducting alloy. Of course, to solve these problems many formidable challenges will have to be overcome and the prospects of success are still quite uncertain.

Bibliography

[1] J. G. Bednorz and K. A. Müller, *Z. Phys.* **B64** (1986) 189

[2] M. K. Wu, J. R. Ashburn, C. J. Torng, P. H. Hor, R. L. Meng, L. Gao, Z. J. Huang, Y. Q. Wang and C. W. Chu, *Phys. Rev. Letts.* **58** (1987) 908

[3] Y. L. Luo A. H. Morrish, Q. A. Pankhurst, G. H. Pelletier G. J. Roy, D. Y. Zhang and X. Z. Zhou, *Can. J. Phys.* **65** (1987) 438

[4] H. Maeda, Y. Tanaka, M. Fukotomi and T. Asano, *Jpn. J. Appl. Phys.* **27** (1988) L209

[5] Z. Z. Sheng and A. M. Hermann, *Nature* **332** (1988) 138

[6] C. G. Kuper, *An Introduction to the Theory of Superconductivity*, Clarendon press. Oxford (1968) p57

[7] B. B. Goodman, *Proc. Phys. Soc. A* **66** (1953) 217

[8] R. E. Glover, III and M. Tinkham, *Phys. Rev.* **108** (1957) 243

[9] R. W. Morse and H. V. Bohm, *Phys. Rev.* **108** (1957) 1094

[10] I. Giaever, *Phys. Rev. Lett.* **5** (1960) 147, 464

[11] E. Maxwell, *Phys. Rev.* **78** (1950) 477

[12] C. A. Reynolds, B. Serin, W. H. Wright, L. B. Nesbitt, *Phys. Rev.* **78** (1950) 487

[13] U. Essmann and H. Träuble, *Phys. Letts. A* **24** (1967) 526

[14] P. L. Gammel, D. J. Bishop, G. J. Dolan, J. R. Kwo, C. A. Murray, L. F. Schneemeyer and J.V. Waszczak, *Phys. Rev. Lett.* **59** (1987) 2592

[15] Z. H. Mai and X. Chu, *Solid State Commun.* **65** (1988) 877

[16] V. L. Ginzburg and L. D. Landau, *JETP* **20** (1950) 1064

[17] J. Bardeen, L. N. Cooper and J. R. Schrieffer, *Phys. Rev.* **108** (1957) 1175

[18] L. C. Bourne, M. F. Crommie, A. Zettl, Hans-Conrad Zur Loye, S. W. Keller, K. L. Leary, A. M. Stacy, K. J. Chang, M. L. Cohen, and D. E. Morris, *Phys. Rev. Lett.* **58** (1987) 2337

[19] Lin Quan, Wei Yu-nian, Yan Qi-wei, Chen Geng-hua, Zhang Pan-lin, Shen Zhi-gong, Ni Yong-ming, Yang Qian-sheng, Liu Chao-xin, Ning Tai-shang, Zhao Jin-kue, Shao You-yu, Han Shun-hui and Li Jing-yuan, *Solid State Commun.* **65** (1988) 869

[20] R. D. Parks, *Superconductivity*, Marcel Dekker Inc. New York, (1969) p71

[21] H. Fröhlich, *Phys. Rev.* **79** (1950) 845

[22] L. N. Cooper, *Phys. Rev.* **104** (1956) 1189

[23] M. Tinkham, *Introduction to Superconductivity*, McGraw-Hill Inc. (1975) p33

[24] B. S. Deaver and W. M. Fairbank, *Phys. Rev. Lett.* **7** (1961) 43

[25] R. Doll and M. Näbauer, *Phys.Rev. Lett.* **7** (1961) 51

[26] C. E. Gough, M. S. Colclough, E. M. Forgan, R. G. Jordan, M. Keene, C. M. Muirhead, A. I. M. Rae, N. Thomas, J. S. Abell and S. Sutton, *Nature* **326** (1987) 855

[27] L. Ya. Vinnikov, L. A. Gurevich, G. A. Emelchenko, G. A. Kazaryan, N. N. Kolesnikov, M. P. Kulakov, D. Ya. Lenchinenko and Yu. A. Ossipyan, *Solid State Commun.* **70** (1989) 1145

[28] J. Niemeyer. M. R. Dietrich, C. Politis, A. R. Moodenbaugh, D. O. Welch and M. Suenaga, *Phys. Rev. B* **39** (1989) 351

[29] P. W. Anderson, *Science* **235** (1987) 1196

[30] A. Khurana, *Physics Today*, **3** (1988) 19

[31] R. J. Cava, B. Batlogg, J. J. Krajewski, R. Farrow, L. W. Rupp Jr, A. E. White, K. Short, W. F. Peck and T. Kometani, *Nature* **332** (1988) 814

[32] W. A. Little, *Science* **242** (1988) 1390

[33] H. F. C. Hoevers, P. J. M. Van Bentum, L. E. C. Van De Leemput, H. Van Kempen, A. J. G. Schellingerhout and D. Van Der Marel, *Physica C* **152** (1988) 105

[34] I. Maartense, *J. Appl. Phys.* **53** (1982) 2466

[35] H. Steinfink, J. S. Swinnea, Z. T. Sui, H. M. Hsu and J.B.Goodenough, *J. Am. Chem. Soc.* **109** (1987) 3348

[36] X. Z. Zhou, A. H. Morrish, Y. L. Luo, M. Raudsepp and I. Maartense, *J. Phys. D* **21** (1988) 1243

[37] C. C. Torardi, M. A. Subramanian, J. C. Calabrese, J. Gopalakrishnan, K. J. Morrissey, T. R. Askew, R. B. Flippen, U. Chowdhry and A. W. Sleight, *Science* **240** (1988) 631

[38] A. Ono and T. Tanaka, *Jpn. J. Appl. Phys.* **26** (1987) L825

[39] S. Takekawa and N. Iyi, *Jpn. J. Appl. Phys.* **26** (1987) L851

[40] Y. Hidaka, Y. Enomoto, M. Suzuki, M. Oda and T. Murakami, *J. Crystal Growth* **85** (1987) 581

[41] R. F. Cook, T. R. Dinger and D. R. Clark, *Appl. Phys. Letts.* **51** (1987) 454

[42] W. Tolksdorf, *Crystal Growth of Electronic Materials*, Edited by E. Kaldis, Elsevier Science Publishers, B. V. (1985) p175

[43] X. Z. Zhou, J. A. Eaton, M. Raudsepp, A. H. Morrish and Y. L. Luo, *J. Phys. D* **20** (1987) 542

[44] M. Raudsepp, F. C. Hawthorne, X. Z. Zhou, I. Maartense, A. H. Morrish, and Y. L. Luo, *Can. J. Phys.* **65** (1987) 1145

[45] A. H. Morrish, X. Z. Zhou, M. Raudsepp, I. Maartense, J. A. Eaton, and Y. L. Luo, *Can. J. Phys.* **65** (1987) 808

[46] B. G. Hyde, J. G. Thompson, R. L. Withers, J. G. Fitzgerald, A. M. Stewart, D. J. M. Bevan J. S. Anderson, J. Bitmead and M. S. Peterson, *Nature* (London) **327** (1987) 402

[47] R. L. Barns and R. A. Laudise, *Appl. Phys. Lett.* **51** (1987) 1373.

[48] N. P. Bansal and A. L. Sandkuhl, *Appl. Phys. Lett.* **52** (1988) 323

[49] R. M. Hazen, *Scientific American* **6** (1988) 74

[50] F. Izumi, H Asano and T. Ishigaki, *Jpn. J. Appl. Phys.* **26** (1987) L617

[51] W. I. F. David, W. T. A. Harrison, J. M. F. Gunn, O. Moze, A. K. Soper, P. Day, J. D. Jorgensen, D. G. Hinks, M. A. Beno, L. Soderholm, D. W. CaponeII, I. K. Schuller, C. U. Segre, K. Zhang and J. D. Grace, *Nature (London)* **327** (1987) 310

[52] M. A. Beno, L. Soderholm, D. W. Capone II, D. G. Hinks J. D. Jorgensen, J. D. Grace and I. K. Schuller, *Appl. Phys. Lett.* **51** (1987) 57

[53] J. D. Jorgensen, B. W. Veal, W. K. Kwok, G. W. Crabtree, A. Umezawa, L. J. Nowicki and A. P. Paulikas, *Phys. Rev. B* **36** (1987) 5731

[54] J. M. Tarascon, W. R. McKinnon, L. H. Greene, G. W. Hull and E. M. Vogel, *Phys. Rev. B* **36** (1987) 226

[55] I. K. Schuller, D. G. Hinks, M. A. Beno, D. W. Capone II, L. Soderholm, J. P. Locquet, Y. Bruynseraede, C. U. Segre and K. Zhang, *Solid State Commun.* **63** (1987) 385

[56] H. M. Rietveld, *J. Appl. Cryst.* **2** (1969) 65

[57] R. J. Hill, *Acta Crystllogr. Sect C: Cryst. Struct. Commun.* **41** (1985) 1281

[58] D. B. Wiles and R. A. Young, *J. Appl. Crystl.* **14** (1981) 149

[59] S. Sato, I. Nakada, T. Kohara and Y. Oda, *Jpn. J. Appl. Phys.* **26** (1987) L663

[60] K. Hestermann and R. Hoppe, *Z. Anorg. Allg. Chem.* **363** (1968) 249

[61] R. J. Cava, B. Batlogg, C. H. Chen, E. A. Rietman, S. M. Zahurak and D. Werder, *Nature* **329** (1987) 423

[62] Gang Xiao, M. Z. Cieplak, D. Musser, A. Gavrin, F. H. Streitz, C. L. Chien, J. J. Rhyne and J. A. Gotaas, *Nature* **332** (1988) 238, *Phys. Rev. B* **35** (1987) 8782

[63] J. M. Tarascon and P. B. Barboux, B. G. Bagley, L. H. Green and G. W. Hull, *Mat. Sci. Eng. B* **1** (1988) 29

[64] R. Poole. *Science* **240** (1988) 146

[65] R. M. Hazen, L. W. Finger, R. J. Angel, C. T. Prewitt, N. L. Ross, C. G. Hadidiacos, P. J. Heaney, D. R. Veblen, Z. Z. Sheng, A. El Ali and A. M. Hermann, *Phys. Rev. Lett.* **60** (1988) 1657

[66] M. Kikuchi, T. Kajitani, T. Suzuki, S. Nakajima, K. Hiraga, N. Kobayashi, H.Iwasaki, Y. Syono and Y. Muto, *Jpn. J. Appl. Phys.* **28** (1989) L382

[67] M. A. Subramanian, J. C. Calabrese, C. C. Torardi, J. Gopalakrishnan, T. R. Askew, R. B. Flippen, K. J. Morrissey, U. Chowdhry and A. W. Sleight, *Nature* **332** (1988) 420

[68] M. Kikuchi, N. Kobayashi, H. Iwasaki, D. Shindo, T. Oku, A. Tokiwa, T. Kajitani, K. Hiraga, Y. Syono and Y. Muto, *Jpn. J. Appl. Phys.* **27** (1988) L1050

[69] G. T. Meaden, *Electrical Resistance of Metals*, Heywood, London, (1966) p147

[70] E. Maxwell and M. Strongin, *Phys. Rev. Lett.* **10** (1963) 212

[71] C. W. Chu, J. Bechtold, L. Gao, P. H. Hor, Z. J. Huang, R. L. Meng, Y. Y. Sun, Y. Q. Wang and Y. Y. Xue, *Phys. Rev. Lett.* **60** (1988) 941

[72] D. K. Finnemore, R. N. Shelton, J. R. Clem, R. W. McCallum, H. C. Ku, R. E. McCarley, S. C. Chen, P. Klavins and V. Kogan, *Phys. Rev. B* **35** (1987) 5319

[73] S. L. McCarthy and R. Viswanathan, *Solid State Commun.* **9** (1971) 569

[74] T. Ishida and H. Mazaki, *Phys. Rev. B* **20** (1979) 131

[75] W. D. Gregory, in *The Science and Technology of Supercoductivity,* edited by W. D. Gregory, W. N. Matthews, Jr., E. Edelsack (Plenum, New York, 1973), Vol. II, p226

[76] L. Landau and E. M. Lifshitz, *Electrodynamics of Continuous Media,* Addison-Wesley Publishing, (1960) p194

[77] M. Ribault, G.Benedek, D.Jerome and K. Bechgaard, *J. Phys. Lett.* **41** (1980) 397

[78] N. Garcia, S. Vieira, A. M. Baro, J. Tornero. M. Pazos, L. Vázquez, J. Gómez, A. Aguiló, S. Bourgeal, A. Buendía, M. Hortal, M. A. López, de la Torre, M. A. Ramos, R. Villar, K. V. Rao, D.-X. Chen, Josep Nogues and N. Karpe, *Z. Phys. B* **70** (1988) 9

[79] T. Ishida and H. Mazaki, *J. Appl. Phys.* **52** (1981) 6798

[80] A. F. Khoder, *Phys. Letts. A* **94** (1983) 378

[81] R. A. Hein, *Phys. Rev. B* **33** (1986) 7539

[82] T. Ishida and H. Mazaki, *Jpn. J. Appl. Phys.* **26** (1987) L1296

[83] Y. Oda, I. Nakada, T. Kohara, H. Fujita, T. Kaneko, H. Toyota, E. Sakagami and K. Asayama, *Jpn. J. Appl. Phys.* **26** (1987) L481

[84] H. Mazaki, M. Takano, Y. Ikeda, Y. Bando, R. Kanno, Y. Takeda, and O. Yamamoto, *Jpn. J. Appl. Phys.* **26** (1987) L1749

[85] Y. Oda, H Takenaka, H. Nagano and I. Nakada, *Solid State Commun.* **35** (1980) 887

[86] D. X. Chen, R. B. Goldfarb, J. Nogues, and K. V. Rao, *J. Appl. Phys.* **63** (1988) 980

[87] H. Kumakura, K. Togano, K. Takahashi, E. Yanagisawa, M. Nakao and H. Maeda, *Jpn. J. Appl. Phys.* **27** (1988) L2059

[88] E. Baggio-Saitovitch, I. S. Azevedo, R. B. Scorzelli, H. Saitovitch, S. F. da Cunha, A. P. Guimaraes, P. R. Silva, and A. Y. Takeuchi, *Phys. Rev. B* **37** (1988) 7967

[89] J. M. Tarascon, P. Barboux, P. F. Miceli, L. H. Greene, and G. W. Hull, *Phys. Rev. B* **37** (1988) 7458

[90] C. W. Kimball, J. L. Matykiewicz, J. Giapintzakis, H. Lee, B. D. Dunlap, M. Slaski, F. Y. Fradin, C. Segre, and J. D. Jorgensen, MRS symposium proceedings, Eds by M. B. Brodsky, R. C. Dynes, K. Kitazawa and H. L. Tuller, MRS, Pittsburgh, (1987) p107

[91] J. M. D. Coey and K. Donnelly, *Z. Phys. B* **67** (1987) 513

[92] E. R. Bauminger, M. Kowitt, I. Felner and I. Nowik, *Solid State Commun.* **65** (1988) 123

[93] Q. A. Pankhurst, A. H. Morrish, M. Raudsepp and X. Z. Zhou, *J. phys. C* **21** (1988) L7

[94] X. Z. Zhou, M. Raudsepp, Q. A. Pankhurst, A. H. Morrish, Y. L. Luo and I. Maartense, *Phys. Rev. B* **36** (1987) 7230

[95] H. Tang, Z. Q. Qiu, Y. W. Du, Gang Xiao, C. L. Chien and J. C. Walker, *Phys. Rev. B* **36** (1987) 4018

[96] E. Simopoulos and D. Niarchos, *Hyperfine Interactions,* **42** (1988) 1256

[97] C. Blue, K. Elgaid, I. Zitkovsky and P. Boolchand, *Phys. Rev. B* **37** (1988) 5905

[98] Z. Q. Qiu, Y. W. Du, H. Tang and J. C. Walker, *J. Mag. Magn. Mat.* **78** (1989) 359

[99] E. Simopoulos and D. Niarchos, *Phys. Rev. B* **38** (1988) 8931

[100] N. N. Greenwood and T. C. Gibb, *Mössbauer Spectroscopy,* Chapman and Hall Ltd. London (1971) p91

[101] C. Y. Yang, S. M. Heald, J. M. Tranquada, Youwen Xu, Y. L. Wang, A. R. Moodenbaugh, D. O. Welch and M. Suenaga, *Phys. Rev. B* **39** (1989) 6681

[102] N. N. Greenwood and T. C. Gibb, *Mössbauer spectroscopy,* Chapman and Hall Ltd. London, 1971 p11

[103] Q. A. Pankhurst, A. H. Morrish and X. Z. Zhou, *Phys. Letts. A* **127** (1988) 231

[104] M. Blume, *Phys. Rev.* **174** (1968) 351

[105] D. S. Ginley, E. L. Venturini, J. F. Kwak, R. J. Baughman, B. Morosin and J. E. Schirber, *Phys. Rev. B* **36** (1987) 829

[106] J. M. Tarascon, P. Barboux, P. R. Miceli, L. H. Greene, G. W. Hull, M. Eibschutz and S. A. Sunshine, *Phys. Rev. B* **37** (1988) 7458

[107] Z. Q. Qiu, Y. W. Du, H. Tang, J. C. Walker, J. S. Morgan and W. A. Bryden, *J. Appl. Phys.* **64** (1988) 5947

[108] S. K. Xia, Z. B. Zhao, C. R. Wang, R. Z. Ma, G. H. Cao and J. Y. Ping, *Solid State Commun.* **70** (1989) 141

[109] J. Giapintzakis, J. M. Matykiewicz, C. W. Kimball, A. E. Dwight B. D. Dunlap, M. Slaski and F. Y. Fradin *Phys. Lett. A* **121** (1987) 307

[110] T. C. Gibb, *Principles of Mössbauer spectroscopy,* Chapman and Hall, London, 1976 p139

[111] J. R. Thompson, J. Brynestad, D. M. Kroeger, Y. C. Kim, S. T. Sekula, D. K. Christen and E. D. Spechet, *Phys. Rev. B* **39** (1989) 6652

[112] A. H. Morrish, X. Z. Zhou and Y. L. Luo, *Progress in High Temperature Superconductivity*, eds. L. H. Bennett, Y. Flom and G. C. Vezzoli, Vol. 17 (World Scientific Publishing Co., Singapore 1989) p319

[113] Y. Iye, T. Tamegai, H. Takeya and H. Takei, *Jpn. J. Appl. Phys.* **26** (1987) L1057

[114] S. Kamba, J. Petzelt, V. Zelezny, E. V. Pechen, S. I. Krasnosvobodtsev, and B. P. Gorshunov, *Solid State Commun.* **70** (1989) 547